ABSTRACT

Wassel, Ronald Andrew Investigating structure property relationships in electroactive molecules via scanning tunneling microscopy **(**Under the direction of Dr. Christopher B. Gorman)

This dissertation will discuss issues related to determining structure property relationships that are relevant to molecular electronics. More specifically, an STM will be used to compare electronic measurements over insulating n-alkanethiolate SAMs and electroactive SAMs composed of ferrocenyl- terminated thiols and viologen terminated thiols, as well as multilayer SAMs created by alternating a metal dication and a thiolate. The surface characterization of these SAMs will be discussed. Current – voltage (I-V) measurements on the SAMs will be discussed as they pertain to the non-linear current voltage behavior of negative differential resistance (NDR). A mechanism for the nature of NDR will be discussed as well as the need to understand how the junctions used to measure I-V curves influence NDR. The attenuation of the apparent tunneling barrier of ferrocenyl-terminated thiolates via non-covalent binding of β-cyclodextrin will be shown. This attenuation will be shown to influence the peak to valley ratio of NDR

Stochastic variation in electroactive molecules inserted into an insulating n-alkanethiolate background SAM was observed and is believed to be a general phenomenon. In this dissertation it will also be shown that the electric field generated by the STM tip increases the rate of replacement of electroactive molecules in to the background SAM.

Investigating structure property relationships in electroactive molecules via scanning tunneling microscopy

By

Ronald Andrew Wassel

A Dissertation Submitted to the Graduate Facility of North Carolina State University
In Partial Fulfillment of the
Requirements for the
Degree of Doctor of Philosophy

Department of Chemistry

Raleigh, North Carolina
October 26, 2004

_____
Dr. Christopher B. Gorman, Chair of Advisory Committee

_____ _____
Dr. Edmond F. Bowden Dr. Daniel L. Feldheim

_____ _____
Dr. T. Brent Gunnoe Dr. Raymond E. Fornes,
Graduate School Representative

DEDICATION

For my wife Deb, Mom, Dad, Todd, Courtney and Harrison

BIOGRAPHY

Ronald Andrew Wassel Jr. was born in Port Hueneme, CA on March 1, 1974 to Ronald and Andréa Wassel. His father was a career Naval Officer and moved every few years until finally settling in Jamestown, RI upon his father's retirement. He graduated from Rensselaer Polytechnic Institute in 1996 with a B.S. in environmental science and received a second B.S. in biology from Roger Williams University in 1997. It was at Roger Williams that Ronald met his future wife Deborah Ann Butkus. He worked for the next few years in various laboratories before starting graduate school in the chemistry department at North Carolina State University in 2000. Ronald married Deb on June 8, 2002 in Whitman MA.

ACKNOWLEDGMENTS

First, I would like to thank Deb, my loving wife, for supporting me through this experience. I would like to thank my Mom, Dad, Todd and Courtney for being there for me. Without you I would not be the man I am today.

I want to thank my advisor, Prof. Christopher B. Gorman, for his support and guidance throughout my graduate school career. I would also like to acknowledge my colleagues and friends who made graduate school an enjoyable experience for me: Drs. Stephan Kramer, Ryan Fuierer, Wyatt McConnell, Grace Credo and Lloyd Carrol. I am very grateful to you all for for friendship and guidance. I would especially like to thank Stephan for putting up with all of my questions and for being my friend.

I would like to thank Christopher Cameron for his help in all things organic as well as our lengthy political discussions (some day you will see that I am right). I would like to thank the rest of the Gorman group especially Holly Robuck and Young-Rae Hong.

TABLE OF CONTENTS

LIST OF FIGURES

LIST OF TABLES

Chapter 1

Establishing the basis for molecular electronics

1.1 The current state of electronics

For the past forty years, computers have become faster and more powerful as the size of the transistor has decreased.[1] A transistor is a device that is used to amplify a signal or open and close a circuit. In a computer, it functions as an electronic switch. Transistors work on the principle that certain materials such as silicon can be made to perform as "solid state" devices. The conductivity of a solid “state device” is related to the number of “free” electrons it has. Silicon has very few free electrons. If impurities (phosphorous or boron) are introduced in a controlled manner, then the free electrons or electron deficiencies (holes) are created and the conductivity is increased. A Material with this type of increase in conductivity is called a semiconductor. Semiconductors that conduct free electrons are called n-type material, while materials which conduct holes are called p-type.

Figure 1.1.1 shows a schematic of a generic transistor. The gray region labeled "silicon substrate" forms the support for the transistor. The source and drain material are the red regions at the very top of the grey silicon substrate. The source and drain can be either p- or n- type material. In between them is the conduction path along which electrons flow. The gate is the yellow area labeled "Gate” and straddles the gap between the source and drain area and controls the switching action of the transistor. An insulating layer is placed in between the source/drain and the gate in order to prevent current from leaking into the conduction path.

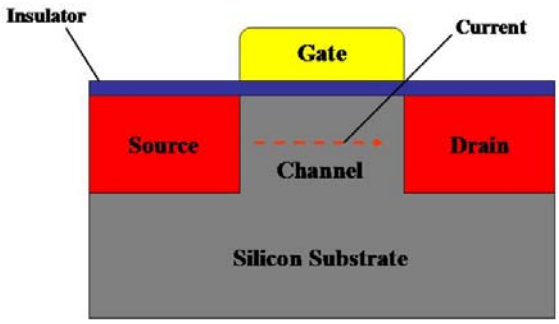

Figure 1.1.1 Schematic of a typical metal oxide semiconductor field effect transistor

The pathway between the source and drain changes from an insulator to a conductor, depending on whether current is applied to the gate. When current is applied to the gate, electrons or holes flow from the source to the drain and the transistor is said to be in the "on" state. It is in the "off" state when no current is applied to the gate. The open or closed switches represent the zeros and ones that are used to store all the data in a computer.

Transistors made today utilize a top down approach: bulk material is removed from the surface to create the desired structure. The most common commercial way to create structures is the use of photolithography and photo resists. The minimum feature size created through photolithography is limited by the wavelength of light used. More advanced methods such as electron-beam lithography, ion beam lithography and x-ray lithography can achieve much better resolution, but are much more expensive to use commercially.

According to Moore's law, the number of transistors per chip doubles every 1.5 years.[2] As the transistor size decreases, the speed of the devices increase and the amount of power needed per unit also decreases. As of the year 2000 gate

structures were about 180 nanometers across, or 1/500 the width of a human hair.[3] Until recently, this increase in density equated to lower cost and added functionality.

Conventional devices are reaching their physical limitations as device sizes of 50 nm and smaller are approached. In 1997 the gate oxide thickness was 25 silicon atoms and by 2012 it is estimated that the gate oxide will only be 5 atoms thick which is the bare minimum for a functional insulating oxide layer.[4] As the dimensions of the gate and the insulating oxide layer decrease, quantum-mechanical tunneling of carriers can occur through the thin gate oxide, from source to drain, and from drain to the body of the transistor.[5-8] At some point the size of these components become so small that their behavior no longer functions like that of the bulk material. For example, controlling the density and location of dopant atoms in the transistor channel and source/drain region becomes increasingly difficult as the dimensions of the transistor decreases.[9] The challenge of molecular electronics is to capitalize on some of these quantum mechanical problems such as tunneling and incorporate them into new device architectures. If devices can be fabricated that are based on tunneling, they can be made both small and fast because tunneling is not limited by carrier mobility as it is in a semiconductor.[8]

It has been proposed that individual molecules or small bundles of molecules could be used to create novel devices whose electronic behavior could be similar to traditional electronic components.[10] The question for molecular electronics then becomes: how does one make small devices and how do we make contact to them? What does “small” even mean? How can materials be easily made with consistent uniform properties and on a small scale?

Present day transistors are still much larger than proposed molecular-scale devices. The International Technology Roadmap for Semiconductors projects that in about 10 years, semiconductors will approach the 50-nm node (a node is a set of requirements composed to support semiconductor manufacturing at a specific minimum line width). Beyond this, however, processes will be required approaching atomic-layer precision.[11] It has been projected that a total molecular device size could be made as small as 12 to 25 nm. If they could be made on the molecular scale, integrated circuits could have as many as 100 billion or more switching devices on a single chip, resulting in terabyte/cm^2 memories.[1] To put this size differential in perspective, if the conventional transistor were scaled up so that it occupied the printed page you are reading, a molecular device would be the period at the end of this sentence.[12]

1.2 Devices based on novel molecular architectures

The integration of large numbers of molecules into a molecular device remains one of the primary difficulties in implementing molecular electronics.[1] A novel approach for the fabrication of molecular scale electronic devices is the bottom up approach. It has been shown that amphiphilic molecules self-assemble on a surface.[13] Self-assembly is the ability of simple building blocks to spontaneously form complex hierarchical structures. This behavior can be observed in nature because any living cell is an example of self assembly.[14] Self-assembled monolayers (SAMs) spontaneously form ordered structures via the adsorption of a surfactant that had an head group with a specific affinity for a surface.[14]

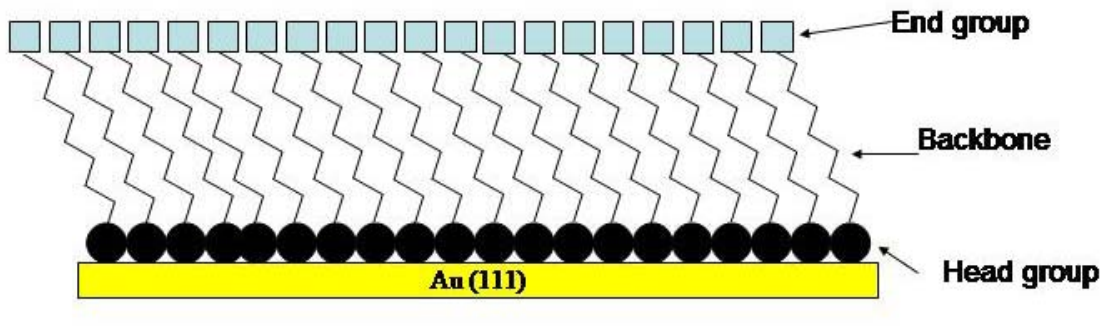

Figure 1.2.1 Schematic of a n-alkanethiolate self assembled monolayer on a Au(111) surface

Figure 1.2.1 shows a schematic of a SAM. The head group is the part of the molecule that binds (preferably covalently) to the substrate. The backbone, in this case an n-alkane chain, makes up the body of the assembly. Collective van der Waals forces in the alkane backbone aid in the ability of the molecules to form densely packed and ordered arrays.[14] The end group is the terminus of the molecule that is sticking up from the surface. Order and structural complexity in SAMs are intrinsically built into the system rather than being dictated by external forces. This has the advantage of virtually unlimited variations in the kinds of molecules that can be assembled on a surface.

1.2.1 Molecular electronics measurements

Performing logic and memory operations with one or a very small collection of molecules would be the ultimate in electronic device miniaturization. For this reason, the field of molecular electronics has received attention that ranges from scientific curiosity to intellectual property generation and venture capital. While new paradigms and financial rewards in nanotechnology will probably come, answers to several key questions are a necessary first step in this evolution. In this regard,

chemists, with their deep understanding of molecular structure/ property relationships, have an exciting task ahead– sorting out the fundamental precepts that will govern this field. A number of central questions have emerged. For example, how does one make contact with a molecule? What is the electronic structure of a molecule when in contact with "wires"? Is it different from the electronic structure that is probed by electrochemistry? Can molecular structure-property relationships be derived that relate the structure of a molecule to current behaviors, switching, and, ultimately, gating? These latter questions have been addressed with some recent, plausible approaches. Such work is highlighted in the following sections.

1.2.2 Strategies for making metal-molecule-metal junctions

In performing nanoscale electronic measurements, the first issue at hand, is how to make electrical contact to these elements. There are several effective strategies for making contact to molecules. The first strategy for making contact to a small collection of molecules began with the mechanical break junction (Figure 1.2.2).[15-21] A break junction is formed by attaching a metal wire onto a flexible substrate and then bending the substrate just until the wire has broken. The gap produced is then exposed to molecules designed to bind across it. The researchers measured the resistance across the gap and were determined to be consistent with the resistance of a single molecule. The structure of each break junction varies from sample to sample, making the data difficult to reproduce. Comparing the behaviors of a range of molecules is difficult, since only one break junction can be made and measured at a time. The lack of data sets to be used for comparisons of molecular

behaviors and the time requirements needed to test a range of molecules leaves much to be desired.

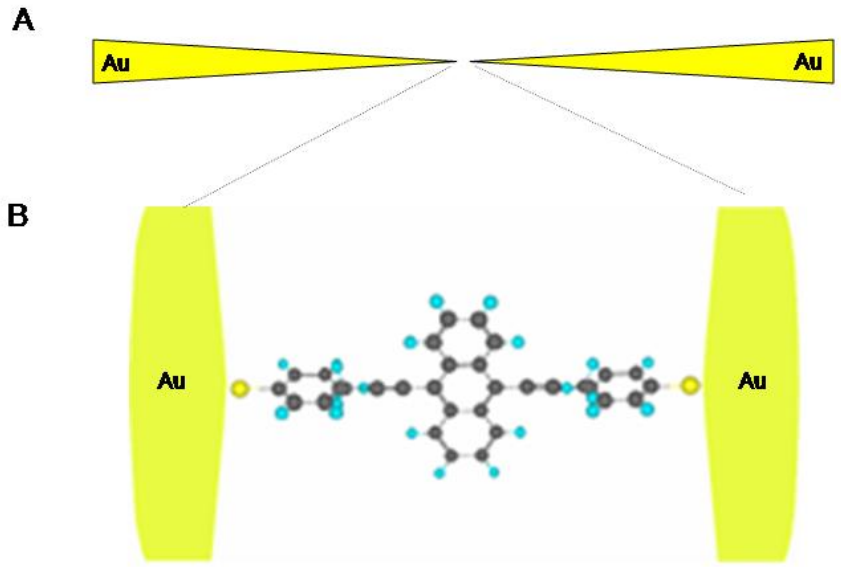

Figure 1.2.2 Schematic of a molecular break junction. (A) Two gold wires with a nanogap in the middle. (B) Zoom of the nanogap showing a molecule inserted into it.

A variation of the break junction can be made by using an STM and a gold substrate. Xiao et al. reported a metal-molecule-metal junction where a molecular junctions was formed by pulling a gold STM tip out of contact with the gold substrate in the presence of sample molecules.[22] Each sample molecule was terminated on both ends with a thiol and can bridge the tip and substrate electrodes to form a molecular junction. The current flow between the tip and substrate was recorded at a fixed bias as the tip is pulled away.[22] As the tip was pulled out of contact with the surface the conductance decreased in a stepwise fashion. When the last gold atom

contact was broken a new sequence of stepwise conductance curves is observed at a high resistance region indicating the presence of a molecular contact. In this work conductance values for benzenedithiol (BDT) and benzenedimethanethiol (BDMT) were compared. The conductance of BDT was shown to be 20 times greater than that of the BDMT.

Haiss et al. have taken this technique a step further. They performed current distance (I-d) measurements on a viologen dithiol.[23] They formed a low coverage phase on gold so that the dithiol was lying down parallel to the surface. The STM tip was brought close to the Au surface to form a stable molecular contact between the tip and the surface. The tip was then withdrawn from the surface and the current-distance relation was measured. The researchers saw two types of I-d curves: one showed a fast exponential decay that is typical for tunneling between a tip and a bare gold substrate (curve 1 in Figure 1.2.3). The second type of curve exhibited a less abrupt decay followed by a characteristic current plateau (curve 2 in Figure 1.2.3). It was proposed that the plateau is related to conduction through the molecule and that direct tunneling from the tip to the substrate does not significantly contribute to the current in this region.

In another type of junction a top contact can be made to a collection of molecules (e.g. a self-assembled monolayer (SAM) or Langmuir-Blodgett (LB) film) via metal evaporation. For example, in a nanopore configuration (Figure 1.2.4)[24,25] the area of the nanopore is designed to be smaller than the domain size of the SAM and the evaporated metal accumulates only on the top of the SAM.

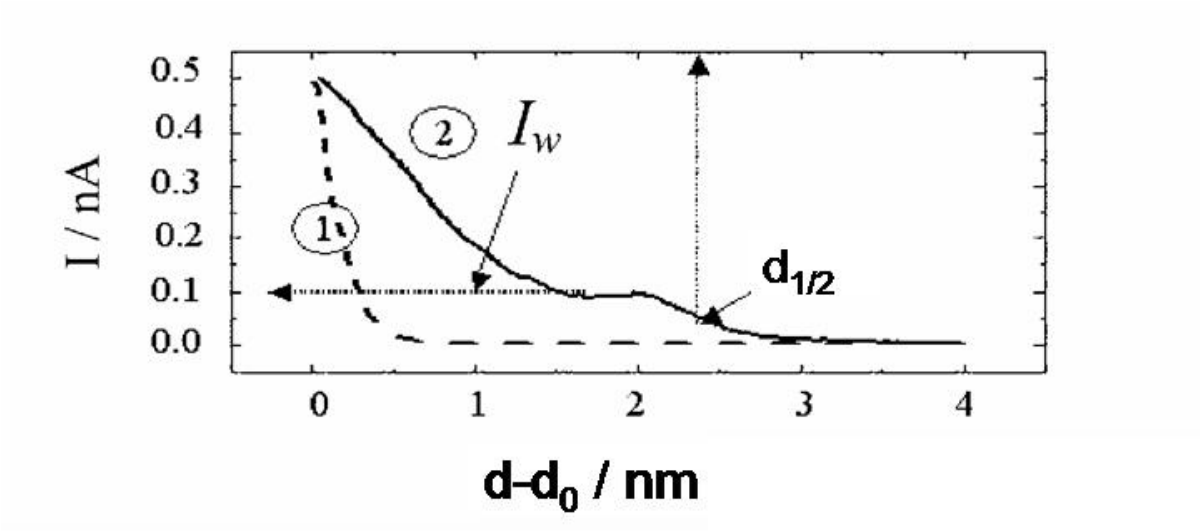

Figure 1.2.3 I-z spectroscopy for C_6-viologen-C_6 dithiol on A(111) in air. Curve 1 shows a baseline for a clean Au surface and curve 2 shows presence of the C_6-viologen-C_6 dithiol between the tip and the substrate. I_w is the plateau current and $d_{1/2} = I_w/2$. (reproduced from Figure 2 in reference 23)

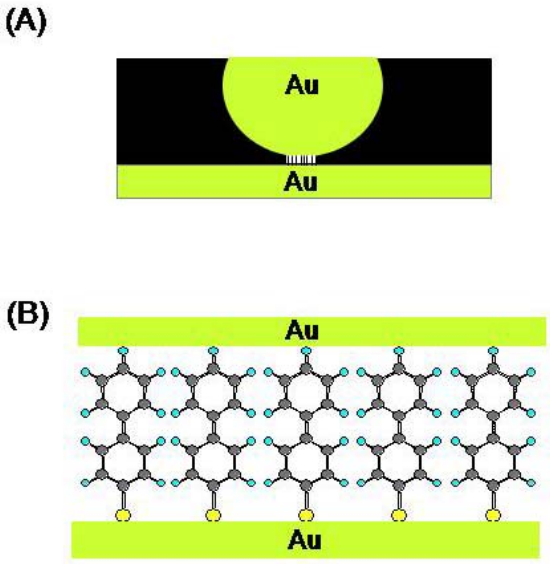

Figure 1.2. 4 Schematic of a nanopore assembly. A) Au top electrode self-assembled monolayer/ Au bottom electrode sandwich structure in the nanopore with a diameter of about 300 Å. B) diagram of the sandwich structure. (reproduced from Figure 1 in reference 25)

Although evaporating a top contact makes a metal-molecule-metal sandwich that most naturally resembles a device, metals are strong reducing agents. Reduced molecules are typically quite chemically reactive- thus, the molecule placed into the sandwich may not be the structure that is ultimately measured. This concern is exacerbated by the fact that the geometry of
the sandwich precludes any spectroscopic characterization of the molecules in that device.

An alternative to evaporated metal contacts is the use of mercury with n-alkanethiolate SAMs formed on its surface. The Hg drop is liquid and can conform to any surface it comes in contact with. In these types of experiments a SAM was formed on a drop of mercury and was brought into contact with another SAM on a metal substrate. This second SAM can be made from the same type of molecule as the SAM on the mercury drop or a different molecule altogether. In these types experiments two types of junctions can be assembled: 1) one in which a SAM(1) and SAM (2) were formed from n-alkanethiols on small drops of mercury (Figure 1.2.5A), and 2) one in which SAM(1) was formed on Hg and SAM(2) was formed on Au or Ag (Figure 1.2.5B). In this case SAMs (1) and (2) can have the same terminal group (Figure 1.2.5A) or different terminal groups (Figure 1.2.5B).[26,27]

Whitesides et al. have used a junction in which one SAM was formed on silver from an aliphatic or aromatic thiol and another SAM was formed on a drop of mercury or where both metal electrodes were mercury. The two SAMs were brought into contact with each other so that the rates of electron transport could be measured across the junction. [26-36]

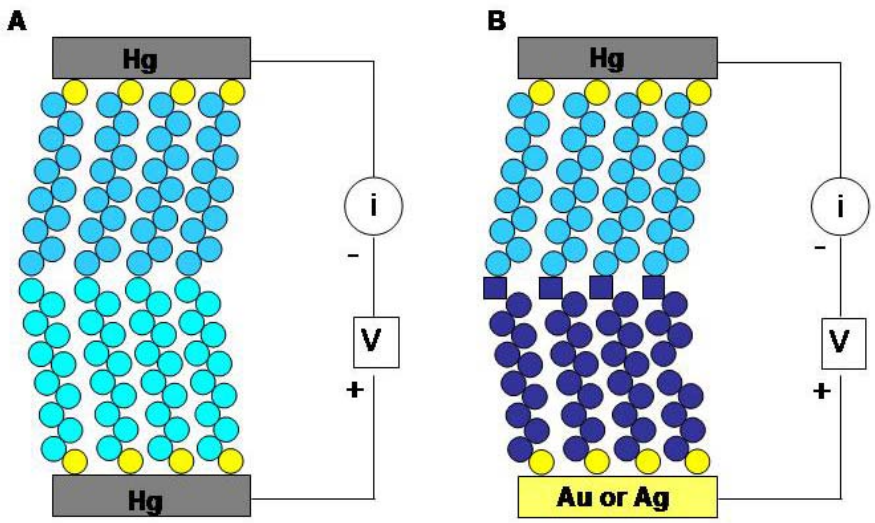

Figure 1.2.5 Mercury drop electrode A) Identical SAMs formed on two drops of mercury B) Mercury/Au or Ag junction with two different SAMs formed on each electrode.

Electron transport can be related to the current measured across these junctions by the equation $I = I_0 e^{-\beta d}$ (where d is the distance between the electrodes, and β is the structure-dependent attenuation factor). Figure 1.2.6 shows a plot of current density vs. length of three different classes of molecules. The β values can be calculated from the slope of these curves. For alkanethiols forming SAM(1) on Ag, $\beta_{(CH_2)_{n-1}CH_3}$ is 0.87 ± 0.1 $Å^{-1}$; for oligophenylene thiols, $\beta_{(Ph)_k}$ is 0.61 ± 0.1 $Å^{-1}$; and for the benzylic derivatives of oligophenylene thiols, $\beta_{CH_2(PH)m}$ is 0.67 ± 0.1 $Å^{-1}$.[27]

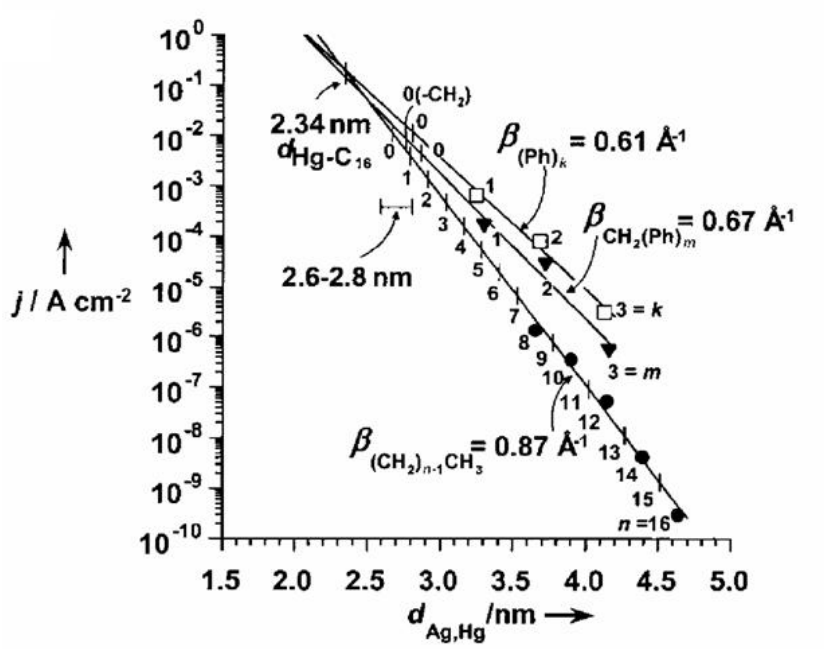

Figure 1.2.6 Plot correlating values of current density and distance between electrodes for $J_{Ag\text{-}SAM(1)//C16\text{-}Hg}$ at V=0.5 V. The lines are linear least-squares fits to the equation ln(I)=-βd+ln(I_0). For alkanethiols forming SAM(1) on Ag, β is 0.87 ± 0.1 $Å^{-1}$; for oligophenylene thiols, β is 0.61 ± 0.1 $Å^{-1}$; and for the benzylic derivatives of oligophenylene thiols, β b is 0.67 ± 0.1 $Å^{-1}$.(Reproduced from Figure 2 in reference 27)

Mercury contacts have also been used to demonstrate negative differential resistance (NDR) in oligo(phenylene-ethynylene) (OPE) SAMs on Au. NDR is characterized by a decreasing current with increasing potential. Le et al. have shown NDR in Hg/C_{14}S-/OPE/Au bilayer junctions. Figure 1.2.7 shows several current-voltage curves for successive bias sweeps form -1.5 to 1.5 V.[37] A NDR peak was observed in the positive bias region and no NDR was observed in the negative region. This technique was demonstrated to be a robust and reproducible junction with which to measure current-voltage curves.

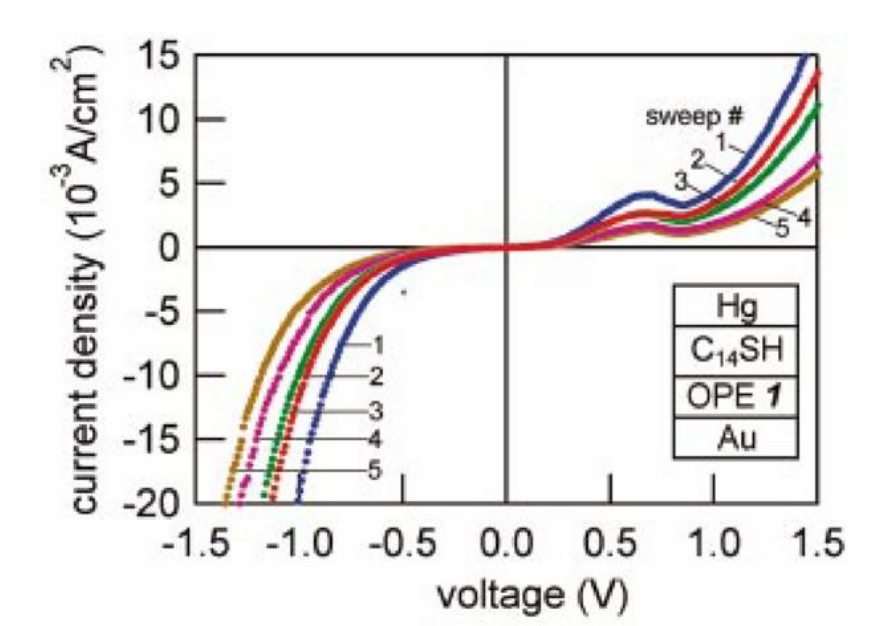

Figure 1.2.7 Current–voltage characteristics for successive bias sweeps for a single Hg/C_{14}S-/OPE/Au bilayer junction at 300 K. The voltage was swept from -1.5 to +1.5 V with a sweep rate of 0.13 V/s and a delay of approximately 30 s between sweeps. The contact area was 1.7 x 10^{-4} cm^2.

A number of investigators have employed a scanning tunneling microscope (or conducting atomic force microscope) tip as a second contact to a molecule (often organized into a self-assembled monolayer).[38-54] In a scanning tunneling setup, a STM tip is held over a conductive surface at a constant potential and tunneling current. Current either flows from the tip to the surface or visa versa. As the tip scans across the surface, it responds to surface features by moving up and down to maintain a constant current. If the tip moves over a more conductive area, there is less resistance and the tip has to increase its distance from the surface in order to maintain a constant current. If the tip moves over a less conductive area, then it has to move closer to the surface to achieve the desired tunneling current. In this way

the STM allows us to create an image that is a convolution of the topography of the sample and its electronic properties. Several STM examples are noted here. Hipps et al. reported orbital mediated tunneling through phthalocyanins and porphyrins containing metal centers.[39-42,55] Resonant tunneling in an STM system occurs when the Fermi energy of the metal tip or the substrate overlaps with that of an orbital in the molecule resulting in a maximum probability of tunneling.[55] In one experiment, mixed monolayers of copper phthalocyanine and cobalt phthalocyanine were deposited on gold. The copper center was observed as a dark hole where the cobalt center was observed as a bright spot. In both molecules the geometric height was the same, however, the electronic behavior of the metal centers were different. Hipps et al. attributed this to the fact that the highest occupied molecular orbital (HOMO) and the lowest unoccupied molecular orbital (LUMO) of the copper were 1 eV away from the Fermi energy, thus decreasing the probability of the resonant tunneling.

Resonant tunneling was also observed by Tao et al., who have shown with an electrochemical STM that there was an increase in the apparent height contrast in the center of iron containing protoporphyrins vs. protoporphyrins without a metal center. At low and high biases, the centers of the two protoporphyrins appear to have the same height. At intermediate biases, the iron containing protoporphyrin appears as a bright spot. The height of this bright spot reached a maximum when the bias of the substrate was close in energy to that of the LUMO of the iron.

Electronic measurements have been performed on a variety of SAMs as well as using apparent height contrast to study variations in molecular conductance. Bard

measured peak shaped I-V curves in phenylene ethynylene oligomers (OPEs) using a tuning fork STM.[43,44] Gorman et al. have studied I-V behavior in patterned, electroactive SAMs using the STM.[38] Weiss et al. inserted individual OPEs into an insulating n-alkanethiolate SAM background and determined that these molecules were more conductive than the background.[45-48] By visualizing individual molecules over time, they also observed changes in conductance over time. These variations in conductance (stochastic switching) were attributed to conformational variations in the molecules rather than the electrostatic effects of charge transfer. Similar stochastic switching behaviors have been observed by Lindsay et al.[54] on carotenoid molecules with a gold nanoparticle on top[50,53] and by Gorman et al. on ferrocenyl-terminated alkanethiols inserted into an n-alkanethiolate SAM.[56] Although these approaches utilizing scanning probe microscopy address several important aspects of molecular contacts, they still leave important issues such as structure-property relationships largely open. The STM allows the investigation of the ordering of molecules on a surface as well as their electronic properties in a straight forward and reproducible way.

1.2.3 The influence of metallic junctions on the electronic behavior of a molecule

Metallic contacts have been shown to influence the electronic structure of the molecule between them. A recent report by Nazin et al. illustrated how the electronic structure of a molecule evolves as it comes in contact with larger and larger metal bridges (Figure 1.2.8).[57]

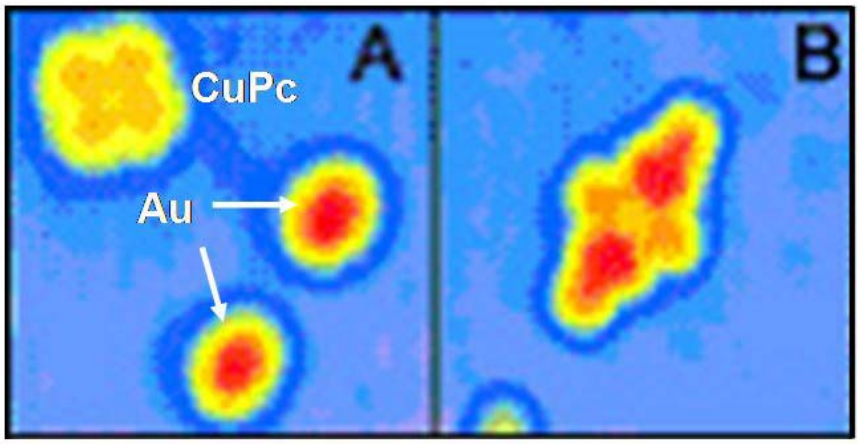

Figure 1.2.8 CuPc@2Au$_3$ hybrid structures A) Bare 2Au$_3$ junctions before the CuPc molecule was added (imaging conditions: V_{bias} = 1 V, I = 1 nA; image size is 47 Å by 47 Å). B) Assembled hybrid structures (V_{bias} = 0.5V, I = 1 nA). (Reproduced from Figure 1 in reference 57)

Nanostructures were assembled on a NiAl(110) surface by thermally evaporating single Au atoms and copper phthalocyanine (CuPc) molecules onto the surface. A low temperature ultra high vacuum STM was used to make nanostructures composed of a CuPc molecule bonded to chains of various numbers of gold atoms. When the STM tip was close enough to the surface it could be employed to pull the Au atoms along the direction of the moving tip. In this way, chains of gold atoms were built along Ni troughs. The authors made two chains of gold atoms separated by 5 Ni-Ni lattice constants (Figure 1.2.8a) and then moved a CuPc molecule into the space between them (Figure 1.2.8b). dI/dV curves taken over the center of the CuPc molecule showed peaks. The peaks in the dI/dV curves that were ascribed to the CuPc were shifted and split when it was contacted to two Au atoms, When more Au atoms were added on to each chain the molecular peaks did not shift further. dI/dV taken over the Au atoms also showed peaks but in different positions compared to the CuPc. The dI/dV curves taken over the last Au atom in the chain

showed peaks that shifted to higher energies when they were compared to peaks observed in dI/dV curves of Au chains that are not in contact with a CuPc molecule. The molecular states of the Au atom that were in direct contact with the molecule were shifted out of resonance with the rest of the Au chain, meaning that there was no peak observed in the dI/dV curve. The Au atoms in contact with the molecule can now be considered to be part of an extended CuPc molecule. From these data, it was illustrated to what extent the degree of coupling between the CuPc and the various Au chains could vary. This variation in coupling will have an important role on the conductivity that will be measured across these junctions. Thus, from a chemist's perspective, metal-molecule-metal junctions should be regarded as extended molecular systems, and the nature and type of the contact is going to be a dominant factor in the rational design of molecular-scale devices.

The effects a of contact to a molecule have also been illustrated by Kubatkin et al. in which electronic transport was measured at 4 K through a single para-phenylene vinylene oligomer deposited into a small (2 nm) gap on a semi-conducting substrate that acted as a gate electrode (Figure 1.2.9).[58] The gate voltage (V_g) of the single electron transistor (SET) was changed in small steps from – 4.3 V to + 4.3 V. Source- drain I-V measurements were taken at each step. Eight different open states in the molecule were probed and the energies of these electronic states were strongly perturbed when compared to those obtained from measurements on the molecule in solution. It was suggested that image charges in the source and drain electrodes could account for this perturbation. This again, shows that the contact between a molecule and a metal is not just a simple

connection. There are many other factors involved when electronic behaviors are investigated.

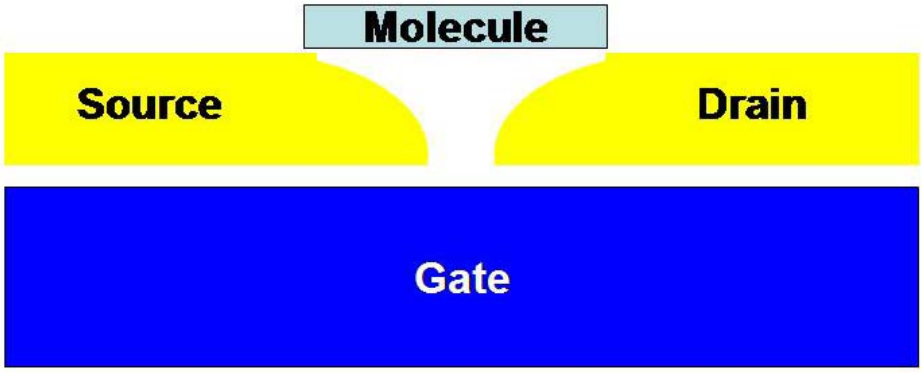

Figure 1.2.9 Schematic of a molecule deposited in a 2 nm gap on a semi conducting surface

1.2.4 Structure - Electronic Property Relationships

A second key issue in molecular electronics is relating an electronic behavior to the structure of the molecule(s) being probed. Chemists have always sought to systematically vary properties with structure to illustrate an optimal molecular structure for a given behavior. However, molecular electronics is still a very young field and establishing structure-electronic property relationships has a vital role. Systematically varying molecular propertied can help support the hypothesis that the behavior under observation is influenced by the structure of the molecule and thus, the behavior is attributable to the molecule. As discussed above the issue of how the molecule is contacted plays an important role in the electronic behavior. However, if the method of contact is the same for all molecules studied, then conclusions can be made concerning structure property relationships.

If one wants to think of a molecule as an analog to a wire, then the issue of conductance though a molecule is of extreme importance. A number of papers have

reported the systematic study of conductance of molecules of various lengths. These studies almost always took place on simple n-alkanethiolate SAMs[45,52] or on SAMs composed of various conjugated or aromatic molecules.[20,21,25,44,46,47,50,54,59-67] They have established that as the conductance varied with molecular length, this variation scaled with the relative rate of discrete electron transfer (e.g. the electron transfer coefficient β for a given molecular architecture was $-\ln k_{et} = \beta r$ where r is the distance between a donor and acceptor group, k_{et} is the rate of electron transfer rate).

The value of β depends strongly on the electronic structure of the molecule. β-values have been calculated by using several different measuring techniques for different molecular archetechtures. Slowinski et al. used alkanethiol SAMs sandwiched between two mercury electrodes to measure tunneling current across the junctions.[28] They determined a value for β of 0.8 $Å^{-1}$ for SAMs of alkanethiols. As discussed previously Holmlin et al have used a similar mercury junction to systematically study electron transport through thin organic films of a series of molecules with different structures.[26,34]

A few groups have used SPM to probe tunneling across molecules in thin organic films. For example, Fan et al. have examined the electrical properties of SAMs of thiolates or OPEs on Au by using shear force-based scanning probe microscopy combined with current-voltage (I-V) and current-distance (I-d) measurements.[44] The I-V curves of hexadecanethiol in the low bias regime were symmetric around 0 V and the current increased exponentially as the bias was increased. Reversible peak-shaped I-V characteristics were obtained for most of the

nitro-based OPE SAMs and were different from the hexadecanethiol indicating that part of the conduction mechanism of these junctions involved resonant tunneling. Current was found to decrease with increasing distance, z, between the tip and substrate. From these I-V and I-z curves the attenuation factor β could be determined. The β of hexadecanethiolate SAM ranged from 1.3 to 1.4 $Å^{-1}$, and was nearly independent of the tip bias. The β -values for nitro-based molecules were lower and depended strongly on the tip bias, ranging from 0.15 $Å^{-1}$ for tetranitro oligo(phenylene ethynylene) thiol, to 0.50 $Å^{-1}$ for dinitro oligo(phenylene) thiol, at a -3.0 V tip bias. Both the beta values of these nitro-based SAMs were also strongly dependent on the structures of the molecules, e.g. the number of electroactive substituent groups on the central benzene, the backbone, the head group, and the end group. It is important to point out that Fan's β is different than the β discussed above. The β observed by Holmlin and Slowinski was derived from plotting current density vs. SAMs composed of molecules of different chain lengths. Fan et al. measured the tunneling current as it was brought into contact with a SAM. Therefore the β they calculate is based on the current recorded over one type of SAM and Holmlin and Slowinski's β is determined from the tunneling current through molecules with the same structure but increasing chain length and the distance between the molecules and the metal junction is always the same.

Conductance in a molecule is not just a result of molecular length or conjugation, another behavior of note is that of Kondo resonance. In general, the Kondo effect involves the coupling between an unpaired electron localized on an impurity and the surrounding delocalized electrons in a metal. The coupling leads to

screening of the localized electron's spin by the delocalized electrons with opposite spin, so that a spin-zero singlet is formed below the Kondo temperature. The phenomenon of Kondo resonance has been exploited in two key papers that credibly related a unique structural feature of a given molecule to an electronic behavior that relies on that feature. In the Kondo effect, the spin state of an "impurity" (here, a molecule) in a wire affects its conductance. Liang et al. displayed Kondo resonance in a single molecule transistor using a single divanadium molecule that could be tuned by changing the gate voltage to alter the spin and charge state of the molecule.[68] A sharp peak in the dI/dV curve was observed when the molecules were set to a S = ½ spin state. The peak was not observed when S = 0.

Another feature of the Kondo resonance is the splitting of peaks in the dI/dV curves for S = ½ by an applied magnetic field. Park et al. have reported Kondo resonance by changing the degree of coupling of a $Co^{2+,3+}$ ion to the electrodes.[69] The $Co^{2+,3+}$ is bonded in an octahedral environment to two terpyridinyl linker molecules with thiol end groups and placed between gold electrodes in a break junction. A peak in the dI/dV curves was observed in the Co^{2+} complex, which was split by applying a magnetic field. Thus, by selecting molecules that could exist in different spin states under the influence of different gate voltages, a link between a molecular property and an electronic property of those molecules in a junction could be established.

Most recently, Mayor et al. have documented how electronic transport through a molecule is affected by its structure.[70] Mechanical break junctions containing two bis-9,10-phenyl-ethynylanthracene molecules were compared in

which the position of the thiol anchor group was varied from para to meta (Figure 1.2.10). The lack of a fully conjugated pathway in the meta-linked molecule significantly reduced the electronic communication between the metal electrodes

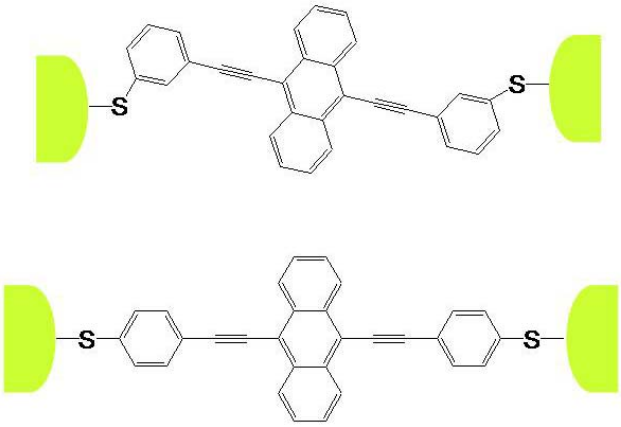

Figure 1.2.10 Cartoon of molecules containing a bis-9,10-phenyl-ethynylanthracene core with thiol linker in the meta (top) and para (bottom) position inserted into a break junction

and the molecule when compared to analogous data obtained with the molecule linked via thiol groups in para position. Specifically, the immobilization of the molecule with the thiol linker in the meta position afforded I-V curves with currents that were almost two orders of magnitude smaller than the values measured for the molecule in the para position. The curves were noisy so I-V curves were measured on the meta-linked molecule at 30 K. At this temperature the meta linked molecule showed step like features in the current, which were attributed to resonant tunneling through the highest occupied molecular orbital of the molecule. The dominating current path seemed to be through the Au - S - C bonds (and not by direct injection from the metal to the pi system of the molecule). Also, at 30 K the reproducibility of the I-V curves seems to be improved because the molecule is electronically less

coupled to the disordered electrodes. The appearance of highly symmetric I-V curves indicates that both contacts are the same.

There are many challenges that need to be addressed before a viable molecular device can be fabricated. The work presented here is revealing as to how the structure of a molecule relates to its electronic properties and how the binding of molecules to bulk metal electrodes influences their electronic properties. These results provide an intriguing step in the evolution of this field.

1.3 Scope

This dissertation will discuss issues related to determining structure property relationships that are relevant to molecular electronics. More specifically, an STM will be used to compare electronic measurements over insulating n-alkanethiolate SAMs and electroactive SAMs composed of ferrocenyl- terminated thiols and viologen terminated thiols, as well as multilayer SAMs created by alternating a metal dication and a thiolate. Chapter 2 will discuss the surface characterization of SAMs composed of ferrocenyl-terminated and viologen terminated thiols. I-V measurements on these SAMs will be discussed as they pertain to the non-linear current voltage behavior of negative differential resistance (NDR). A mechanism for the nature of NDR will be discussed as well as the need to understand how the junctions used to measure I-V curves influence NDR. Chapter 3 will show NDR in multilayer SAMs composed of dication metals and surface characterization of these systems. Chapter 4 will show stochastic variation in electroactive molecules inserted into an insulating n-alkanethiolate background SAM. In this chapter it will

also be shown that the electric field generated by the STM tip increases the rate of replacement of electroactive molecules in to the background SAM. In Chapter 5 the attenuation of the apparent tunneling barrier of ferrocenyl-terminated thiolates via non-covalent binding of β-cyclodextrin will be shown. This attenuation will be shown to influence the peak to valley ratio of NDR. Appendix 1 will describe the instrumentation used to measure the I-V behavior of the SAMs discussed in chapters 2 and 3 and 5

1.4 References

(1) Goldhaber, G., D.; Montemerlo, M. S.; Love, J. C.; Opiteck, G. J.; Ellenbogen, J. C. *Proc. IEEE* **1997**, *85*, 521.

(2) Moore, G. *IEDM Tech. Digest* **1975**, 11.

(3) Dunn, P. *Semiconductor Manufacturing* http://www.facsnet.org/tools/sci_tech/tech/fundaments/scale2.php3, 2000.

(4) Schulz, M. *Nature* **1999**, *399*, 729.

(5) Wong, H.-S. P.; Frank, D.; Solomon, P. M.; Wann, H.-J.; Welser, J. *Proc. IEEE* **1999**, *87*, 537.

(6) Frank, D.; Dennard, R.; Nowak, E.; Solomon, P. M.; Taur, Y.; Wong, H.-S. *Proc. IEEE* **2001**, *89*, 259.

(7) Packan, P. *Science* **1999**, *285*, 2079.

(8) Switzer, J. A.; Maune, B. M.; Raub, E. R.; Bohannan, E. W. *J. Phys. Chem. B* **1999**, *103*, 395.

(9) Wong, P. *IBM Jounal of Research and Development* **2002**, *46*, 133.

(10) Drexler, E. *Nanosystems: molecular machinery, manufacturing, and computation*; Wiley, 1992.

(11) Solomon, P. M. *IBM Jounal of Research and Development* **2002**, *46*, 119.

(12) Reed, M. A.; Tour, J. M. *Sci.Am.* **2000**, *282*, 86.

(13) Whitesides, G. M.; Bain, C. D. *Angew. Chem. Int. Ed. Engl.* **1989**, *28*, 506.

(14) Schreiber, F. *Prog. Surf. Sci.* **2000**, *65*, 151.

(15) Reichert, J.; Ochs, R.; Beckmann, D.; Weber, H. B.; Mayor, M.; von Lohneysen, H. *Phys. Rev. Lett.* **2002**, *88*, 01.

(16) Weber, H. B.; Reichert, J.; Weigend, F.; Ochs, R.; Beckmann, D.; Mayor, M.; Ahlrichs, R.; von Lohneysen, H. *Chem. Phys.* **2002**, *281*, 113.

(17) Mayor, M.; Weber, H. B. *Chimia* **2002**, *56*, 494.

(18) Weber, H. B.; Reichert, J.; Ochs, R.; Beckmann, D.; Mayor, M.; von Lohneysen, H. *Physica E* **2003**, *18*, 231.

(19) Kergueris, C.; Bourgoin, J. P.; Palacin, S.; Esteve, D.; Urbina, C.; Magoga, M.; Joachim, C. *Phys. Rev. B* **1999**, *59*, 12505.

(20) Reichert, J.; Weber, H. B.; Mayor, M.; von Lohneysen, H. *Appl. Phys. Lett.* **2003**, *82*, 4137.

(21) Reed, M. A.; Zhou, C.; Muller, C. J.; Burgin, T. P.; Tour, J. M. *Science* **1997**, *278*, 252.

(22) Xiao, X. Y.; Xu, B. Q.; Tao, N. J. *Nano Lett.* **2004**, *4*, 267.

(23) Haiss, W.; van Zalinge, H.; Higgins, S. J.; Bethell, D.; Hobenreich, H.; Schiffrin, D. J.; Nichols, R. J. *J. Am. Chem. Soc.* **2003**, *125*, 15294.

(24) Chen, J.; Reed, M. A.; Rawlett, A. M.; Tour, J. M. *Science* **1999**, *286*, 1550.

(25) Zhou, C.; Deshpande, M. R.; Reed, M. A.; Jones, L.; Tour, J. M. *Appl. Phys. Lett.* **1997**, *71*, 611.

(26) Holmlin, R. E.; Haag, R.; Chabinyc, M. L.; Ismagilov, R. F.; Cohen, A. E.; Terfort, A.; Rampi, M. A.; Whitesides, G. M. *J. Am. Chem. Soc.* **2001**, *123*, 5075.

(27) Holmlin, R. E.; Ismagilov, R. F.; Haag, R.; Mujica, V.; Ratner, M. A.; Rampi, M. A.; Whitesides, G. M. *Angew. Chem.-Int. Edit.* **2001**, *40*, 2316.

(28) Slowinski, K.; Majda, M. *J. Electroanal. Chem.* **2000**, *491*, 139.

(29) Slowinski, K.; Chamberlain, R. V.; Miller, C. J.; Majda, M. *J. Am. Chem. Soc.* **1997**, *119*, 11910.

(30) Slowinski, K.; Fong, H. K. Y.; Majda, M. *J. Am. Chem. Soc.* **1999**, *121*, 7257.

(31) Boussaad, S.; Xu, B. Q.; Nagahara, L. A.; Amlani, I.; Schmickler, W.; Tsui, R.; Tao, N. J. *J. Chem. Phys.* **2003**, *118*, 8891.

(32) Schmickler, W.; Rampi, M. A.; Tran, E.; Whitesides, G. M. *Faraday Discuss.* **2004**, *125*, 171.

(33) Ranganathan, S.; Steidel, I.; Anariba, F.; McCreery, R. L. *Nano Lett.* **2001**, *1*, 491.

(34) Holmlin, R. E.; Haag, R.; Chabinyc, M. L.; Ismagilov, R. F.; Cohen, A. E.; Terfort, A.; Rampi, M. A.; Whitesides, G. M. *J. Am. Chem. Soc.* **2002**, *124*, 8762.

(35) Chabinyc, M. L.; Chen, X. X.; Holmlin, R. E.; Jacobs, H. O.; Rampi, M. A.; Whitesides, G. M. *Abstr. Pap. Am. Chem. Soc.* **2001**, *221*, U308.

(36) Haag, R.; Rampi, M. A.; Holmlin, R. E.; Whitesides, G. M. *J. Am. Chem. Soc.* **1999**, *121*, 7895.

(37) Le, J. D.; He, H.; Hoye, T. R.; Mead, C. C.; Kiehl, R. A. *Appl. Phys. Lett.* **2003**, *83*, 5518.

(38) Gorman, C.; Carroll, R. L.; Fuierer, R. *Langmuir* **2001**, *17*, 6923.

(39) Deng, W. L.; Hipps, K. W. *J. Phys. Chem. B* **2003**, *107*, 10736.

(40) Hipps, K. W.; Barlow, D. E.; Mazur, U. *J. Phys. Chem. B* **2000**, *104*, 2444.

(41) Lu, X.; Hipps, K. W.; Wang, X. D.; Mazur, U. *J. Am. Chem. Soc.* **1996**, *118*, 7197.

(42) Lu, X.; Hipps, K. W. *J. Phys. Chem. B* **1997**, *101*, 5391.

(43) Fan, F. R. F.; Yang, J. P.; Dirk, S. M.; Price, D. W.; Kosynkin, D.; Tour, J. M.; Bard, A. J. *J. Am. Chem. Soc.* **2001**, *123*, 2454.

(44) Fan, F. R. F.; Yang, J. P.; Cai, L. T.; Price, D. W.; Dirk, S. M.; Kosynkin, D. V.; Yao, Y. X.; Rawlett, A. M.; Tour, J. M.; Bard, A. J. *J. Am. Chem. Soc.* **2002**, *124*, 5550.

(45) Bumm, L. A.; Arnold, J. J.; Dunbar, T. D.; Allara, D. L.; Weiss, P. S. *J. Phys. Chem. B* **1999**, *103*, 8122.

(46) Bumm, L. A.; Arnold, J. J.; Cygan, M. T.; Dunbar, T. D.; Burgin, T. P.; Jones, L.; Allara, D. L.; Tour, J. M.; Weiss, P. S. *Science* **1996**, *271*, 1705.

(47) Cygan, M. T.; Dunbar, T. D.; Arnold, J. J.; Bumm, L. A.; Shedlock, N. F.; Burgin, T. P.; Jones, L.; Allara, D. L.; Tour, J. M.; Weiss, P. S. *J. Am. Chem. Soc.* **1998**, *120*, 2721.

(48) Donhauser, Z. J.; Mantooth, B. A.; Kelly, K. F.; Bumm, L. A.; Monnell, J. D.; Stapleton, J. J.; Price, D. W.; Rawlett, A. M.; Allara, D. L.; Tour, J. M.; Weiss, P. S. *Science* **2001**, *292*, 2303.

(49) Gorman, C. B.; Carroll, R. L.; He, Y. F.; Tian, F.; Fuierer, R. *Langmuir* **2000**, *16*, 6312.

(50) Leatherman, G.; Durantini, E. N.; Gust, D.; Moore, T. A.; Moore, A. L.; Stone, S.; Zhou, Z.; Rez, P.; Liu, Y. Z.; Lindsay, S. M. *J. Phys. Chem. B* **1999**, *103*, 4006.

(51) Cui, X. D.; Primak, A.; Zarate, X.; Tomfohr, J.; Sankey, O. F.; Moore, A. L.; Moore, T. A.; Gust, D.; Harris, G.; Lindsay, S. M. *Science* **2001**, *294*, 571.

(52) Cui, X. D.; Zarate, X.; Tomfohr, J.; Sankey, O. F.; Primak, A.; Moore, A. L.; Moore, T. A.; Gust, D.; Harris, G.; Lindsay, S. M. *Nanotechnology* **2002**, *13*, 5.

(53) Ramachandran, G. K.; Hopson, T. J.; Rawlett, A. M.; Nagahara, L. A.; Primak, A.; Lindsay, S. M. *Science* **2003**, *300*, 1413.

(54) Ramachandran, G. K.; Tomfohr, J. K.; Li, J.; Sankey, O. F.; Zarate, X.; Primak, A.; Terazono, Y.; Moore, T. A.; Moore, A. L.; Gust, D.; Nagahara, L. A.; Lindsay, S. M. *J. Phys. Chem. B* **2003**, *107*, 6162.

(55) Hipps, K. W.; Lu, X.; Wang, X. D.; Mazur, U. *J. Phys. Chem.* **1996**, *100*, 11207.

(56) Wassel, R. A.; Fuierer, R. R.; Kim, N. J.; Gorman, C. B. *Nano Lett.* **2003**, *3*, 1617.

(57) Nazin, G. V.; Qiu, X. H.; Ho, W. *Science* **2003**, *302*, 77.

(58) Kubatkin, S.; Danilov, A.; Hjort, M.; Cornil, J.; Bredas, J. L.; Stuhr-Hansen, N.; Hedegard, P.; Bjornholm, T. *Nature* **2003**, *425*, 698.

(59) Samanta, M. P.; Tian, W.; Datta, S.; Henderson, J. I.; Kubiak, C. P. *Phys. Rev. B* **1996**, *53*, R7626.

(60) Magoga, M.; Joachim, C. *Phys. Rev. B* **1997**, *56*, 4722.

(61) Langlais, V. J.; Schlittler, R. R.; Tang, H.; Gourdon, A.; Joachim, C.; Gimzewski, J. K. *Phys. Rev. Lett.* **1999**, *83*, 2809.

(62) Ishida, T.; Mizutani, W.; Akiba, U.; Umemura, K.; Inoue, A.; Choi, N.; Fujihira, M.; Tokumoto, H. *J. Phys. Chem. B* **1999**, *103*, 1686.

(63) Ishida, T.; Mizutani, W.; Choi, N.; Akiba, U.; Fujihira, M.; Tokumoto, H. *J. Phys. Chem. B* **2000**, *104*, 11680.

(64) Ishida, T.; Mizutani, W.; Aya, Y.; Ogiso, H.; Sasaki, S.; Tokumoto, H. *J. Phys. Chem. B* **2002**, *106*, 5886.

(65) Howell, S.; Kuila, D.; Kasibhatla, B.; Kubiak, C. P.; Janes, D.; Reifenberger, R. *Langmuir* **2002**, *18*, 5120.

(66) Kushmerick, J. G.; Holt, D. B.; Yang, J. C.; Naciri, J.; Moore, M. H.; Shashidhar, R. *Phys. Rev. Lett.* **2002**, *89*, 086802.

(67) Stapleton, J. J.; Harder, P.; Daniel, T. A.; Reinard, M. D.; Yao, Y. X.; Price, D. W.; Tour, J. M.; Allara, D. L. *Langmuir* **2003**, *19*, 8245.

(68) Liang, W. J.; Shores, M. P.; Bockrath, M.; Long, J. R.; Park, H. *Nature* **2002**, *417*, 725.

(69) Park, J.; Pasupathy, A. N.; Goldsmith, J. I.; Chang, C.; Yaish, Y.; Petta, J. R.; Rinkoski, M.; Sethna, J. P.; Abruna, H. D.; McEuen, P. L.; Ralph, D. C. *Nature* **2002**, *417*, 722.

(70) Mayor, M.; Weber, H. B.; Reichert, J.; Elbing, M.; von Hanisch, C.; Beckmann, D.; Fischer, M. *Angew. Chem.-Int. Edit.* **2003**, *42*, 5834.

Chapter 2

Negative differential resistance in electroactive monolayers.

2.1 Introduction

Metal–molecule–metal junctions exhibiting nonlinear current - voltage properties are currently the subject of several research efforts, due to their proposed use as elements in molecule-scale electronic components.[1-43] The interpretation of experiments used to evaluate the electronic behavior of metal molecule junctions was very difficult and could lead to misleading conclusions.[44] Several factors need to be taken into account when trying to understand-metal-molecule metal junctions. First, metal – molecule - junctions, as discussed in Chapter 1, should be considered extended molecular systems where the nature of the junction plays a role in the electronic behavior. Second, if an electronic behavior can be ascribed to a specific molecular feature then the behavior should be general enough to test on other molecules that have similar features. Third, if the electronic behavior was observed in other, more traditional electronic devices, than the molecular behavior should be able to be modified in a similar way to that of the traditional electronic devices. This chapter will address each of these three points to provide evidence of an electronic behavior that can be ascribed to a specific molecular feature.

Negative differential resistance (NDR) is a non-linear current – voltage behavior that is of interest because it could serve as a nanoscale analogue to conventional multistate electronic swiches.[2,3,5,45] NDR is characterized by a decreasing current with increasing voltage (Figure 2.1.1).[16] Gorman group has observed NDR in electroactive self assembled monolayers (SAMs).[16]

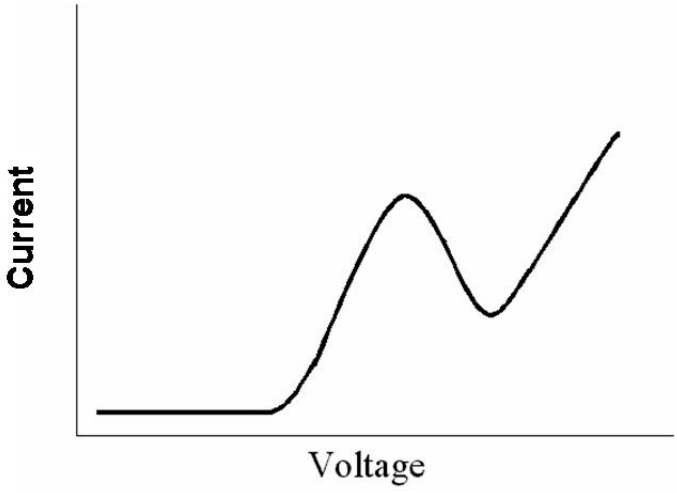

Figure 2.1.1 Characteristic I –V curve exhibiting negative differential resistance. NDR is characterized by a decreasing current with increasing voltage

There are several mechanisms that can cause NDR. Resonant tunneling is a mechanism for molecular systems the exhibit NDR. In traditional semiconductor technology a resonant tunneling diode is a device that shows NDR. This diode consists of a quantum well separated from two electrical contacts by two tunnel barriers. RTDs are of interest because they offer the potential to integrate multi-state logic into computing architectures.[33,46-48] From the standpoint of a basic logic operation a simple system can exist in either an "on" or "off" state (i.e. perform a "Yes" or "No" function). A multi-state device could be capable of existing in more than just an "on" or "off" state. A system like this could be capable of performing much more complicated logic functions with fewer components such as AND, OR, XOR and XNOR.[48] A molecular multi-state device has the potential for implementing more complex logic functions with fewer components than today's current transistor technology.

For traditional devices, the quantum well is composed of a narrow layer of material characterized by accessible quantized states (as in the well/barrier system GaAs/AlGaAs).[49] In resonant tunneling, the tunnel barriers control the probability of electrons moving from one electrode to the other through the quantum well. The energy of the quantum states in the potential well on the island can be adjusted relative to the energy bands in the source and drain (Figure 2.1.2). Increasing the applied bias progressively lowers the energy (depending on the polarity) of all the states in the well relative to the source. When the bias is sufficient to move the energy of an unoccupied quantum state within the range of the energy of the source, current flows and the well is said to be "on". Otherwise the current through the device is blocked or out of resonance and the well is said to be "off". In an analogous molecular device, electroactive molecules appear to serve a similar role via accessible energy levels for electron tunneling. Molecular systems that show NDR and resonant tunneling are of great interest as components of molecular versions of RTDs.[16]

In RTDs, the magnitude of the NDR current peak, directly related to the resonant tunneling probability, is affected by the height and width of the barriers on each side of the well.[50-53] Tunability for conventional RTDs suggests that NDR behavior in molecular-scale systems should also exhibit predictable changes based on tunnel barrier modifications. Boulas et al. have shown that organic SAMs have tunneling barrier heights that are very close the theoretical tunneling limit.[1] They have shown that the conductivity by direct electron tunneling is completely suppressed by monolayers that are ~2 nm thick. Beebe

et al. have shown that the height of the barrier to charge transport in metal – molecule – metal junctions based on aliphatic SAMs decreases with increasing metal work function.[3] Appenzeller et al. have compared carbon nanotube FETs (CNFETs) to p-type MOSFETs. They found the that the CNFETs performed similarly to conventional MOSFETs however the electrical characteristics observed in the CNFET were controlled by schottky barriers in the source drain region instead of the nanotube itself.[52] These studies suggest that molecule-based tunnel barriers can be constructed in a rational manner.[1,3,52]

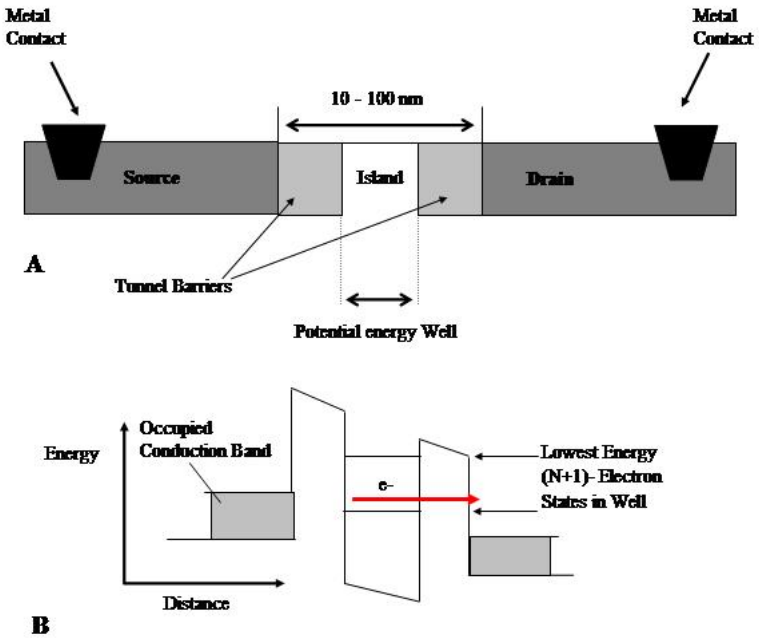

Figure 2.1.2 Typical diagram of a RTD. The energy of states in the potential well on the island can be adjusted to the energy of the bands in the source and drain. B) Increasing the bias lowers the energy of all the states in the well relative to the source. When the bias is low enough that the energy of an unoccupied quantum state is within range of energies of the source the device is in resonance and electrons will flow.

Negative differential resistance has been observed in many types of molecules.[5,7,8,12,16,21,31,32,34,38,42,43,54-61] One of the first examples of NDR was

demonstrated by Reed and Tour. The observed NDR in a phenyl ethynyl molecule sandwiched between two gold electrodes at 60 K with a peak to valley ratio of >1000:1 (Figure 2.1.3).[7,8] The peak to valley ratio (PVR) is the ratio between the maximum current value of NDR and the minimum value of NDR (i.e. the minimum current after the peak). If one considers the NDR maximum as the "on" state and the minimum as the "off" state a large peak to valley ratio is desired because the larger the ratio, the more well defined these two states would be, and the less one has to worry about noise in the system. So far large PVR (1000:1) can only be achieved at very low temperatures.

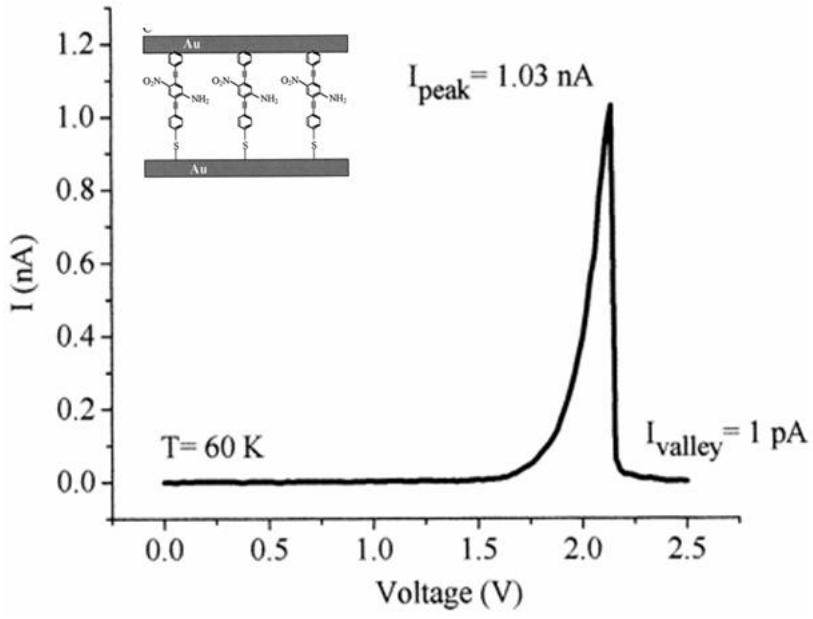

Figure 2.1.3 I(V) characteristics of a Au-(2'-amino-4-ethynylphenyl-4'-ethynylphenyl-5'-nitro-1-benzenethiolate)-Au device at 60 K with a the PVR is 1030:1. The Inset is a scheme of the Au-SAM-Au junction.

The nature of molecular NDR is debatable and there are most likely different mechanisms for different molecules. For example it has been proposed by Chen et al. that their phenylene ethynyene oligomers (OPEs) undergo a two-step reduction mechanism (Figure 2.1.4)[7]. Reducing this molecule would modify the charge transport through it. As the potential is increased, the molecule undergoes a one-electron reduction to form the radical anion, supplying a charge carrier. (Figure 2.1.4 B). As the bias continues to increase, the molecule undergoes another reduction to form the dianion (Figure 2.1.4 C). The dianion is an insulating state, blocking the flow of electrons. Ab initio calculations were used to model the resonant behavior of the molecule when an external voltage was applied. The findings were in agreement with the proposed mechanism.[62,63]

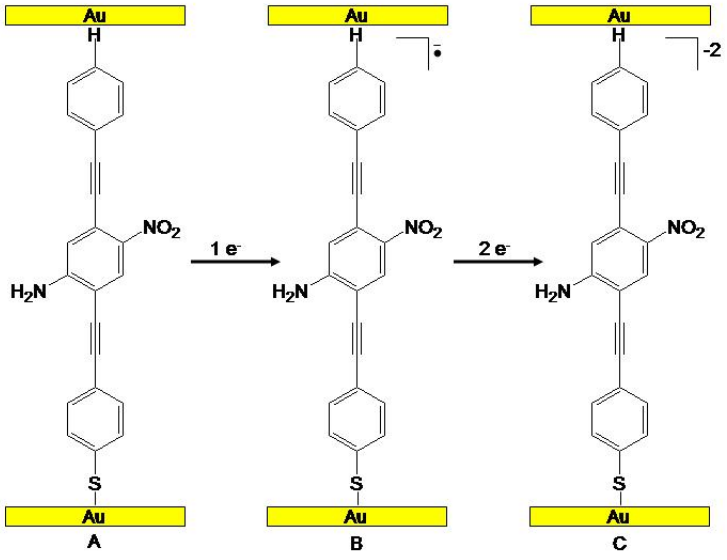

Figure 2.1.4 Two step reduction mechanism in a phenylene ethynyene oligomer In a metal molecule metal junction.

Several other mechanisms have been proposed for molecular NDR in OPEs.[12,64,65] They are based upon charging of the molecules, which results in

changes in the structure of the lowest unoccupied molecular orbital (LUMO). Conformational changes in the molecule have also been proposed. These conformational changes would modulate the current based on changes in the extended π-overlap. As the voltage is increased, the molecules in discrete nanodomains would enter into differing electronic states. On the other hand it has been pointed out that molecular-based switching might not be an inherently molecular phenomenon. Switching might result from surface bonding rearrangements that are molecule/metal contact in origin (i.e., a sulfur atom changing its hybridization state such as subangstrom shifts between different Au surface atom bonding modes or molecular tilting).[57,66]

NDR was observed in junctions where the molecules were removed. Tour et al. have observed NDR in nanocell experiments Figure (2.1.5) with and without OPEs present and suggested that the NDR was due to electromigration of the deposited gold.[67]

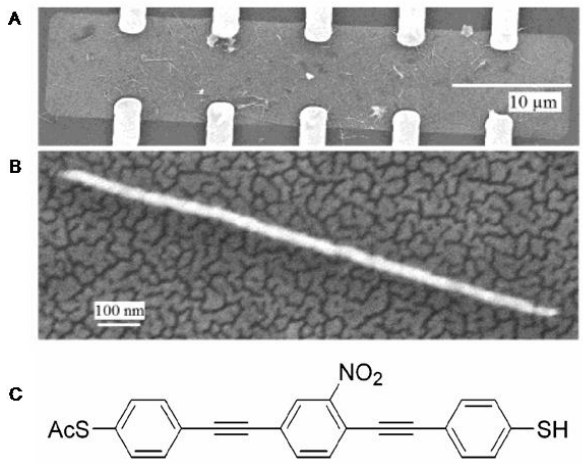

Figure 2.1.5 SEM image of the NanoCell after assembly of the Au nanowires and the molecule (C). A) five pairs of fabricated leads across the NanoCell, and some Au nanowires are barely visible on the internal rectangle of the discontinuous Au film. B) is a higher magnification of the NanoCell's central portion showing the disordered discontinuous Au film with an attached Au nanowire, which is attached via the OPE-dithiol (C). (Reproduced from Figure 1 in reference 67)

The NDR observed was due to the formation of metal filaments between the two metal contacts as the bias was swept. The effect of the electric field on the broken filaments (or on contacts that very close to each other) can cause the formation of bridges between the separated metal junctions through small filaments or clusters of gold atoms that give rise to electronic behaviors such as NDR.[44] Basically, as the bias is swept, the filaments form and then at a higher voltage the filaments break causing a decrease in the current. This work shows that electrically active molecules can behave in very different ways depending on how the metal - molecule junctions are formed.

The Gorman group has previously shown that negative differential resistance (NDR) can be observed in electroactive SAMs via scanning tunneling microscopy.[16] A different mechanism for NDR was given other than that of Tour's OPEs. A qualitative model for the mechanism of NDR in a STM tip / molecule / substrate tunnel junction is shown in Figure 2.1.6. In describing this molecular junction and the proposed resonant tunneling model, an electroactive molecule is placed between an atomically sharp Pt-Ir tip and a gold substrate. In this kind of system molecular orbitals act like the quantum well in a traditional RTD. The two tunnel junctions are created between the tip and the molecule and between the molecule and the substrate. It is important to note that, in this model, the tip is considered to be atomically sharp and is assumed to have a reduced local density of states (LDOS).

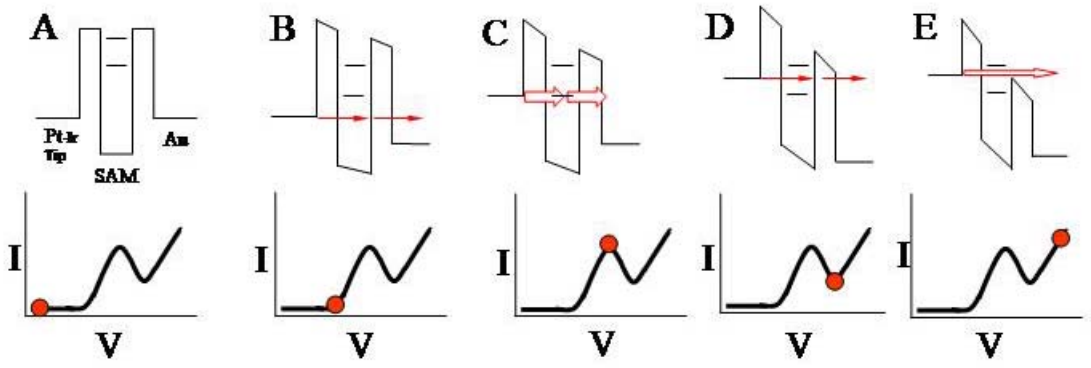

Figure 2.1.6 Qualitative model for the attenuation of NDR peak current by modification of the STM tip/ferrocenyl tunnel junction. (A) Schematics of the two junctions and energy level diagrams indicating the two junctions (B) at zero applied bias, (C) in resonance with the molecular orbital (MO) associated with the ferrocenyl headgroups,(D) out of resonance with the MO associated with the ferrocenyl headgroups, and (E) exhibiting an increase in non-resonant current.

It has been proposed that if there is a tunneling barrier between two parts of the conducting system, and there are narrow features in the density of states in the energy range of interest, then NDR is likely to occur.[42] Schematics of a double barrier junction and energy level diagrams indicating the two junctions at zero applied bias are shown in Figure 2.1.6A. At low bias the Fermi energies of the tip and substrate are lower than the energies of the discrete molecular orbitals (MO) of a molecule. As an increasing negative potential is applied to the Pt-Ir tip the Fermi energy of the tip moves closer in energy to the MO. A narrow local density of states (LDOS) allows for an overlap with the MO, increasing the probability of tunneling through the barrier (Figure 2.1.6B). A maximum in this probability is reached when the Fermi level of the tip is aligned with a MO in the molecule. The Fermi energy is said to be in resonance with the molecular orbital associated with the molecule (Figure 2.1.6C). As the Fermi energy of the tip continues to increase, it moves out of resonance with the MO (Figure 2.1.6D) and the current

decreases until the potential is so large that it over comes one of the barriers and the system exhibits an increase in non-resonant current (Figure 2.1.6E).

If molecular NDR is indeed related to a molecular feature (ie the molecule has accessible molecular states) then it should be a general phenomenon that can be observed any molecule that has accessible molecular states. This chapter will deal with understanding molecular NDR by systematically varying the components that are required to see resonant tunneling NDR (i.e. the type of junction used, the tunneling barrier and the molecular architecture). First understanding how metal – molecule - junctions that are formed when molecules are placed in between two macroscopic metal contacts affect NDR. Second, if NDR is due to resonant tunneling between accessible molecular orbitals in an electroactive molecule. Resonant tunneling is general enough phenomenon to be able to test on other electroactive molecules. Third, NDR can be attenuated in traditional semiconductor devices by changing the tunneling barrier. Therefore it should be possible to change the tunneling junction in analogous molecular systems. This chapter will address each of these three points to provide evidence of an electronic behavior that can be ascribed to a specific molecular feature.

2.1.1 Exploring Non-linear I-V Behavior in Metal / Molecule / Metal Junctions

Scanning tunneling microscopy (STM) is one approach for accessing single molecules or a small number of molecules on a surface. With an atomically sharp metal tip held precisely over a surface at a constant bias, the topography of the surface is sensed by a number of tunneling electrons that flows

between the surface and the tip. By rastering the tip across the surface, an image is created that is a convolution of electronic properties and surface features of the substrate. This image allows one to be able to differentiate between regions that have different conductivities as well as regions that are of different physical height. The use of the STM enables controlled two terminal measurements to be performed without greatly perturbing the chemical environment. The STM provides a stable system for studying metal-molecule-metal junctions. The development of the STM has allowed new experimental approaches for demonstrating and probing electron transport through individual molecules. [30]

As has been shown by Gorman et al., NDR can be observed in an electroactive $FcC_{11}S$- SAM (Figure 2.1.7) and on a galvinol terminated alkanethiolate SAM at room temperature.[16] In non electroactive n-alkanethiolate SAMs NDR was not observed. The position of the NDR peak varies within each data set. The distribution of peak positions can be fit to a Gaussian curve to determine an average peak position. It has been hypothesized that if NDR is due to tunneling through accessible molecular orbitals, then the NDR peak position should shift in molecules with different redox potentials. Gorman group have explored whether the NDR peak potential can be correlated to the redox potential of the molecule. It has been estimated that the Fermi energy of a $FcC_{11}SH$ lies just above the Fermi energies of the Pt-Ir STM tip and the Au substrate (Figure 2.1.8). The Fermi energy of the ferrocenyl moiety has been estimated at -4.8 eV vs vacuum.[68,69]

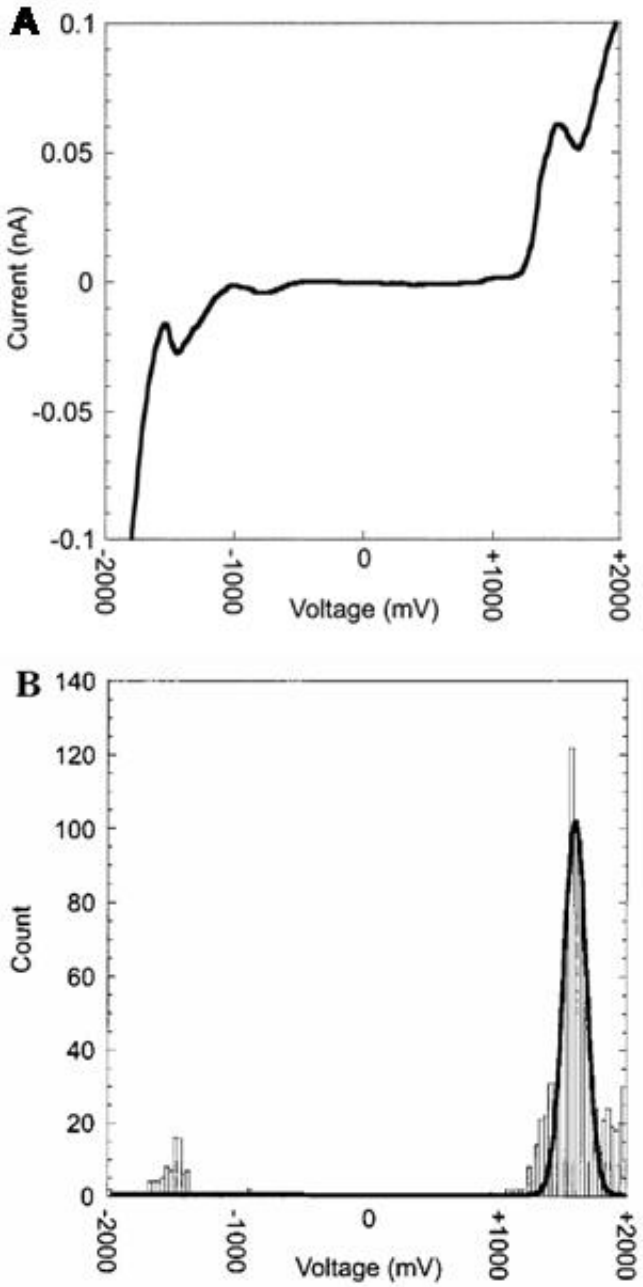

Figure 2.1.7 A) Graph of a typical I-V curve collected from the Fc-C11S- SAM under dodecane during CITS, B) Histogram representing the position of NDR (Gaussian Fit) in the $FcC_{11}S$-SAM under dodecane (Reproduced from Figure 1 in reference 16)

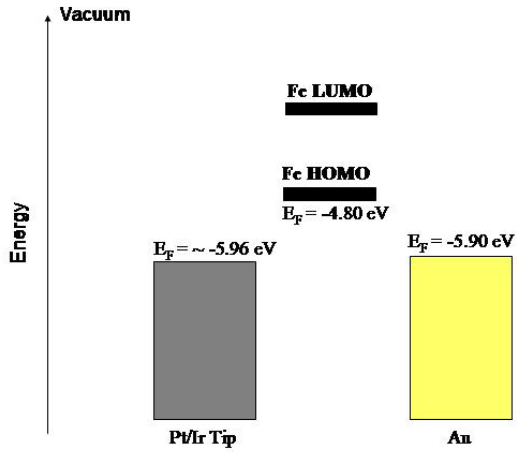

Figure 2.1.8 Fermi levels of Pt/Ir tip and Au vs $FcC_{11}S$-SAM

The Gorman group found that, after fitting the NDR position for different electroactive molecules to a histogram, they could not see a clear trend in the histogram peak position. There are many factors that can contribute to this variability particularly; variation in the tip, not only from tip to tip, but the shape of the tip can also change between I-V measurements thus changing the tunnel junction. Second, there is also variation between monolayers which will affect the chemical environment the tip senses.

Control of the parameters governing NDR behavior in molecular systems is just beginning to be explored experimentally[3,70-72] and theoretically.[2,70,73-75] NDR behavior in conventional semiconductor-based resonant tunneling diodes (RTDs) has been tuned by modifying the materials, dopant concentration, and the physical configuration of the device.[49-53] Recent scanning probe microscopy studies have described the use of electroactive moieties in molecular junctions to facilitate the appearance of nonlinear current–voltage behavior.[5,73,76] Several

reports have examined the relationship between NDR and electroactivity in organic[5,76,77] and inorganic systems.[5,78]

Many questions still remain about the nature of NDR in this system. NDR is clearly observed only in electroactive molecules and not in non-electroactive molecules. However, the influence the type of junction has on the NDR is still unclear. This chapter will discuss basic characterization of electroactive SAMs and experiments where the type of junction is changed. This chapter will also explore how the negative differential resistance (NDR) peak current observed in redox active self-assembled monolayer-based molecular junctions varies with the redox potential of the molecule.

2.2 Results and Discussion

2.2.1 Surface Characterization of Electroactive SAMs

Before performing STM measurements on SAMs composed of different electroactive molecules they were characterized by cyclic voltammetry (CV). CV was performed with the goal of 1) confirming the different redox potentials of the electroactive SAMs and 2) calculating the surface coverage of the SAMs. Figure 2.2.1 shows typical cyclic voltammograms for $FcC_{11}S$-SAM, $FcCOC_{10}S$-SAM and $MVC_{10}S$-SAM. Table 2.2.1 shows the redox potentials, $E_{p1/2,}$ the peak splitting and the calculated surface coverage for the ferrocene terminated thiol ($FcC_{11}S$) (Table 2.2.1A), ferrocene ketone thiol ($FcCOC_{10}S$-) (Table 2.2.1B) and viologen terminated thiol ($MVC_{11}S$-) (Table 2.2.1C).

Table 2.2.1

	Molecule	E_{pc} (mV)	E_{pa} (mV)	$E_{p1/2}$ (mv)	Peak Splitting	Surface Coverage (Moles/cm^2)
A		283	351	317	68	~5 x 10^{-10}
B		562	576	569	14	~1.5 x 10^{-9}
C	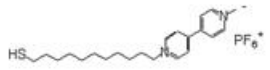	-426	-395	411	31	~5 x 10^{-10}

Molecules studied A) $FcC_{11}SH$, B) $FcCOC_{10}SH$ C) $ViologenC_{11}SH$, D) HSC_8FcC_8HS. E_{pc} = potential at which the peak cathodic current occurs, E_{pa} = potential at which the peak anodic current occurs, $E_{p1/2}$ = potential halfway between E_{pc} and E_{pa}. Peak splitting was the difference between E_{pc} and $E_{pa.}$, Surface coverage (Moles/cm^2)

The $FcC_{11}S$- SAM had a $E_{1/2}$ of 317 mV, the $FcCOC_{10}S$- had a $E_{1/2}$ of 569 mV and the $MVC_{11}S$- had and $E_{1/2}$ of -411 mV. The surface coverage (Γ) of the monolayers can be calculated from the equation:

$$\Gamma = \frac{Q}{nFA}$$

Where Q is the charge in coulombs (C), n is the number of electrons transferred, F is faradays constant $\left(\frac{96500\ C}{mol \bullet e^-}\right)$ and A is the electrode area in cm^2 (in this case .32 cm^2). The charge is calculated by integrating the redox peaks in the CV. The surface coverage for an n-alkanethiolate SAM has been reported to be 9.3 x

10^{-10} mol/cm^2.[79] The calculated surface coverage of $FcC_{11}S$- SAM was ~5 x 10^{-10} moles/ cm^2, for $FcCOC_{10}S$- SAM the surface coverage was ~1.5 x 10^{-9} moles/ cm^2 and for the $MVC_{11}S$- the surface coverage was ~5 x 10^{-10} moles/ cm^2. The surface coverage for the Fc and MV SAMs were comparable to literature values.[80-82]

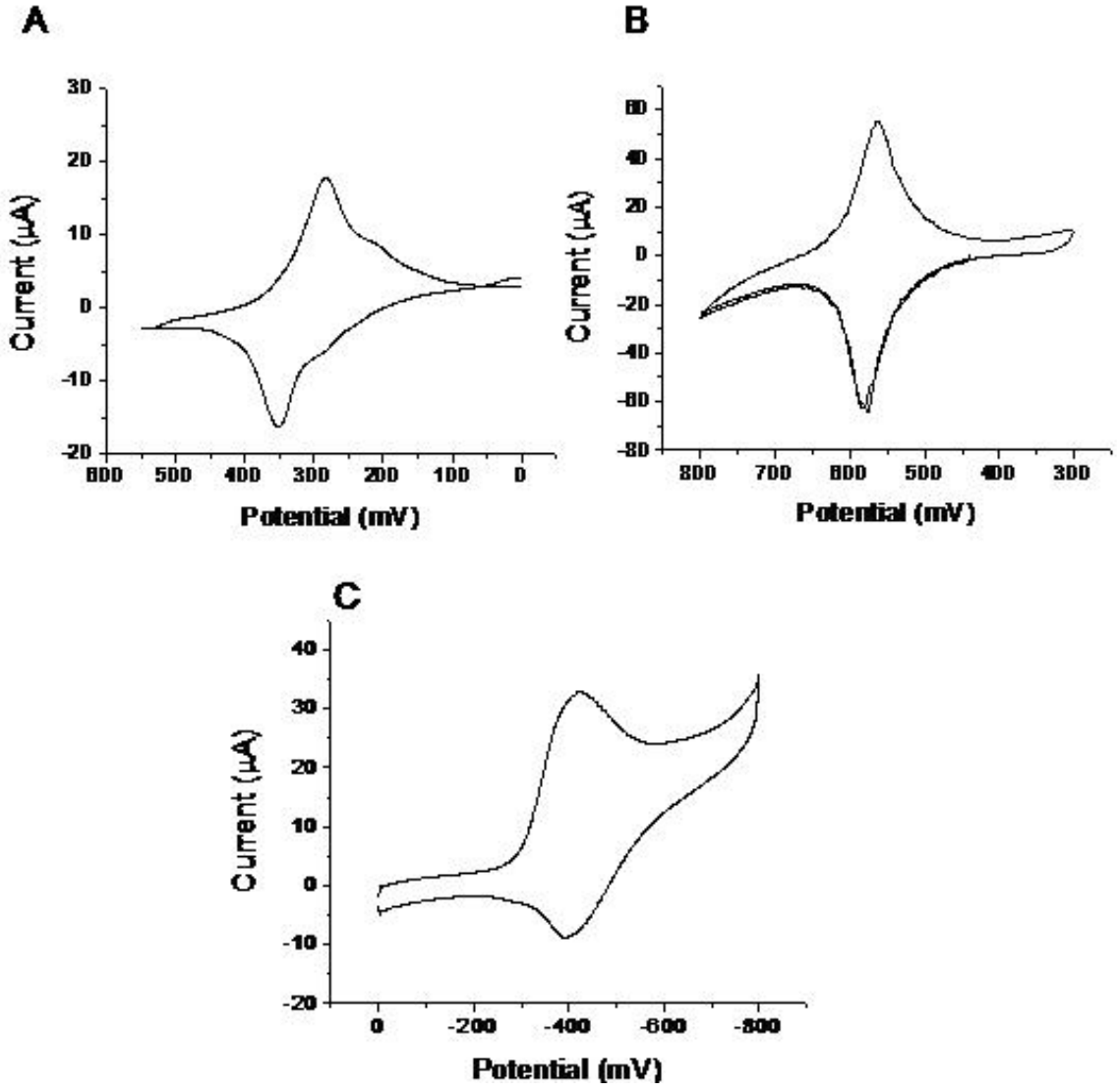

Figure 2.2.1 CV's of A $FcC_{11}S$-SAM, B) $FcCOC_{10}S$-SAM and C) Viologen terminated SAM. Both Fc SAMs were scanned in 1M $HClO_4$ at 100 mV/s with a Ag/AgCl reference. The viologen terminated SAM was scanned in .1M Na_2SO_4 purged in N_2 for 30 min at 200 mV/s with a Ag/AgCl reference.

The lower surface of these electroactive SAMs is due to a higher degree of disorder compared to a n-alkanethiolate SAM. The disorder is due to the mismatch between the sizes of the bulky electroactive head groups and the polymethylene chain.[82] The surface coverage for the $FcCOC_{10}S$- SAM was larger than the other electroactive SAMs by a factor of 3. It is unclear why the coverage is higher than that of the $FcC_{11}S$-SAM. The presence of the carbonyl should not influence the packing density that much. While more investigation was needed it was decided to move on and study current – voltage properties with STM.

2.2.2 Metal / Molecule / Metal Junctions

2.2.2a STM tip / Molecule / Gold Substrate Junctions

Current – voltage (I-V) curves were taken using a Digital Instruments Nanoscope E scanning tunneling microscope. Imaging was done at a bias of 1 V and a setpoint of 10 pA under a low dielectric solvent (dodecane).[83] Dodecane allows one to collect images and I-V curves with very small leakage currents (~2-3 pA @1V). SAMs of $FcC_{11}S$- , $FcCOC_{10}S$-, and $MVC_{11}S$- were formed on Au(111) substrates (see experimental).

It was hypothesized that the position of NDR could be related to the redox potential of the electroactive molecules. NDR in iso-structural ferrocene terminated thiols ($FcC_{11}S$- vs $FcCOC_{10}S$-) as well as a Viologen terminated thiol (MV-$C_{10}S$-) were looked at extensively (Figure 2.2.2). Iso-structural molecules allows one to vary the redox potential while maintaining a similar molecular

architecture and packing in the SAM. MV-C_{10}S- was chosen because it had a redox potential completely different from that of the ferrocene terminated SAMs.

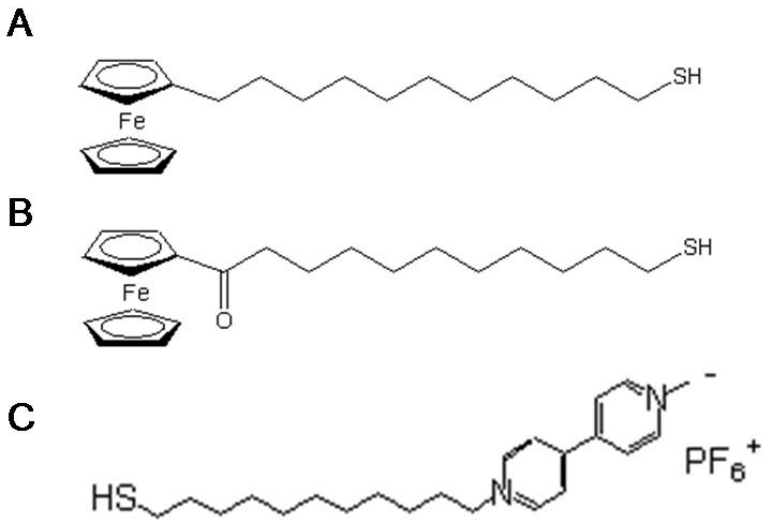

Figure 2.2.2 A) structure of $FcC_{11}SH$, B) structure of $FcCOC_{10}SH$, C) structure of $MVC_{11}SH$

Various experiments were attempted to try to reduce variability in the histogram peak position. The first attempt was to expose a $FcC_{11}S$- SAM to a solution of decanethiol with the hope that as it adsorbed into the $FcC_{11}S$- monolayer it would force the $FcC_{11}S$- to adopt a more rigid conformation and thus decrease variability in the monolayer. While backfilling the $FcC_{11}S$-SAM with dodecanethiol did increase order in the SAM, the variability in the average peak position did not change.[58] Reducing the surface free energy of the Pt Ir tip by coating it with 2,2,2-trifluoroethanethiol was attempted. This molecule was chosen because its short chain would not greatly affect the tunnel junction and because the fluorines give the molecule a low surface free energy. It was thought that by coating the tip, a more homogeneous junction for tunneling could

be provided. Surface contamination on the tip could change the Fermi energy. By coating the tip with a low surface energy molecule the tip could be less prone to contamination and the Fermi energy will be more consistent. However is was shown that it did not reduce the variability in the average peak potential.[58] It was concluded there was too much variability in the data sets for any kind of conclusion to be drawn. This variability seems to be an innate property of the electronic measurements.

Representative curves of $FcC_{11}S$-SAM , $FcCOC_{10}S$-SAM, and $MVC_{11}S$-SAM are shown in Figure 2.2.3. NDR peaks are observed at both negative and positive potentials (see appendix 1 for a discussion of how the I-V curves were collected). The NDR seen in the positive region on the $FcCOC_{10}S$-SAM have a much lower maximum peak current that the other two types of SAMs. The reason for the apparent lower peak current is still being investigated. As can be observed in these curves, there is variation in the position of the peak potential. This variation in peak position has been documented previously.[7,8,16,22,54,57] There are different explanations for this variation. These include surface features such as terraces and pits can influence the I-V curve because when the tip comes back to the pre-selected spot to perform an I-V measurement, the position of the tip over the SAM would not be the same as when the height was recorded due to drift in the piezo material. Thus, the tip could be over an area with a completely different surface topography. Since tunneling current has an exponential relationship with distance, any change in the height when the tip goes out of feedback will result in non-ideal I-V curves (curves showing current

saturation or no current at all). The electroactive molecules have bulky head groups which will lead more disordered SAM than SAMs formed from n-alkanethiolates. Also, the $MVC_{11}S$- is charged leading to repulsion of the head groups which results in a lower packing density. A disordered SAM will increase the degrees of freedom of the molecule. This increase in freedom allows the molecules to rotate and twist more freely. This motion can cause the electroactive head groups to move and to flop over on the surface, changing the structure of the SAM. The STM tip senses different chemical environments due to the increased motion of the molecule. During electron transfer, the electrons could tunnel from the electroactive head group down the through the alkane chain, or if the molecule is leaning over, the electrons could hop from the head group straight to the substrate or it could hop from head group to head group before tunneling to the gold electrode. Adsorbates on the tip could also cause variability in I-V behavior. The shape of the tip can also cause variation from sample to sample, and is considered to be important if NDR is expected to be observed via a resonant tunneling mechanism.

To maintain some amount of consistency between data sets, only tips that could achieve molecular resolution on a $C_{12}S$- SAM were used. Molecular resolution was the best way to determine if the tip was atomically sharp and therefore suitable for collecting I-V curves. Once molecular resolution was achieved, the tip was retracted and the sample was exchanged with a $FcC_{11}S$-SAM and I-V collection was begun.

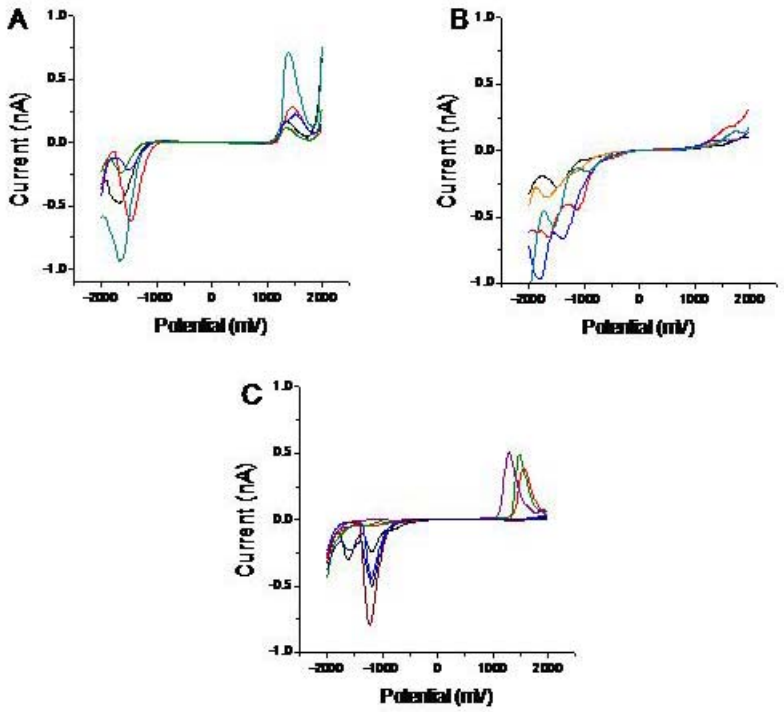

Figure 2.2.3 Representative I-V curves of A) $FcC_{11}S$-SAM, B) $FcCOC_{10}S$-SAM and C) Viologen terminated SAM.

The NDR peak positions for >1000 curves were plotted as a histogram. Figure 2.2.4 shows representative histograms of the various electroactive molecules. The $FcC_{11}S$- SAM for example shows a peak distribution of about 1000 mV for both the negative and positive peaks and with an average peak position of -1636 mV and 1547 mV at the center of the Gaussian fit. This average peak position is highly variable and it is impossible to ascribe any average peak potential for each different molecule. Gorman group members have spent a large amount of time trying to determine whether the average peak position changed with the different redox active molecules. It was concluded that the average peak position changed too much in each sample and from sample to

sample to be able to tell the difference between the NDR behavior in the different SAM based junctions.[58]

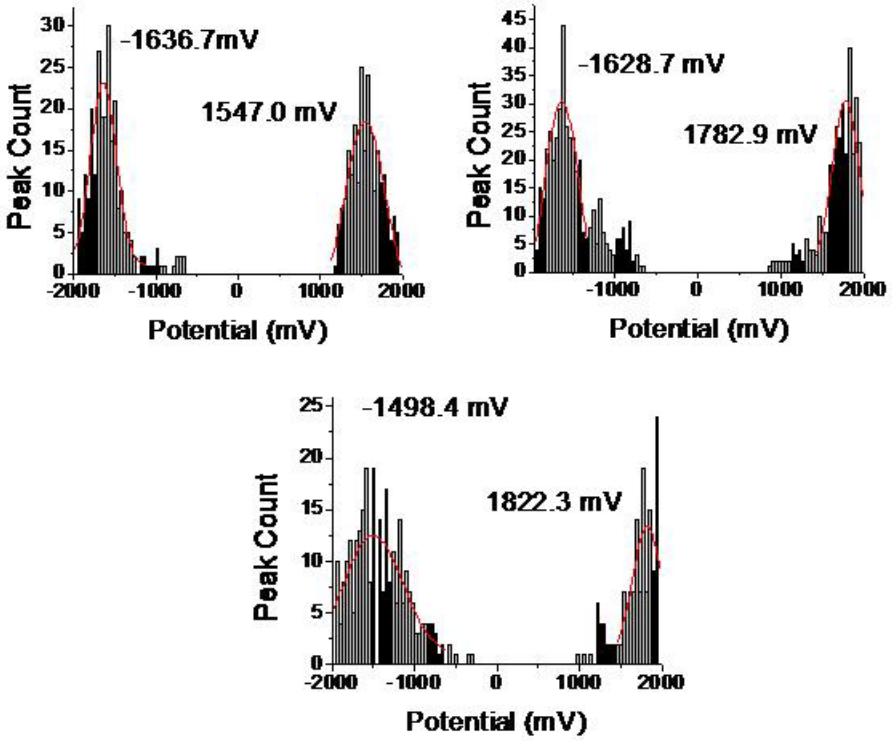

Figure 2.2.4 Representative Histograms of NDR peak positions of A) $FcC_{11}S$-SAM, B) $FcCOC_{10}S$-SAM and C) Viologen terminated SAM. Histograms were fit using a Gaussian model

I-V curves taken over a Fc-C_{11}S-SAM were directly compared to an insulating C_{12}S-SAM by employing replacement lithography. Briefly, replacement lithography involves using an STM to locally remove one type of thiolate and replace it with another type of thiolate from solution to produce nanometer scale patters. Figure 2.2.5 shows a scheme of how replacement lithography works. An n-alkanethiolate monolayer is imaged at a bias of 1 V and a setpoint of 10 pA to find an area suitable for replacement, typically 400 nm x 400 nm or greater was preferred (Figure 2.2.5A). Dodecane was used as the solvent for the

replacement thiol. Desorption of the n-alkanethiolate was induced by increasing the bias to ca. 3.2 volts (Figure 2.2.5B). As the thiolate is removed from the surface the desired replacement thiol that is in the dodecane replaces into the freshly exposed gold surface (Figure 2.2.5C).

Figure 2.2.6 shows an image of $FcC_{11}S$- replaced into a $C_{12}S$- SAM. A lithographic writing program was used to control the tip speed, direction and bias to write the desired Fc pattered. In this case the letters 'F' and 'c' were replaced in to the background SAM to designate the replacement of ferrocene. As can be observed in Figure 2.2.6A the replaced Fc terminated alkanethiol shows an increased apparent height contrast compared to the background SAM, at 1.5 V, even though the two molecules are roughly the same height. As the bias was lowered to 100 mV the height contrast was also lowered until the height of the background SAM appears to be the same height as the $FcC_{11}S$- (Figure 2.2.6C). Bias dependent height contrast was a phenomenon that has been studied previously by our group and others.[16,17,22,84]

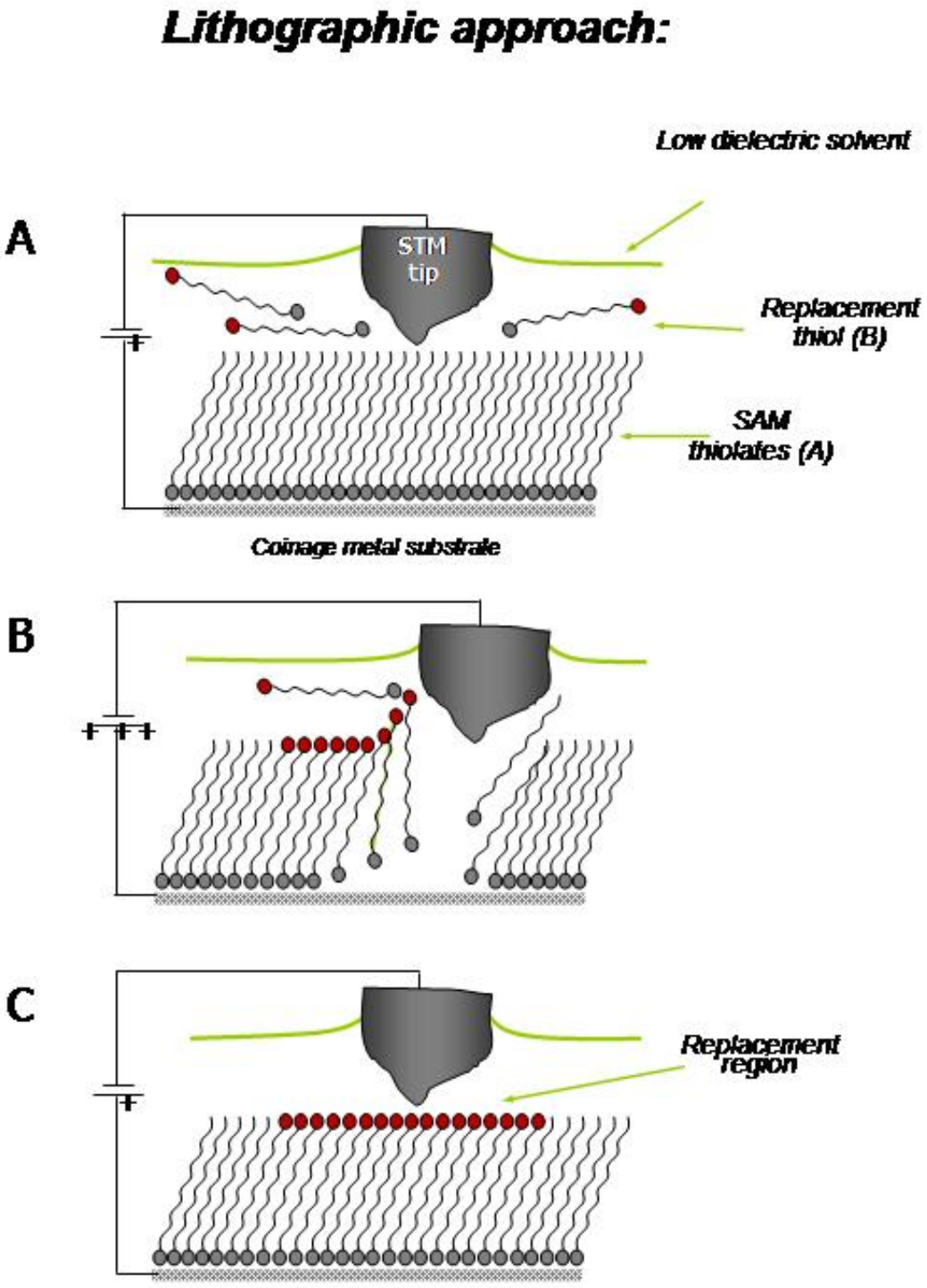

Figure 2.2.5 Schematic of replacement lithography. A) SAM imaged at non-perturbative imaging bias to locate an area free from defects and substrate facet terraces suitable for patterning. B) Upon an increase in substrate bias, the SAM thiolates are desorbed in proximity of the tip, resulting in the removal of the SAM. The replacementmolecules in solution assemble in to the freshly exposed regions of the gold. C) The pattern was assessed under imaging bias.

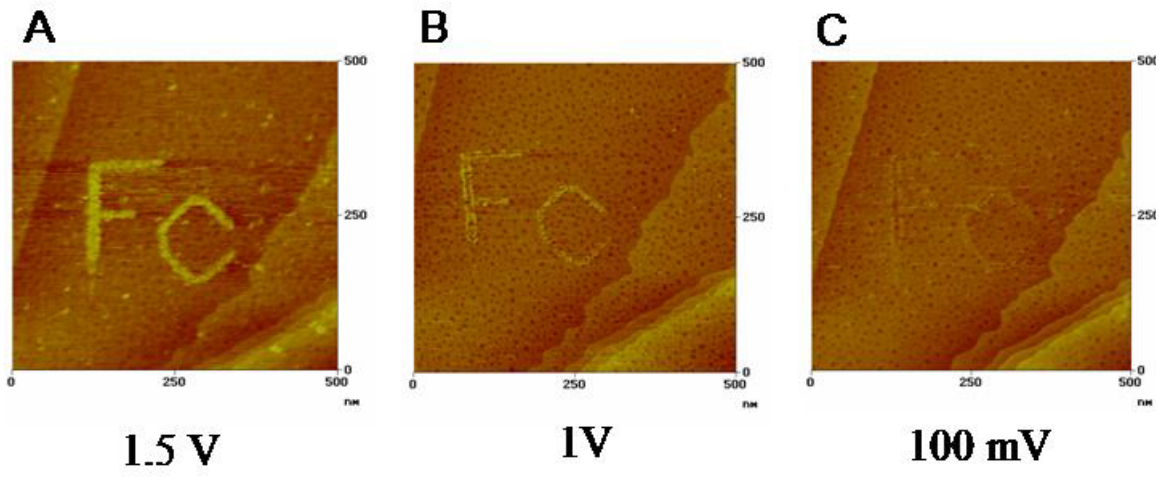

Figure 2.2.6 Replacement of $FcC_{11}S$- in to a $C_{12}S$- background SAM at A) 1.5 V, B) 1.0 V and C)100 mV (500nm x 500 nm)

The increase in height contrast with increasing bias was due to an increase in conductance of the ferrocenyl head group putatively via resonant tunneling. We have proposed that this phenomenon was due to resonant tunneling similar to that explained in Figure 2.1.3.[16] Visual observation of resonant tunneling in electroactive SAMs is valuable because it lends credence claim that NDR is a molecular feature. Replacement lithography allows one to compare two different molecular architectures directly.

For the purpose of collecting I-V curves a square was replaced into the flat area of the background SAM by reducing the scan area to 300 nm x 300 nm (Figure 2.2.7A) and increasing the bias to 3.3 volts. This bias was maintained for the duration of one full scan and then a 700 nm x 700 nm image was collected at 1.2 V (Figure 2.2.7B).

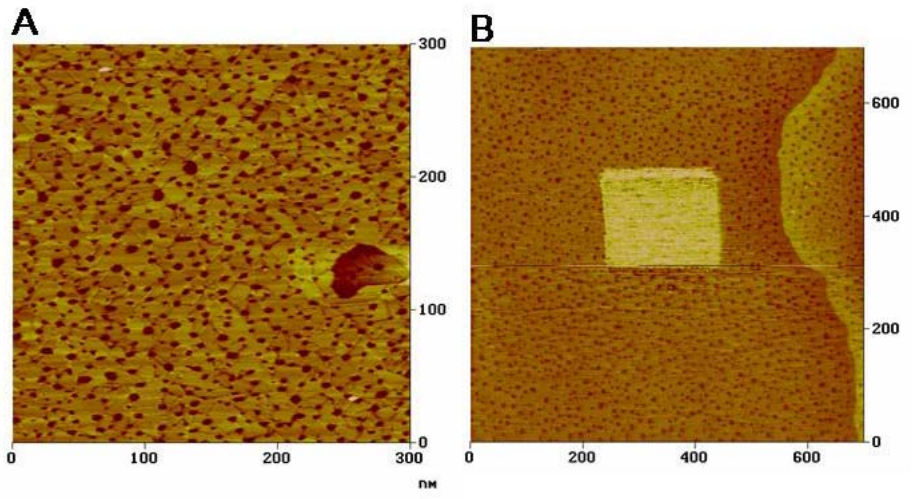

Figure 2.2.7 A) $C_{12}S$- SAM 300 nm x 300 nm @ 1.0 V 10 pA B) $FcC_{11}SH$ replaced into $C_{12}D$ SAM 700 nm x 700 nm @ 1.2 V 10 pA

It has been observed by the Gorman group that if the $FcC_{11}S$- in the dodecane solution was left in the cell for long periods of time it will adventitiously replace into the background SAM. Adventitious replacement, to put it simply, is when the solvated molecule inserts into defect sites in the SAM such as domain boundaries, step edges and pits. Adventitious replacement can cause problems when trying to accurately compare I-V curves in the background SAM to the electroactive SAM. $FcC_{11}S$- can also adsorb onto the tip, which in turn could increase the variability in I-V curves. Pulsing the tip at high bias usually ca. 5.0 V can remove these adsorbed molecules but the molecules not desorbed from the tip at the potential range that I-V curves are collected at (-2.0 V to 2.0 V). The solution to these problems was to replace the dodecane solvent in the cell with fresh dodecane. This step provides some technical problems of its own because, in order to replace the solvent, the tip has to be retracted. Retracting the tip moves it in such a way that when the tip approaches again the area being

scanned can be hundreds to thousands of nanometers away from where the $FcC_{11}SAc$- was replaced into the background SAM. When performing the replacement, 5 squares were replaced in different areas at least 500 nm apart from each square. The tip was then retracted and the solvent was removed with a syringe with careful attention paid to not bumping any part of the tip or sample with the syringe. Clean dodecane was then added and then removed with a syringe and dodecane was added again. The tip was then approached to the sample and imaging was resumed

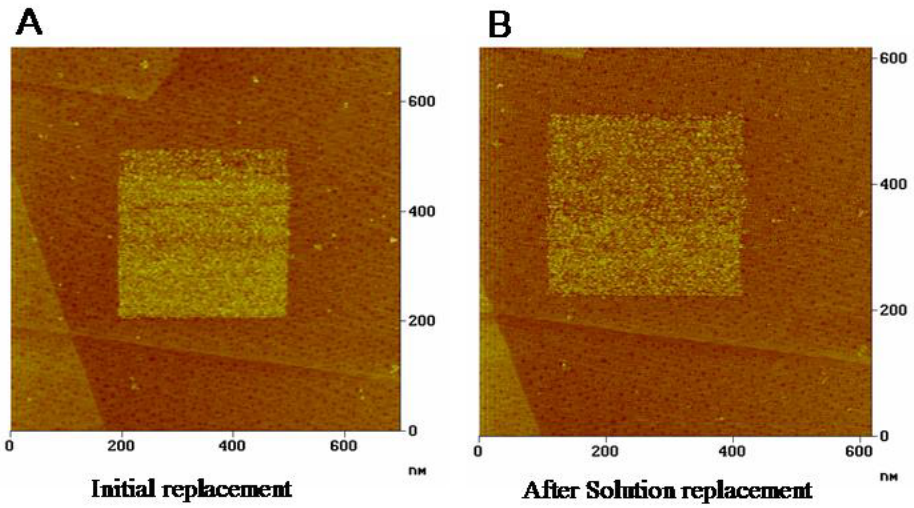

Figure 2.2.8 (A) replacement of $FcC_{11}S$- into $C_{12}S$- background SAM and (B) after dodecane solution was replaced with fresh dodecane

The scan area was then increased to cover a larger area while searching for a $FcC_{11}S$- square. It usually took anywhere from 10 minutes to 1.5 hours to find one of the replaced square. Figure 2.2.8A and B show a replaced pattern before and after rinsing with clean dodecane. This procedure is very complicated and very sensitive to error. However it is extremely effective in removing concerns

about collecting I-V curves over adventitiously replaced electroactive thiolates. Once the replace square is found CITS can be performed over it and the surrounding region for comparison.

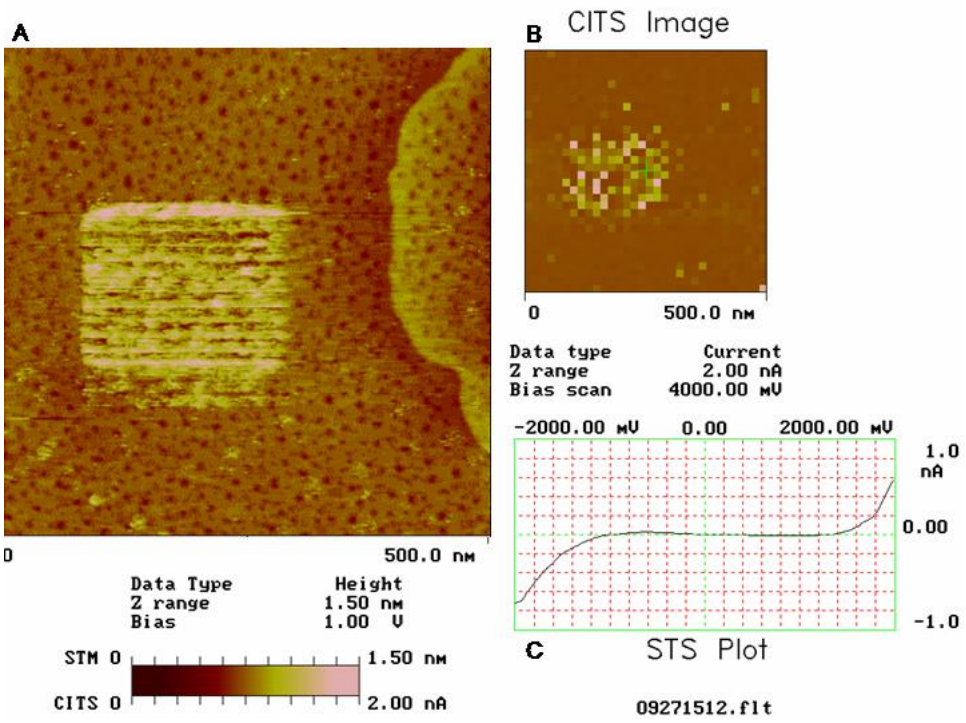

Figure 2.2.9 A) Image of $FcC_{11}S$- replaced into a $C_{12}S$- background SAM at 1.0 V B) CITS image of same region and C) STS plot showing one I-V curve

Figure 2.2.9 shows a typical screen shot of a CITS image of a replaced square and its surrounding background SAM. Figure 2.2.9A shows the topographical image and Figure 2.2.9B shows the CITS image; which displays the current response. The brighter the region, the higher the current response was observed in the CITS image at a given voltage. Figure 2.2.9C shows a typical I-V curve that does not display NDR. The area that has been replaced

with $FcC_{11}S$- shows a brighter region in the CITS image than that of the background $C_{12}S$-SAM.

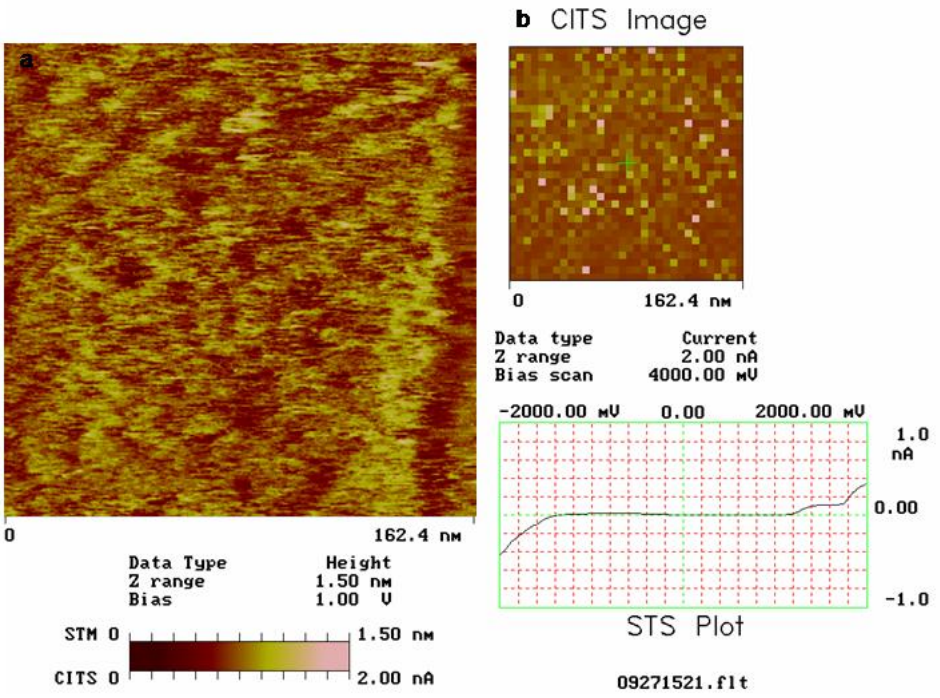

Figure 2.2.10 A) Image taken completely inside a $FcC_{11}S$- square that was replaced into a $C_{12}S$- background SAM B) CITS image of same region and C) STS plot showing one I-V curve

CITS measurements were then performed inside the replaced square to collect more data points over the $FcC_{11}S$-. Figure 2.2.10A shows a typical image of a pure $FcC_{11}S$- SAM which lacks any features in the image such as pits, and domain boundaries that one could attribute to an ordered monolayer. Figure 2.2.10B shows the corresponding CITS plot. These images were analyzed as previously described and the histograms were compared.[16]

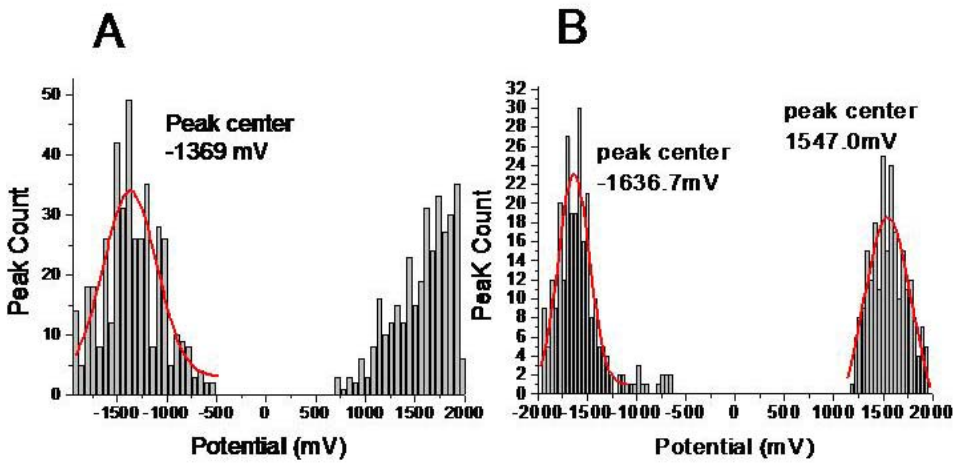

Figure 2.2.11 (A) Representative histograms of Fc square replaced into a C_{12}S- SAM (B) Histogram of FcC_{11}S- SAM Histograms were fit using a Gaussian Model

Figure 2.2.11A shows a typical histogram of curves collected in the replaced region. Histograms of the mono-component FcC_{11}S- SAMs (Figure 2.2.11B) were observed to be experimentally similar those of histograms of curves collected in the replaced FcC_{11}S-SAM region. Replacement of FcC_{11}S- into backround SAMs allows for direct comparison of electroactive and non electroactive molecules. This comparison showed that NDR is observed only in the electroactive SAMs and that the replaced SAMs exhibit the same variation as that of pure SAMs. Replacement lithography was an excellent way to evaluate molecular structure – electronic property relationships.

2.2.2b STM tip / Dithioate / Gold Substrate Junctions

As discussed in chapter 1 Haiss et al have demonstrated that current - distance (I-d) spectroscopy could be used to show that a unimolecular junction between a gold STM tip and a gold substrate could be formed. [20] It was

hypothesized that I-V measurements could be taken once these junctions were formed. These junctions were made with a dithiol covalently linked to a Au substrate and a Au STM tip. If the tip was not pulled back far enough to break the molecular contact it could be possible to measure a I-V curve through the molecule. It was further hypothesized that NDR could be observed in a Fc dithiol if connected to two gold electrodes. In this experiment a C_8 dithiol or $Fc(COC_5SH)_2$ (Figure 2.2.12) was deposited on a gold(111) surface, from a 50 μM solution. A low concentration of dithiol in soulution was shown to produce dithiolates that were lying down parallel to the surface.[20]

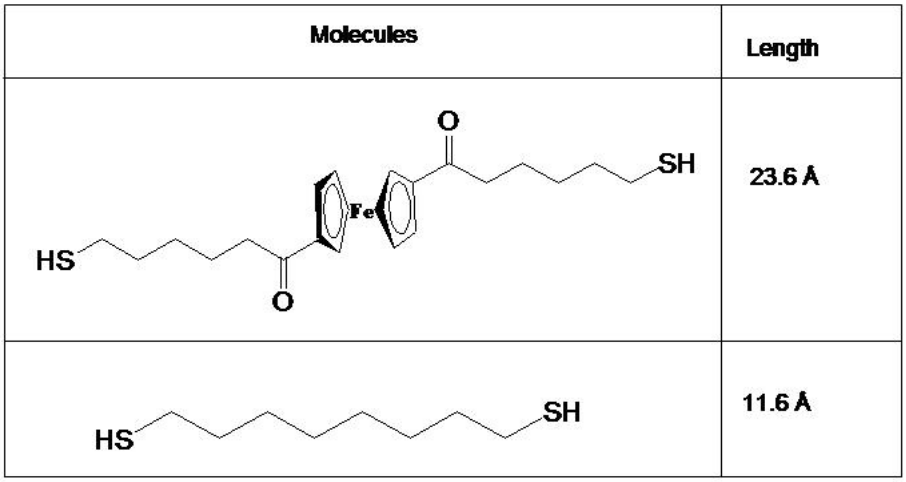

Figure 2.2.12 A) 1,1'-di(mercaptohexanoyl)Ferrocene, B) Octanedithiol Molecular lengths were calculated using Chem Draw software

Then a gold STM tip was brought close to the surface an then retracted a few nanometers. Curve 1 in Figure 2.2.13 shows a rapid exponential decrease in the current with distance. This was consistent with tunneling over a metal surface with out a molecule in the junction. Curve 2 shows a slower decrease in current with distance and a plateau region where the current was not dependent on

distance which was consistent with tunneling through the C_8dithiol.[20] This plateau region should be approximately the length of the molecule. The length can be calculated by subtracting the distance at which the plateau begins from the inflection point (I_s) in the exponential decrease of the curve after the end of the plateau region. The calculated length is 12.5 Å, which is similar to the calculated length of C_8 dithiol (11.6 Å).

I-z spectroscopy was then done with Fc-dithiol and similar results were obtained. Figure 2.2.14 shows a typical curve without a molecular contact (curve 1). After the contact a plateau region can be observed in curve 2 representing a contact to the Fc dithiol. There is more noise in the plateau region than observed in the C_8 dithiol. The current appears to increase as the tip is retracted in the plateau region and then decreases exponentially again. It is speculated that this increase in current is due to increased tunneling through the ferrocenyl moiety. The Fc dithiol was calculated to be approximately 12 Å longer than the C_8 dithiol. However, the length of the plateau region was calculated to be 14.3 Å. It is unclear as to why the plateau region is does not correspond to the calculated length better, further study is required.

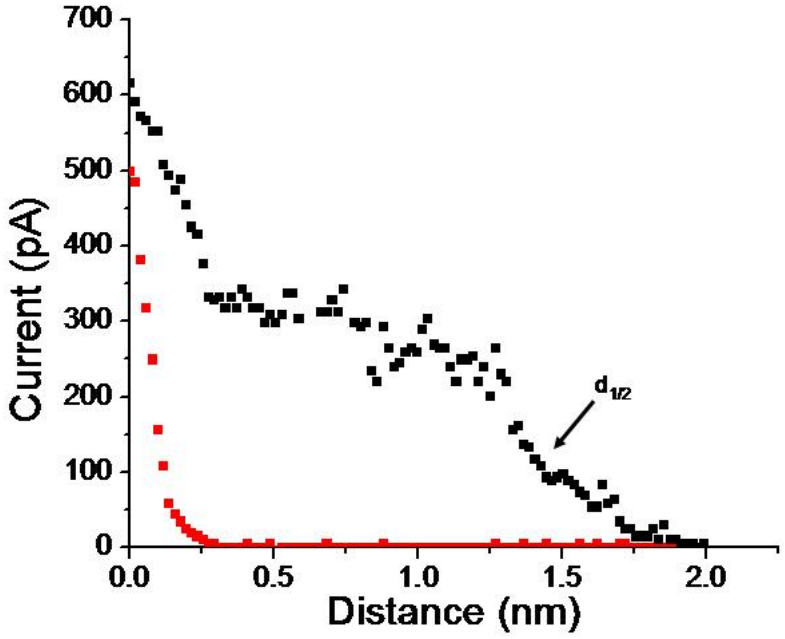

Figure 2.2.13 I-z curves over C_8dithiol. Curve 1 shows a rapid exponential decrease in the current with distance. Curve 2 shows a slower decrease in current with distance and a plateau region where the current was not dependent on distance which was consistent with tunneling through the C_8dithiol $d_{1/2}$ is the inflection point

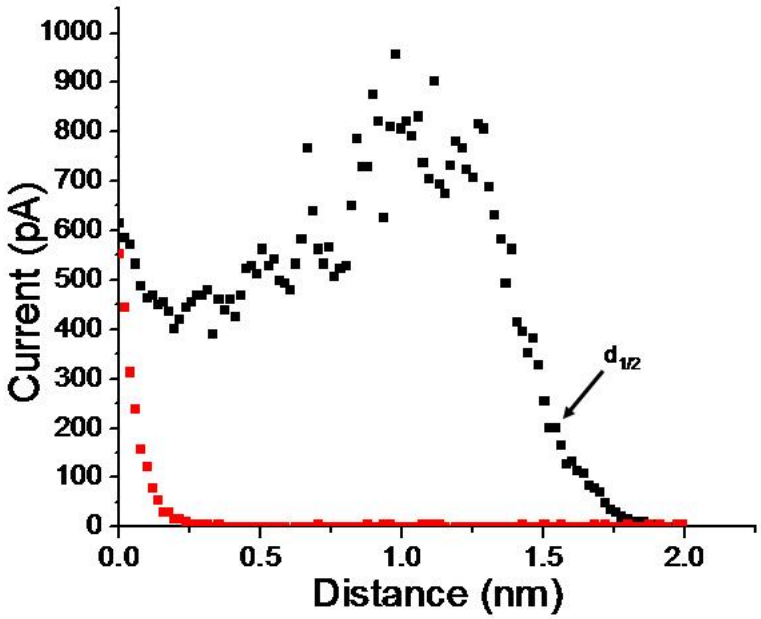

Figure 2.2.14 I-z curves of over bare gold (curve 1) and after the contact to Fc dithiol (curve 2) I_s is the inflection point

Immediately after a junction was shown by I-z measurements, I-V curves were taken. Figure 2.2.15 shows an I-V curve taken over bare metal (open circles) and one after a molecular junction with C_8 dithiol was formed (closed squares). An increase in the non linearity of the curve was consistent with tunneling through a molecular junction. Figure 2.2.16 shows I-V curves obtained on a Fc dithiol junction. Again the Fc dithiol I-V curve (closed black square) shows behavior consistent with tunneling through a molecule (i.e. an increase in the nonlinearity of the I-V curve). NDR like behavior is seen in both curves. It was unclear as to whether this NDR behavior is noise or due to resonant tunneling. A more intense peak is seen for the curve that has a Fc dithiol in the junction. Also note that NDR behavior is not seen in the C_8 dithiol junction nor in the I-V curve without a C_8 dithiol in the junction.

A closer examination of the curves shows NDR like behavior in a few samples (Figure 2.2.17) in the negative region between -600 and -700 mV and not at positive potentials. It was observed that NDR behavior at negative potentials occurred more frequently than at positive potentials. Two representative curves are shown here. This behavior was not observed in the C_8 dithiol curves. Figure 2.2.18 shows a curve obtained on C_8 dithiol compared with an I-V curve obtained with a Fc dithiol. The red squares are the Fc dithiol in which NDR can be observed in and the black open circles show a typical C_8 dithiol in which NDR was not observed.

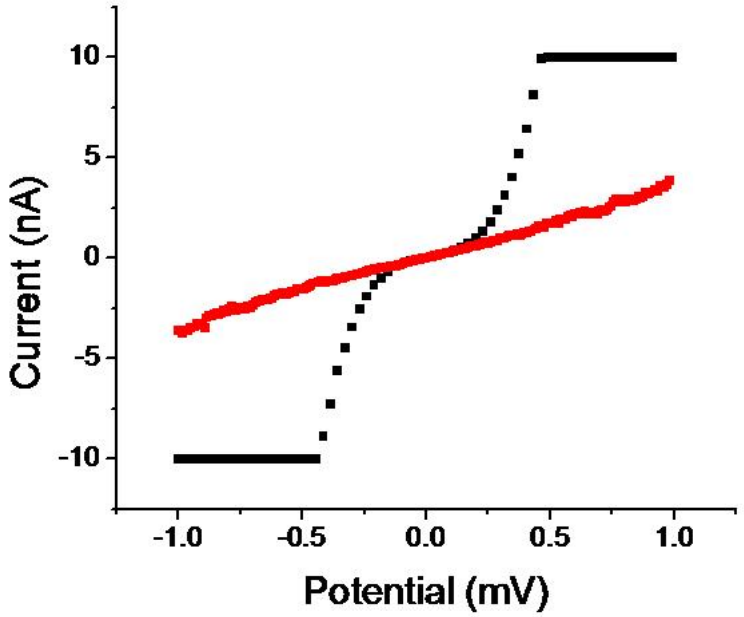

Figure 2.2.15 I-V curve taken over bare metal (open circles) and a curve after a molecular junction with c_8 dithiol was formed (closed squares). An increased in the non linearity of the curve was consistent with tunneling through a molecular junction

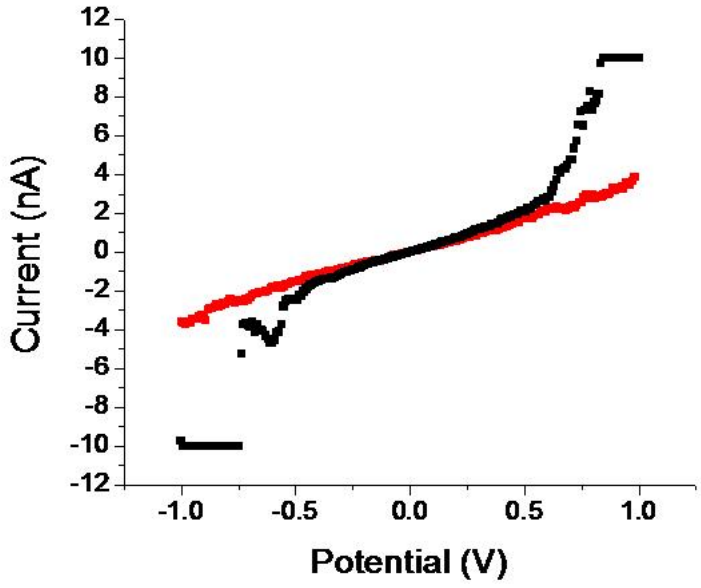

Figure 2.2.16 I-V curve taken over bare metal (open circles) and a curve after a molecular junction with Fc dithiol was formed (closed squares). An increased in the non linearity of the curve was consistent with tunneling through a molecular junction

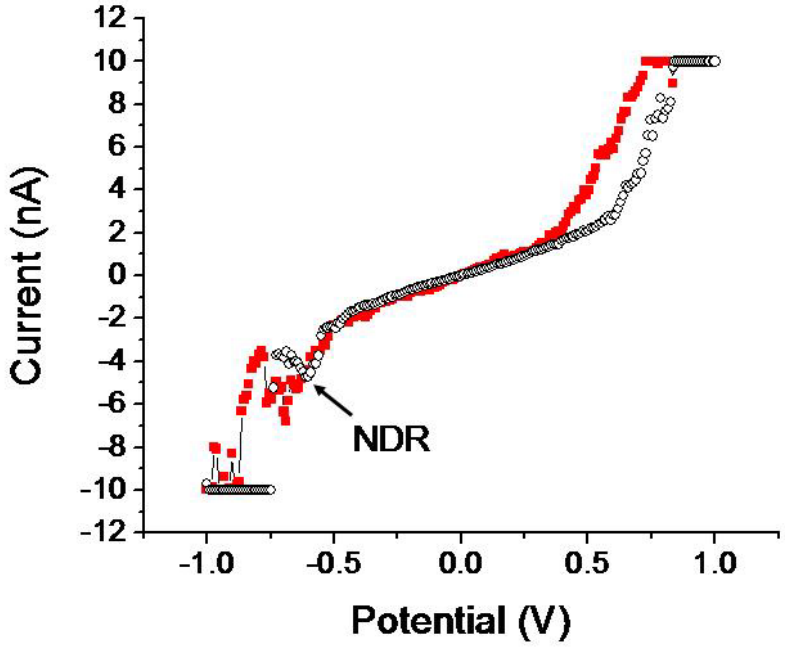

Figure 2.2.17 Two Fc dithiol curves exhibiting NDR like behavior in the negative region between -600 and -700 mV.

imaged. In hundreds of I-z curves only a very small percentage showed NDR like behaivior.

This experiment was very difficult in that it relies on randomly picking up a molecule because due to the quality of the gold tip the surface can not be attachment and out of that the ones that did, only a few I-z curves showed tunneling through a molecule. The lack of I-V curves showing a molecular junction was presumably due to either the molecule disengaging from the contact during I-z measurements or being remove from the junction during I-V collection. Out of the "good" I-V curves even fewer show NDR. There was not enough NDR for any type of statistical analysis to be made. These experiments do demonstrate that presence of NDR the $Fc(COC_5SH)_2$ and not in the C_8 dithiol.

Even after expressing the caveats expressed above, the I-V curves lend further support to the hypothesis that NDR is based on molecular resonant tunneling.

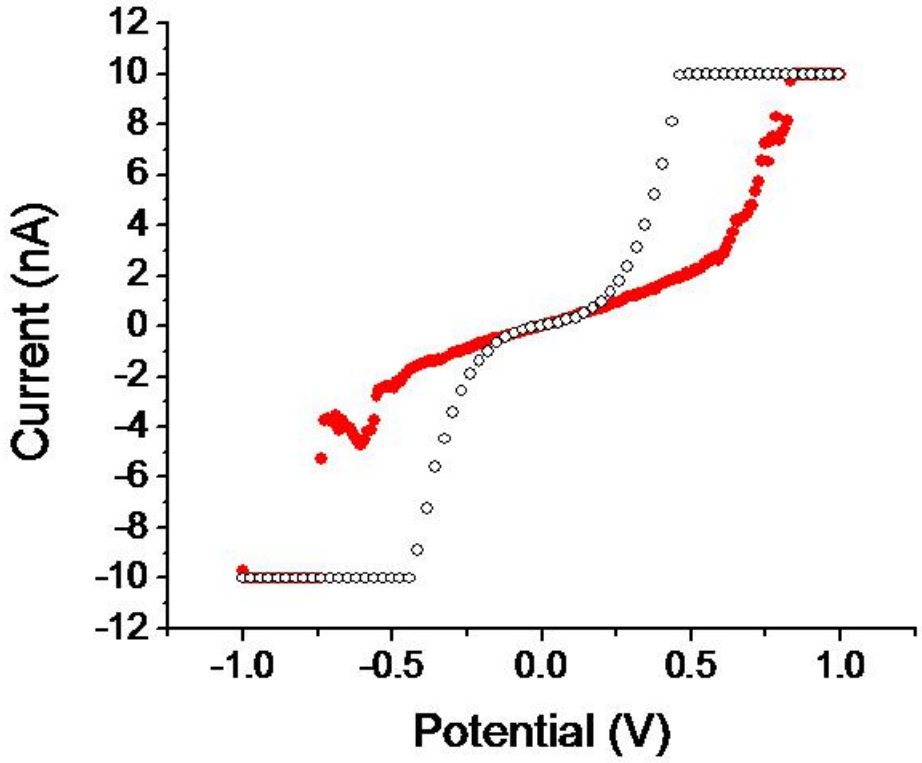

Figure 2.2.18 I-V curves comparing C_8 dithiol (black open circles) to Fc dithol (red squares). NDR was observed in the Fc dithiol and not in the C_8 dithiol.

2.2.2c Mercury drop junctions

Having observed NDR with STM, it was proposed to explore whether or not it could be observed in a mercury – molecule - gold junctions. As discussed previously in Chapter 1, Le et al. have observed NDR in OPEs using mercury drop junctions.[34] Monolayers formed on Hg were quite useful to study electron tunneling through SAM due to the ability of n-alkanethiols to form monolayers that maintain defect free impermeable characteristics. A defect free SAM was

important because mercury amalgamates when contacted to gold. In this experiment a 1000 µl syringe was used to create a small drop of mercury. This drop of mercury was connected to a PAR M273 potentiostat. The Hg drop was connected as the working electrode. The counter and auxiliary electrodes were connected to either another syringe containing mercury covered in a 1 mM $C_{16}SH$ thiol in ethanol or a gold substrate also covered by a 1 mM $C_{12}SH$ or $C_{16}SH$. The first goal in this experiment was to show that two mercury electrodes could be contacted and measured with our equipment. Figure 2.2.19 shows a CV of 5 cycles of two $C_{16}S$ thiolate SAMs formed on two mercury electrodes. This CV shows that stable contact could be made between two SAMs and their I-V behavior could be measured. It was first thought that the peak in the negative region could be due to reductive desorption of the thiol.[79,82,85,86] However, reductive desoorption of the thiol as the cause of the peak was not clear because potential sweeps of $C_{12}S$- SAMs and $FcC_{11}S$- SAMs did not show this kind of peak as well as the fact that the initial negative scan in Figure 2.2.19 does not show a peak either. The peak was also observed on a $C_{16}S$-SAM in a Hg-Au junction. One would expect the peak potential to be different on a Au substrate vs on Hg. It has been reported that the potential for the reductive desorption of a thiolate with a chain length greater than 13 carbons is greater then -1.1 V vs Ag/AgCl.[86]

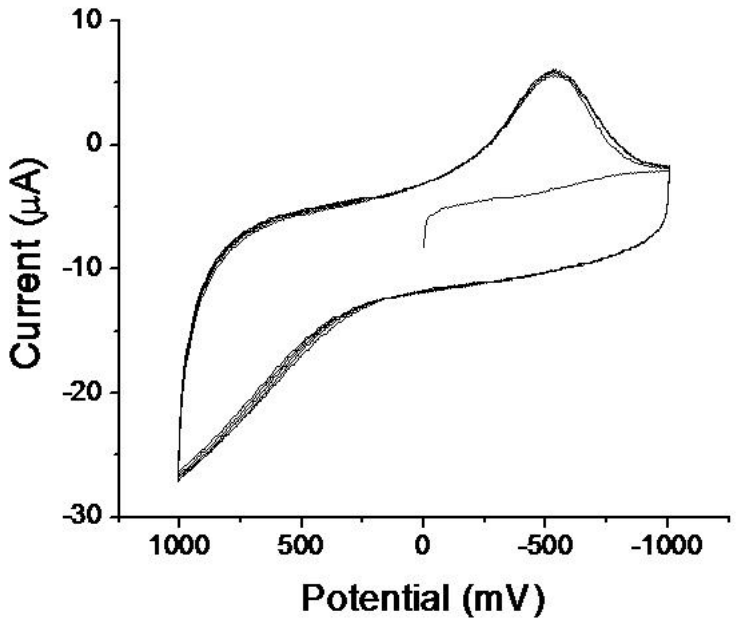

Figure 2.2.19 CV of Hg-C_{16}S-SAM-Hg junction @ 50 mV/s, 5 cycles. The counter and reference were shorted together.

In the mercury drop experiment the reference was shorted to the counter so no comparison of the reduction waves can be made. However, since this peak was not observed all the time nor was it observed on C_{12}S-SAM or FcC_{11}S-SAM it was most likely due to some type of impurity in the C_{16}SH solution.

The next series of experiments was designed to show that contact between the mercury drop and a gold substrate could be formed without the amalgamation of the two metals. Figure 2.2.20A shows a chronoamperommetry (CA) where current was measured as a function of time. This technique was used to determine when the two SAMs were contacted with each other.

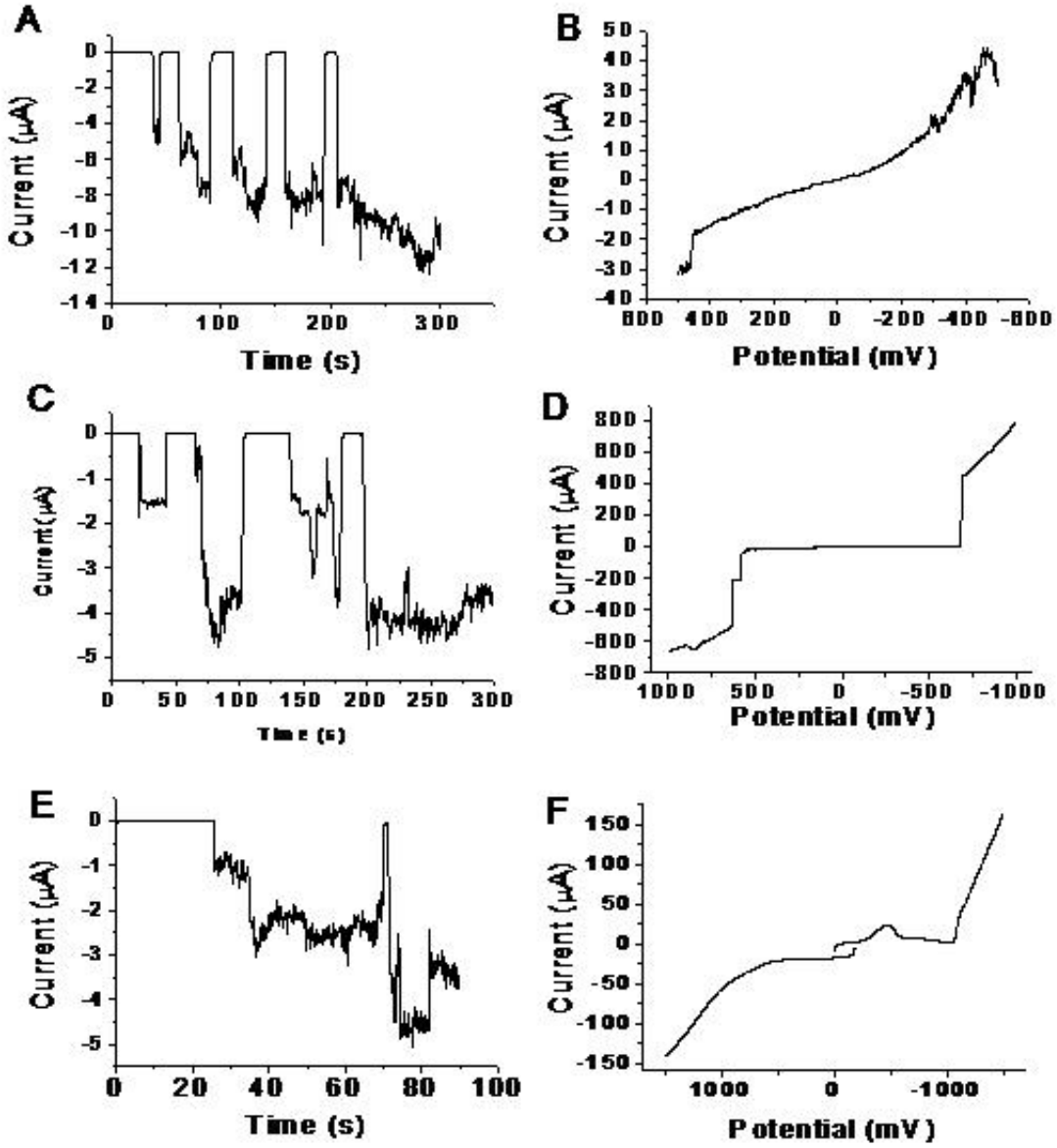

Figure 2.2.20 Hg-C_{16}S-SAM-Au junction A), C) and E) are chronoamperometry measurements with a potential of 200 mV; B), D), and F) are linear sweep voltammetry experiments at 100 mV/s

With a constant potential of 200 mV and the two SAMs being separate, no tunneling current was measured. As the Hg drop approaches the gold the current increases due to tunneling through the junction when the two SAMs just make contact with each other. When contact was made a jump in the current was observed. The Hg drop was then disengaged from the surface and approached again several times. This shows that the contact was robust and reproducible. Figure 2.2.20B shows a representative I-V curve taken with this junction. The junction was first swept from 0 V to -500 mV, then the Hg drop was disengaged then engaged to as observed by CA then the potential was swept form 0 to 500 mV. The curve shows a slightly non-linear I-V curve consistent with tunneling. Figure 2.2.20C shows another CA experiment, with the Hg drop engaged and disengaged four times. Once contact was made the potential was swept from 0 V to -1.0 V and the Hg drop was disengaged and engaged and the potential was swept from 0 V to 1.0 V. Figure 2.2.20D shows a curve that was observed on many occasions where the current does not increase much and then sharply increases. The potential where this occurs was very symmetrical. It was very similar to curves that show destruction of the monolayer and an amalgamation of the metals, however, in this example the Hg drop was retracted and then contacted again demonstrating that this kind of I-V was not indicating the breakdown potential. Figure 2.2.20E shows contact via CA and I-V (Figure 2.2.20F) curves swept first from 0 to -1.5 V and then from 0 to 1.5 V. In these curves a peak was observed on the negative region at the same potential as that

observed in the Hg/-SC_{16}/C_{16}S-/Hg junction. The shape of the I-V curves were variable from data set to data set, but reproducible within each set.

Having demonstrated the reproducibility of I-V measurements over a Hg/-SC_{16}/C_{16}S-/Au junction a comparison of Hg/-SC_{12}/C_{12}S-/Au to Hg/-SC_{12}/FcC_{11}S-/Au was performed. C_{12}S-SAM was used because it was approximately the same SAM length as the FcC_{11}S-SAM. Figure 2.2.21 show typical I-V curves of the two junctions. As can be observed the I-V curves of the FcC_{11}S-SAM (Figure 2.2.21 curve 1) the current was roughly 5 times larger than in the C_{12}S-SAM (Figure 2.2.21 curve 2). This behavior was consistent with tunneling through a molecule with a smaller tunneling barrier. NDR was never observed in any I-V curve taken. In retrospect the lack of NDR make sense because if resonant tunneling is the mechanism that causes NDR, a reduced local density of states is required for it to be observed. The lack of NDR in the mercury drop experiment should then be expected.

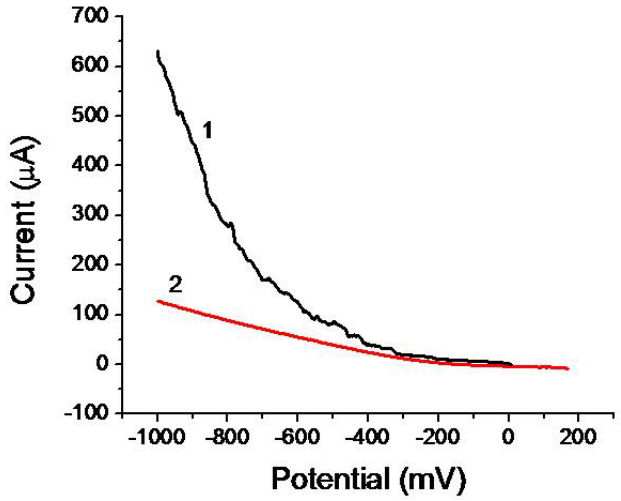

Figure 2.2.21 Linear sweep voltammetry comparison of Hg-C_{12}S-SAM-Au junction (curve 2) and Hg-FcC_{11}S-SAM-Au (curve 1) at 100 mV/s

2.3 Conclusion

NDR can be seen in electroactive molecules. The mechanism for NDR is proposed to be via resonant tunneling through the electroactive moiety. Alternate molecular contact strategies were employed and NDR was not observed in Hg drop experiments, which is not surprising due to the absence of a narrow density of states in the junction. NDR behavior was observed in the STM tip-molecule-gold substrate junction using a dithiol. The amount of NDR observed was not sufficient for any definitive statements to be made. The results presented in this chapter suggest that NDR does seem to be a real molecular phenomenon based on resonant tunneling.

2.4 Experimental

Materials. Dodecane and n-alkanethiols ($HS(CH_2)_{n-1}CH_3$ (n = 3, 6, 7, 12, 16) were purchased from Aldrich and were used without further purification. 11 Ferrocenylundecanethiol and11 Ferrocenylundecanethiolacetate (Fc(CH2)11SH, abbreviated here as $FcC_{11}SH$ and $Fc(CH_2)_{11}SAc$) was prepared according to previously published procedures.[5,87] n-Alkanethiols were dissolved in anhydrous ethanol (Aaper Alcohol and Chemical Co.) to form 1 mM stock solutions. All solutions were discarded after each use.

SAM Preparation. Sample substrates were flame-annealed Au(111) facets on a gold bead formed at the end of a gold wire (Alfa Aesar, 99.999%). The wire stem was alloyed to a platinum foil (Alfa Aesar) base. Prior to monolayer

deposition, the substrates were cleaned in piranha solution (3:1 H_2SO_4:H_2O_2 (30%) by volume). Caution: Piranha solution was corrosive. In addition, care should be taken to not store piranha solution for extended lengths of time due to the formation of explosive oxides. Au(111) substrates were incubated in 1 mM ethanol solution of ferrocenyl undecylthiol for at least 24 h at room temperature to form a ferrocenyl-terminated self-assembled monolayer ($FcC_{11}S$-SAM). After copious rinsing in ethanol and drying in a di-nitrogen stream, the sample was mounted in a custom Kel-F fluid cell in preparation for scanning in solvent. Samples were subsequently studied by STM without further delay. The STM tips used in this work were etched Pt:Ir (90:10, Alfa Aesar, 0.254 mm diameter) wire.

Scanning Tunneling Microscopy (STM). All current–voltage data were collected on a Digital Instruments (Santa Barbara, CA) Nanoscope E, equipped with a multimode base, an E-scanner, and low-current converter with a picoamp boost stage or a RHK (Troy, MI) SPM 1000 controller with the same Digital Instruments multimode base, E-scanner, and low-current converter. All experiments were performed at room temperature under ambient conditions. The sample was scanned in a low dielectric solvent (dodecane) Typical scanning conditions were a bias voltage of 1 V and a set-point current of 10 pA.

Scanning Tunneling Spectroscopy (I–V Data Collection):.

Current–voltage curves were collected for these experiments using the CITS (current imaging tunneling spectroscopy) mode in the Digital Instruments

scanning software. At least three data sets for each type of experiment were collected. Each set consisted of 1024 curves collected at regularly spaced intervals (32 x̣ 32 array) when scanning a square region. During the collection of a current–voltage curve, the instrument stopped lateral tip scanning and turned off the feedback. The sweep time for each curve was 150 μs, and the bias limits were –2.0 V to +2.0 V.

Each data set was subjected to a screening process where saturated responses were removed as described previously.[16] The peak currents and valley currents were determined by analyzing the first derivative of each I–V curve. These values were used to calculate a peak-to-valley ratio (PVR) for each peak. The large number of samples per scanning area (1024 per 0.04 μm^2 area (200 nm x̣ 200 nm)) permitted the collection of a large number of data for each sample.

Once imaging was complete, the raw I-V data was exported in ASCII and imported into Kaleidagraph (Synergy Software). Macros that were written by previous group members were used to analyze the data (see Appendix 1 for more information). Curves that did not show any increase in current (e.g. they remained flat) were rejected as well as curves that were saturated. The curves that were not rejected were further analyzed to determine the potential at which the NDR occurs as well as to determine the ratio between the maximum current value of NDR and the minimum value of NDR (we call this the peak to valley ration of PVR). The NDR peak positions can be plotted as histograms and then fit to a Gaussian curve.

2.5 References

(1) Boulas, C.; Davidovits, J. V.; Rondelez, F.; Vuillaume, D. *Phys. Rev. Lett.* **1996**, *76*, 4797.

(2) Avouris, P. *Accounts Chem. Res.* **2002**, *35*, 1026.

(3) Beebe, J. M.; Engelkes, V. B.; Miller, L. L.; Frisbie, C. D. *J. Am. Chem. Soc.* **2002**, *124*, 11268.

(4) Boussaad, S.; Xu, B. Q.; Nagahara, L. A.; Amlani, I.; Schmickler, W.; Tsui, R.; Tao, N. J. *J. Chem. Phys.* **2003**, *118*, 8891.

(5) Carroll, R. L.; Fuierer, R.; Gorman, C. B. In *Molecules as Components of Electronic Devices*; Amer. Chem. Soc.: Washington, 2003; Vol. 844, pp 10.

(6) Chabinyc, M. L.; Holmlin, R. E.; Haag, R.; Chen, X. X.; Ismagilov, R. F.; Rampi, M. A.; Whitesides, G. M. In *Molecules as Components of Electronic Devices*; Amer. Chem. Soc.: Washington, 2003; Vol. 844, pp 16.

(7) Chen, J.; Reed, M. A.; Rawlett, A. M.; Tour, J. M. *Science* **1999**, *286*, 1550.

(8) Chen, J.; Wang, W.; Reed, M. A.; Rawlett, A. M.; Price, D. W.; Tour, J. M. *Appl. Phys. Lett.* **2000**, *77*, 1224.

(9) Collier, C. P.; Jeppesen, J. O.; Luo, Y.; Perkins, J.; Wong, E. W.; Heath, J. R.; Stoddart, J. F. *J. Am. Chem. Soc.* **2001**, *123*, 12632.

(10) Cui, X. D.; Primak, A.; Zarate, X.; Tomfohr, J.; Sankey, O. F.; Moore, A. L.; Moore, T. A.; Gust, D.; Harris, G.; Lindsay, S. M. *Science* **2001**, *294*, 571.

(11) Cui, X. D.; Zarate, X.; Tomfohr, J.; Sankey, O. F.; Primak, A.; Moore, A. L.; Moore, T. A.; Gust, D.; Harris, G.; Lindsay, S. M. *Nanotechnology* **2002**, *13*, 5.

(12) Fan, F. R. F.; Yang, J. P.; Cai, L. T.; Price, D. W.; Dirk, S. M.; Kosynkin, D. V.; Yao, Y. X.; Rawlett, A. M.; Tour, J. M.; Bard, A. J. *J. Am. Chem. Soc.* **2002**, *124*, 5550.

(13) Fuierer, R. *Probing the Electronic Properties of Materials that Self-Assemble*; North Carolina State University: Raleigh, 2004.

(14) Fuierer, R. R.; Carroll, R. L.; Feldheim, D. L.; Gorman, C. B. *Adv. Mater.* **2002**, *14*, 154.

(15) Gittins, D. I.; Bethell, D.; Schiffrin, D. J.; Nichols, R. J. *Nature* **2000**, *408*, 67.

(16) Gorman, C. B.; Carroll, R. L.; Fuierer, R. R. *Langmuir* **2001**, *17*, 6923.

(17) Gorman, C. B.; Carroll, R. L.; He, Y. F.; Tian, F.; Fuierer, R. *Langmuir* **2000**, *16*, 6312.

(18) Gorman, C. B.; Miller, R. L.; Chen, K. Y.; Bishop, A. R.; Haasch, R. T.; Nuzzo, R. G. *Langmuir* **1998**, *14*, 3312.

(19) Hahn, J. R.; Hong, Y. A.; Kang, H. *Appl. Phys. A-Mater. Sci. Process.* **1998**, *66*, S467.

(20) Haiss, W.; van Zalinge, H.; Higgins, S. J.; Bethell, D.; Hobenreich, H.; Schiffrin, D. J.; Nichols, R. J. *J. Am. Chem. Soc.* **2003**, *125*, 15294.

(21) Han, J. E.; Crespi, V. H. *Appl. Phys. Lett.* **2001**, *79*, 2829.

(22) Han, W. H.; Durantini, E. N.; Moore, T. A.; Moore, A. L.; Gust, D.; Rez, P.; Leatherman, G.; Seely, G. R.; Tao, N. J.; Lindsay, S. M. *J. Phys. Chem. B* **1997**, *101*, 10719.

(23) Hipps, K. W.; Barlow, D. E.; Mazur, U. *J. Phys. Chem. B* **2000**, *104*, 2444.

(24) Holmlin, R. E.; Haag, R.; Chabinyc, M. L.; Ismagilov, R. F.; Cohen, A. E.; Terfort, A.; Rampi, M. A.; Whitesides, G. M. *J. Am. Chem. Soc.* **2001**, *123*, 5075.

(25) Holmlin, R. E.; Ismagilov, R. F.; Haag, R.; Mujica, V.; Ratner, M. A.; Rampi, M. A.; Whitesides, G. M. *Angew. Chem.-Int. Edit.* **2001**, *40*, 2316.

(26) Huang, C. Y.; Morris, J. E.; Su, Y. K.; Kuo, T. H. *Electron. Lett.* **1994**, *30*, 1012.

(27) Ito, T.; Buhlmann, P.; Umezawa, Y. *Anal. Chem.* **1998**, *70*, 255.

(28) Ito, T.; Buhlmann, P.; Umezawa, Y. *Anal. Chem.* **1999**, *71*, 1699.

(29) Jiang, P.; Liu, Z. F.; Wang, Y. C.; Cai, S. M. *Mol. Cryst. Liquid Cryst.* **1999**, *337*, 317.

(30) Joachim, C.; Gimzewski, J. K.; Aviram, A. *Nature* **2000**, *408*, 541.

(31) Kaba, M. S.; Song, I. K.; Barteau, M. A. *J. Vac. Sci. Technol. A-Vac. Surf. Films* **1997**, *15*, 1299.

(32) Karzazi, Y.; Cornil, J.; Bredas, J. L. *J. Am. Chem. Soc.* **2001**, *123*, 10076.

(33) Kwon, Y. K.; Tomanek, D.; Iijima, S. *Phys. Rev. Lett.* **1999**, *82*, 1470.

(34) Le, J. D.; He, H.; Hoye, T. R.; Mead, C. C.; Kiehl, R. A. *Appl. Phys. Lett.* **2003**, *83*, 5518.

(35) Slowinski, K.; Fong, H. K. Y.; Majda, M. *J. Am. Chem. Soc.* **1999**, *121*, 7257.

(36) Slowinski, K.; Majda, M. *J. Electroanal. Chem.* **2000**, *491*, 139.

(37) Wold, D. J.; Frisbie, C. D. *J. Am. Chem. Soc.* **2000**, *122*, 2970.

(38) Wold, D. J.; Frisbie, C. D. *J. Am. Chem. Soc.* **2001**, *123*, 5549.

(39) Wong, E. W.; Collier, C. P.; Behloradsky, M.; Raymo, F. M.; Stoddart, J. F.; Heath, J. R. *J. Am. Chem. Soc.* **2000**, *122*, 5831.

(40) Xiao, X. Y.; Xu, B. Q.; Tao, N. J. *Nano Lett.* **2004**, *4*, 267.

(41) Xu, B. Q.; Xiao, X. Y.; Tao, N. J. *J. Am. Chem. Soc.* **2003**, *125*, 16164.

(42) Xue, Y. Q.; Datta, S.; Hong, S.; Reifenberger, R.; Henderson, J. I.; Kubiak, C. P. *Phys. Rev. B* **1999**, *59*, R7852.

(43) Xue, Y. Q.; Datta, S.; Ratner, M. A. *J. Chem. Phys.* **2001**, *115*, 4292.

(44) Seminario, J. M.; Araujo, R. A.; Yan, L. M. *J. Phys. Chem. B* **2004**, *108*, 6915.

(45) Altfeder, I. B.; Golovchenko, J. A.; Narayanamurti, V. *Phys. Rev. Lett.* **2001**, *87*, 0568011.

(46) Roth, K. M.; Gryko, D. T.; Clausen, C.; Li, J. Z.; Lindsey, J. S.; Kuhr, W. G.; Bocian, D. F. *J. Phys. Chem. B* **2002**, *106*, 8639.

(47) Roque, A.; Pina, F.; Alves, S.; Ballardini, R.; Maestri, M.; Balzani, V. *J. Mater. Chem.* **1999**, *9*, 2265.

(48) Pina, F.; Roque, A.; Melo, M. J.; Maestri, I.; Belladelli, L.; Balzani, V. *Chem.-Eur. J.* **1998**, *4*, 1184.

(49) Sun, J. P.; Haddad, G. I.; Mazumder, P.; Schulman, J. N. *Proc. IEEE* **1998**, *86*, 641.

(50) Alvarez, J.; Liu, J.; Roman, E.; Kaifer, A. E. *Chem. Commun.* **2000**, 1151.

(51) Besenbacher, F. *Rep. Prog. Phys.* **1996**, *59*, 1737.

(52) Appenzeller, J.; Knoch, J.; Martel, R.; Derycke, V.; Wind, S. J.; Avouris, P. *IEEE Trans. Nanotechnol.* **2002**, *1*, 184.

(53) Schulman, J. N.; Santos, H. J. D.; Chow, D. H. *IEEE Electron Device Lett.* **1996**, *17*, 220.

(54) Kinne, M.; Barteau, M. A. *Surf. Sci.* **2000**, *447*, 105.

(55) Leonard, F.; Tersoff, J. *Phys. Rev. Lett.* **2000**, *85*, 4767.

(56) Paulsson, M.; Stafstrom, S. *Phys. Rev. B* **2001**, *6403*.

(57) Rawlett, A. M.; Hopson, T. J.; Nagahara, L. A.; Tsui, R. K.; Ramachandran, G. K.; Lindsay, S. M. *Appl. Phys. Lett.* **2002**, *81*, 3043.

(58) Robuck, H. E. *Molecular-Based Negative Differential Resistance Across a Self-Assembled Monolayer: Its Dependence on Monolayer Coverage and Tunneling Gap*; North Carolina State University: Raleigh, 2004.

(59) Selzer, Y.; Salomon, A.; Ghabboun, J.; Cahen, D. *Angew. Chem.-Int. Edit.* **2002**, *41*, 827.

(60) Song, I. K.; Kaba, M. S.; Barteau, M. A. *Langmuir* **2002**, *18*, 2358.

(61) Zhao, P. J.; Cui, H. L.; Woolard, D.; Jensen, K. L.; Buot, F. A. *J. Appl. Phys.* **2000**, *87*, 1337.

(62) Seminario, J. M.; Zacarias, A. G.; Derosa, P. A. *J. Chem. Phys.* **2002**, *116*, 1671.

(63) Seminario, J. M.; Zacarias, A. G.; Tour, J. M. *J. Am. Chem. Soc.* **2000**, *122*, 3015.

(64) Cornil, J.; Karzazi, Y.; Bredas, J. L. *J. Am. Chem. Soc.* **2002**, *124*, 3516.

(65) Seminario, J. M.; Derosa, P. A.; Bastos, J. L. *J. Am .Chem. Soc.* **2002**, *communication*, 10266.

(66) Donhauser, Z. J.; Mantooth, B. A.; Kelly, K. F.; Bumm, L. A.; Monnell, J. D.; Stapleton, J. J.; Price, D. W.; Rawlett, A. M.; Allara, D. L.; Tour, J. M.; Weiss, P. S. *Science* **2001**, *292*, 2303.

(67) Tour, J. M.; Cheng, L.; Nackashi, D. P.; Yao, Y. X.; Flatt, A. K.; St Angelo, S. K.; Mallouk, T. E.; Franzon, P. D. *J. Am. Chem. Soc.* **2003**, *125*, 13279.

(68) Koepp, H. M.; Wendt, H.; Strehlow, H. *Zeitschrift Fur Elektrochemie* **1960**, *64*, 483.

(69) Bolink, H. J. *Photorefractive polymers*; University Library Groningen: Groningen, 1997.

(70) Basch, H.; Ratner, M. A. *J. Chem. Phys.* **2004**, *120*, 5771.

(71) Agarwal, M.; De Guire, M. R.; Heuer, A. H. *J. Am. Ceram. Soc.* **1997**, *80*, 2967.

(72) Barteau, M. A.; Song, I. K.; Lyons, J. E. *Abstr. Pap. Am. Chem. Soc.* **2002**, *223*, U22.

(73) Bredas, J.; Cornil, J.; Karzazi, Y. *J. Am. Chem. Soc.* **2001**, *123*, 10075.

(74) Damle, P.; Rakshit, T.; Paulsson, M.; Datta, S. *IEEE Trans. Nanotechnol.* **2002**, *1*, 145.

(75) Abdelghani, A. *Mater. Lett.* **2001**, *50*, 73.

(76) Barlow, D.; Scudiero, L.; Hipps, K. W. *Ultramicroscopy* **2003**, *97*, 47.

(77) Altfeder, I. B.; Chen, D. M. *Phys. Rev. Lett.* **2000**, *84*, 1284.

(78) Barteau, M. A.; Kaba, M. S.; Song, I. K. *J. Vac. Sci. Technol. A* **1997**, *15*, 1299.

(79) Widrig, C. A.; Chung, C.; Porter, M. D. *J. Electroanal. Chem.* **1991**, *310*, 335.

(80) Tang, X. Y.; Schneider, T. W.; Walker, J. W.; Buttry, D. A. *Langmuir* **1996**, *12*, 5921.

(81) Viana, A. S.; Kalaji, M.; Abrantes, L. M. *Langmuir* **2003**, *19*, 9542.

(82) Walczak, M. M.; Popenoe, D. D.; Deinhammer, R. S.; Lamp, B. D.; Chung, C. K.; Porter, M. D. *Langmuir* **1991**, *7*, 2687.

(83) Dean, J. A. *Lange's Handbook of Chemistry*; Thirteenth ed., 1985.

(84) Tao, N. J. *Phys. Rev. Lett.* **1996**, *76*, 4066.

(85) Zhong, C. J.; Zak, J.; Porter, M. D. *J. Electroanal. Chem.* **1997**, *421*, 9.

(86) Kakiuchi, T.; Usui, H.; Hobara, D.; Yamamoto, M. *Langmuir* **2002**, *18*, 5231.

(87) Uosaki, K.; Sato, Y.; Kita, H. *Langmuir* **1991**, *7*, 1510.

Chapter 3

Negative differential resistance in ω-thiolate/ metal multilayer assemblies

3.1 Introduction

As discussed in Chapter 2 scanning tunneling microscopy (STM) is an approach to access single molecules on a surface that allows us to take a large number of measurements in a relatively short time frame. STM has been shown to be a versatile technique for investigating molecular structure - electronic property relationships. This chapter will focus on resonant tunneling based Negative Differential Resistance (NDR) (Figure 2.1.1) in self assembled multilayers.

The observation of NDR in a few specific electroactive species (as discussed in Chapter 2), prompted studies involving a variety of electroactive architectures. It was further proposed that the magnitude of the peak to valley ratio would increase with the density of redox active sites due to increased tunneling ability. This phenomenon was explored using multilayers of alkanethiol chains, formed with redox active metal ions deposited in between them (Figure 3.1.1.)

A multilayer construction strategy has been developed by Mallouk et al. capitalizing on the strong ionic binding between zirconium ion and organic phosphonates.[1,2] Multilayers were formed by immersion of a functionalized substrate in solutions containing $ZrOCl_2$ and a bis-(phosphonic acid). Another method for multilayer formation was based on the interaction of a Cu^{2+} ion with

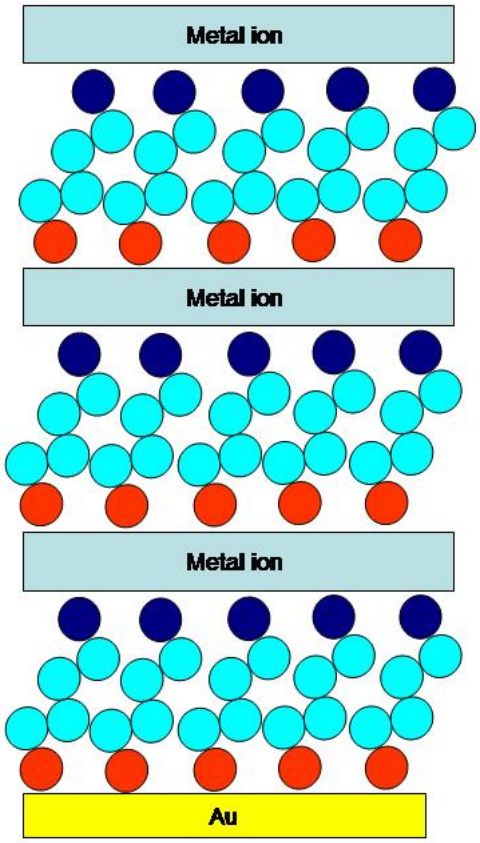

Figure 3.1.1 Schematic of self multilayer assembly. α-ω alkane thiols are deposited between metal cations (Cu^{2+} or Zn^{2+})

carboxylic acids and thiols.[3] A bifunctional thiol, mercaptodecanoic acid ($HS(CH_2)_{10}COOH$), was deposited onto a Au substrate. This –COOH terminated monolayer was then exposed to a Cu^{2+} salt to form a Cu-carboxylate at the surface of the SAM. The SAM was then exposed to the bifunctional thiol solution. The thiol group, bound to the Cu-carboxylate sites resulting in layers of Cu in between a carboxylate group and a thiol group.[3] Bard and co-workers also looked at this strategy for multilayer formation by using a dithiol instead of a carboxylic acid terminated thiol.[4]

It was not clear that NDR could be seen in all electroactive SAMs, especially of the type that involve metal ions placed in between alkanethiols. To

test whether or not NDR could be seen in these types of multilayers, simple SAMs were formed with benzenedimethanethiol (BDMT) and Cu^{2+}. If the multilayers include a metal ion that has an accessible molecular orbital, then NDR should be seen. NDR should not be seen in molecules that have lower lying HOMOs and higher lying LUMOs (i.e., harder to reduce and oxidize) and therefore inaccessible. Candidate metals were evaluated based on their redox potential using cyclic voltammetry (CV).

NDR should be different for orbitals with varying energies. NDR is seen in $FcC_{11}S$-SAM, presumably because it has accessible orbitals that can overlap with the Fermi levels of the tip and Au substrate (Figure 2.1.6).[5] Rough calculations show that the Fermi energy of the tip and substrate lie below the HOMO of the FC-SAM. The Fermi energy for gold was derived by first calculating the electron density (N/V) for gold. The number of moles per m^3 was calculated using the following equation (the density of gold is 19.32 x 10^3 kg/m^3):

$$mol/m^3 = \frac{19.32\times10^3 kg/m^3}{0.197\ kg/mol} = 9.81\times10^4 mol/m^3$$

Avogadro's number is then used to find the number of gold atoms per cubic meter, which will be the same as the number of electrons because each gold atom contributes one electron.

$$n/m^3 = (9.81\times10^4 mol/m^3)(6.02\times10^{23} atoms/mol) = 5.9\times10^{28} atoms/m^3$$

The Fermi energy for gold can then be calculated using this equation:

$$\varepsilon_F = \frac{h^2}{2m}\left(\frac{3}{8\pi}\frac{N}{V}\right)^{2/3} = \frac{(6.626\times10^{-34} Js)^2}{2(9.11\times10^{-31} kg)}\left(\frac{3}{8\pi}(5.9\times10^{28}/m^3\right)^{2/3} = 8.857\times10^{-19} J = 5.50eV$$

The same calculation can be applied to platinum to yield a Fermi energy of 5.96 eV.

The HOMO level for ferrocene has been estimated at 4.8 eV.[6,7] At zero bias the initial Fermi levels of the tip and substrate of a double barrier junction with a ferrocene terminated SAM lie below the HOMO of the Fc molecule.

One might then assume that the potential at which NDR occurs should be different for molecules with orbitals at different energies. As discussed in Chapter 2, the position of NDR could not be correlated to molecules with different redox potential. However if two molecules are compared where one molecule has a much more negative redox potential one would assume that its molecular states would be less accessible than the molecule with a more positive redox potential.

3.2 Results and discussion

Cu^{2+} and Zn^{2+} were chosen to be the metal ions used to form multilayers. The reduction of Cu^{2+} occurs at a much more positive potential than the reduction of Zn^{2+}.[8] Since Zn^{2+} is reduced at higher biases it was proposed that multilayers with Zn would not exhibit NDR in the bias window that was used (-2.0 V to 2.0 V).

The purpose of these experiments was to build multilayers by alternating organic molecules with metal ions (Cu^{2+} and Zn^{2+}) and to collect I-V measurements over them. The Zn^{2+} ions were assumed to form the same types of multilayers as the Cu^{2+}. It was hypothesized that NDR could be controlled by

changing the metal in the multilayers and that the peak to valley ratio would increase as the number of layers was increased. Three different molecules were used for these experiments; 1,4 benzenedimethanethiol (BDMT), mercaptopropionic acid (MPA) and 4-mercaptobenzoic acid (MBA) (Table 3.2.1).

Table 3.1.1

1,4-Benzenedimethanethiol (BDMT)	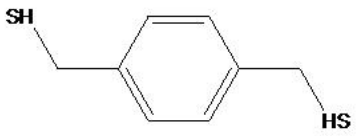
Mercaptopropionic acid (MPA)	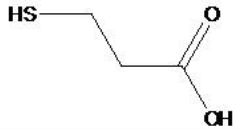
4-Mercaptobenzoic acid (MBA)	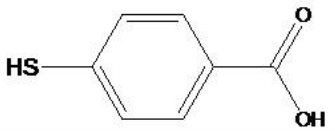

Molecules used for multilayer experiments.

Dithiols and acid-terminated thiols were investigated because these multilayers have precedent in the literature.[3-5] Multilayers were formed by alternating one-hour depositions of thiol and metal in solution. Surface characterization was used to demonstrate that multilayers were in fact formed. Ellipsometry, Surface IR, X-ray Photoemission Spectroscopy (XPS) were taken in order to verify the thickness and composition of the multilayers and Cyclic Voltammetry (CV) measurements were taken on the SAMs to measure redox activity. STM imaging and Current–Voltage (I-V) measurements were performed to measure NDR.

3.2.1 Surface Characterization

3.2.1a X-ray Photoemission Spectroscopy (XPS)

XPS measurements were taken in order to determine the presence of copper in the multilayer. For this experiment BDMT/Cu^{2+} multilayers were used. Four samples were compared: the first sample was made with copper on top of one layer of BDMT, the second sample had a layer of butanethiol on top of the Cu, the third sample had two BDMT/Cu layers with butanethiol on top, the fourth sample had five BDMT/Cu layers with butanethiol on top. Butanethiol was used to cap the multilayers because leaving exposed copper ions increased the possibility of surface contamination due to its larger surface free energy than a methyl terminated alkanethiol.

Figure 3.2.1 shows the XPS Cu 2p 3/2 peaks at 933 eV and 953 eV. These peaks are consistent with those observed in the same multilayered systems.[3,4,9] With one layer of BDMT and Cu on top there is a pronounced Cu peak seen (Figure 3.2.1A). The Cu peak was attenuated when the top layer was capped with the butanethiol (Figure 3.2.1B). Figure 3.2.1C and Figure 3.2.1D represent 2 and 5 layers respectively. Both layers were also capped with butanethiol and showed an increase in the Cu 2p intensity as the layers increase, verifying that more and more Cu was being added to the surface with each layer.

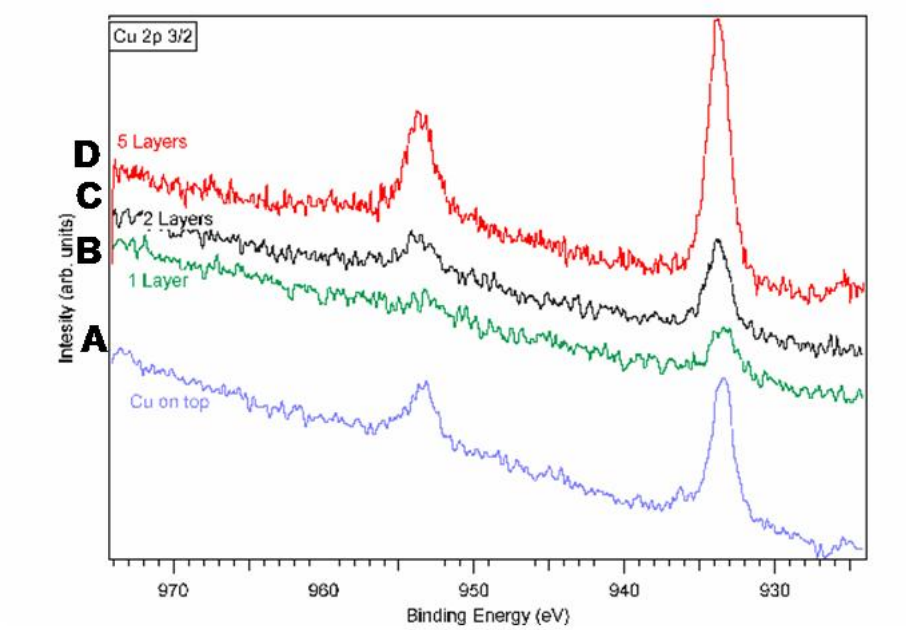

Figure 3.2.1 XPS of Cu 2p 3/2, A) BDMT Cu^{2+}, B) BDMT/Cu/C_4S-, C) BDMT/Cu/BDMT/C_4S-, D) 5 BDMT/Cu Layers capped with C_4S- As can be seen the intensity of the Cu 2p peak increases as more layers are built up.

Figure 3.2.2 shows the S 2p peak at ~163 eV. Figure 3.2.2 A, shows the first monolayer with Cu on top and Figure 3.2.2 B shows the first monolayer with a butanethiol cap on top of the Cu. There is very little signal in either case. The signal intensity does increase as the number of layers was built up from 2 and 5 layers (Figure 3.2.2 C and D respectively). These data also support the growth of multilayers by showing that there is more sulfur in the film as the number of layers increases.

Figure 3.2.3 shows the Au 4f peaks for the substrate. The first monolayer with Cu on top (Figure 3.2.3A) shows an excellent signal to noise ratio. This is due to Au having a very high sensitivity factor compared to the other expected atom's signals from the surface surface. A very small amount of gold produces a

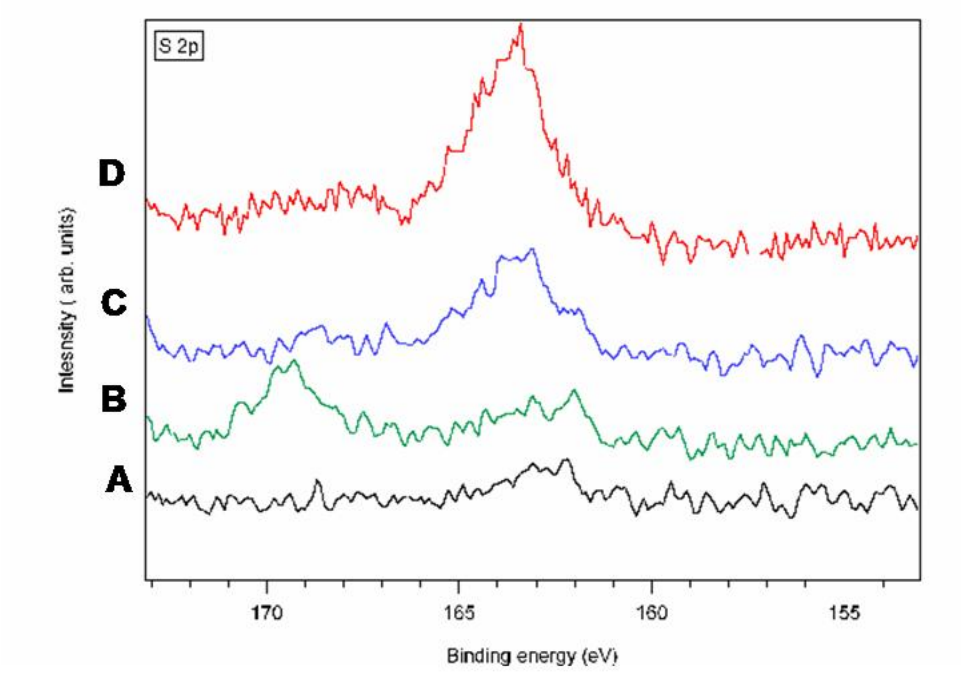

Figure 3.2.2 XPS of S 2p A) BDMT Cu2+, B) BDMT/Cu/C4S-, C) BDMT/Cu/BDMT/C4S-, D) 5 BDMT/Cu Layers capped with C4S- As can be seen the intensity of the S 2p peak increases as more layers are built up.

very large signal. When the butanethiol cap is put on, the peak height decreases (Figure 3.2.3B). A comparison of 5 multilayers (Figure 3.2.3D) to 1 layer (Figure 3.2.3A) shows that the peak intensity is dramatically decreased. This indicates the distance from top of the multilayer to the gold substrate is increasing and shows that multilayers were formed; however no conclusions could be drawn regarding the order in these multilayers.

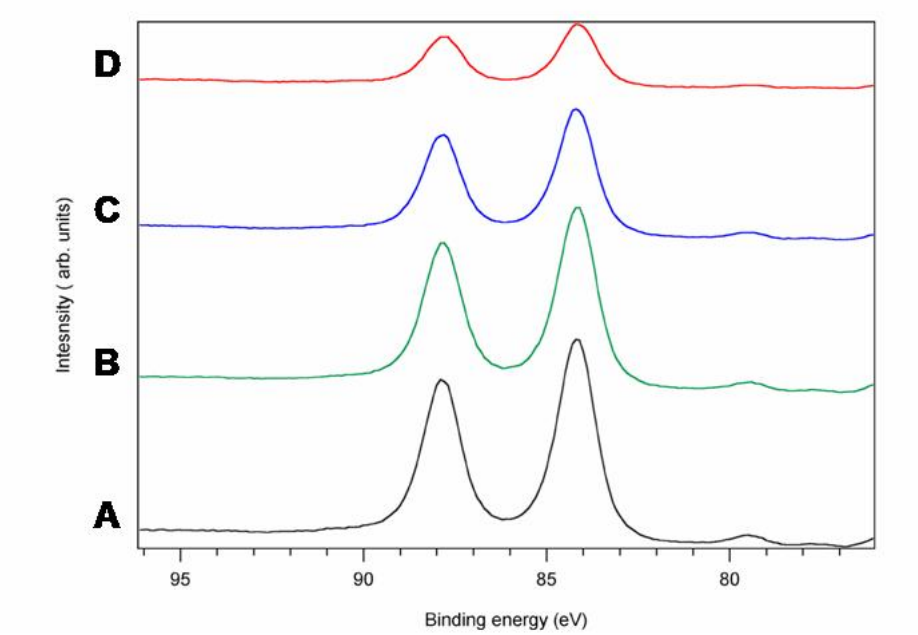

Figure 3.2.3 XPS of Au 4f 7/2 A) BDMT Cu2+, B) BDMT/Cu/C4S-, C) BDMT/Cu/BDMT/C4S-, D) 5 BDMT/Cu Layers capped with C4S- As can be seen the intensity of the Au 4f 7/2 peak decreases with increasing layers

3.2.1b Surface IR

An Infrared spectrum was taken of a multilayer of BDMT to show the presence of the multilayer on the surface. The thickness of the monolayer of BDMT was too small for the peaks to be resolved, so a sample with 5 layers was prepared. A comparison of the absorbance's in the fingerprint region resulting from the stretching from the benzene ring in the BDMT molecule (Figure 3.2.4 A) to BDMT in NUJOL (Figure 3.2.4 B) shows similar peaks. Figure 3.2.5 shows peaks at 2850 and 2930 cm^{-1} and are due to symmetric (d+) and anti-symmetric

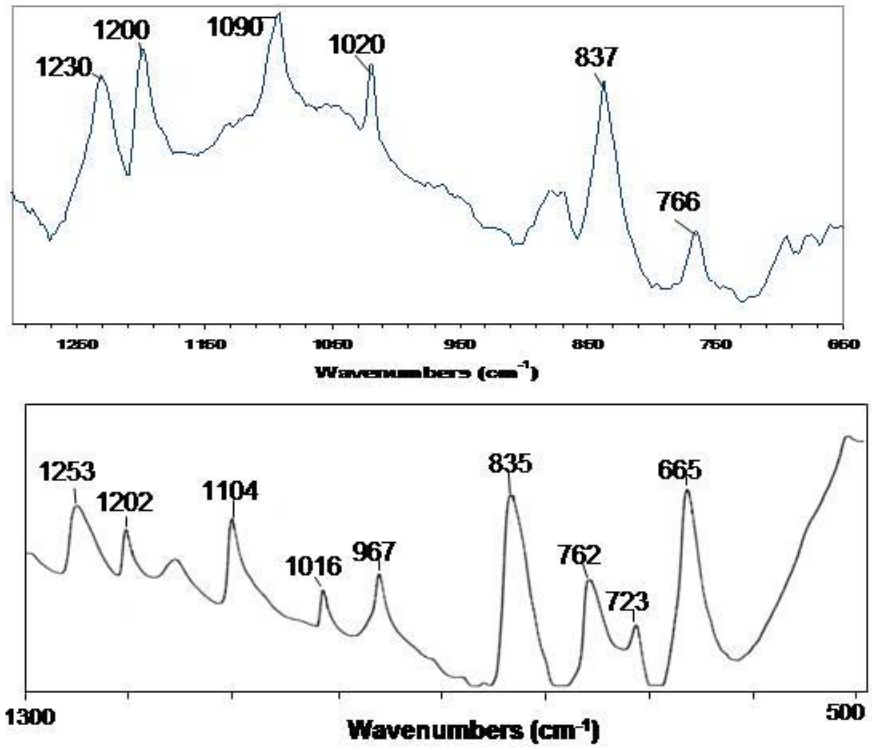

Figure 3.2.4 Infrared spectrums of fingerprint region in A) surface confined 1,4 BDMT monolayer are B) 1,4 BDMT in NUJOL

(d-) methylene stretching modes, respectively. The peak positions for d+ and d- modes of crystalline alkyl chains are reported typically to be in the range of 2846 – 2850 and 2915 – 2918 cm^{-1} for all trans extended chains and at approximately 2856 and 2928 cm^{-1} for liquid like disordered chains.[10] We can conclude that the SAMs are not completely crystalline. Thus XPS and IR results confirm that multilayers were formed by alternating an aryl thiol and a metal ion.[4]

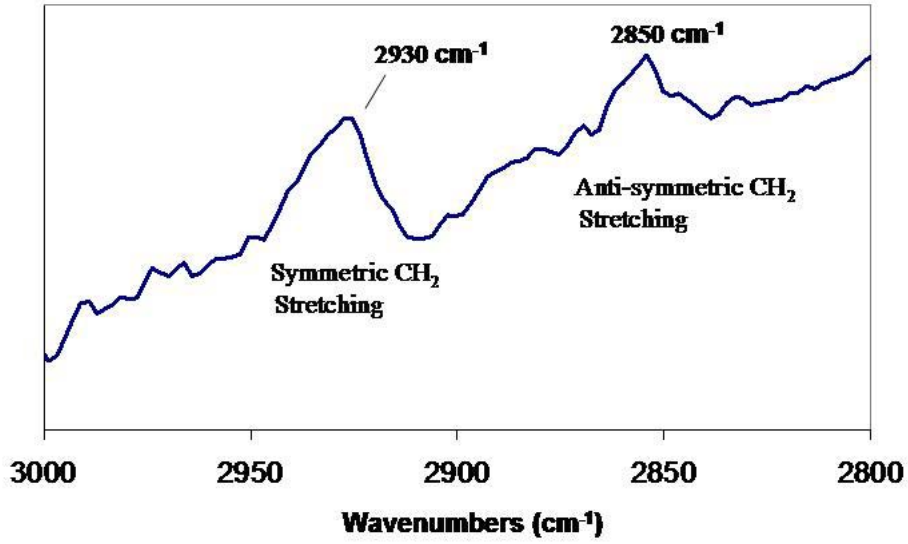

Figure 3.2.5 Surface FT-IR of 1,4 BDMT monolayer showing symmetric and anti symmetric methylene stretches.

3.2.1c Ellipsometry

Ellipsometric measurements were taken in order to determine the thickness of the multilayers. Ellipsometric data was averaged from 5 gold slides with 3 samples per slide for a total of 15 samples. Control measurements were collected on a hexadecanethiol SAM, because this system is known to form a well-packed monolayer. A thickness of 21 Å ± 3 Å was consistently achieved for $C_{16}S$- SAMs; which was consistent with reported literature values.[11] MPA/Cu^{2+} multilayers were then studied. Theoretical calculations of the approximate thickness of a monolayer of MPA yield 6 Å. The experimental thickness with a layer of Cu was 8 Å ± 3 Å. Figure 3.2.6 shows the average thickness of 1 through 5 MPA/Cu^{2+} layers. The first three layers increased linearly and then the

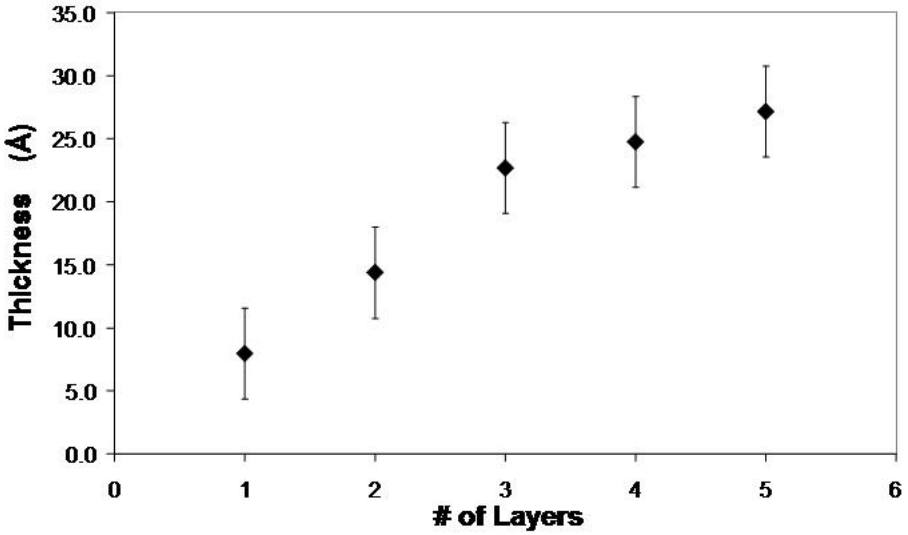

Figure 3.2.6 Ellipsometry data of 1 through 6 mercaptopropionic/Cu^{2+} multilayers on evaporated gold on glass.

rate of growth begins to plateau in layers 4 and 5. This is attributed to disorder in the layers as they are added to each other as well as surface contamination. Visual inspection of the gold slides showed an iridescent film formed after the 3rd layer. This film is most likely due to impurities in the solution. This contamination contributes to the disorder with increasing multilayer thickness. Since a linear growth rate could only be shown for the first three layers they were the only ones that would be looked at by CITS measurements. The normal deposition times for MPA and the copper was one hour per layer. Shorter deposition times of 3, 10, 15, 20 and 30 minutes were used to try and optimize the multilayer deposition, none of which gave reproducible thicknesses. Formation of hexadecanethiolate (HDT) SAMs was also attempted at these shorter deposition times, all of which were unsuccessful. Based on these results it was decided to keep the deposition time for MPA and Cu^{2+} at 1 hour.

Well packed monolayers were not observed at shorter times for this system and for the HDT. XPS showed an increase in the Cu^{2+} signal for 5 layers and the intensity of the Au 4f peaks decrease for 5 layers which was consistent with multilayer formation. Ellipsometric data demonstrated that a linear increase in thickness could only be demonstrated for the first 3 layers. Future electrochemical work will be confined to measuring the redox change in just these layers.

3.2.2 Electronic Properties

3.2.2a Cyclic Voltammetry

The purpose of the next set of experiments was to characterize the selected multilayer systems by cyclic voltammetry (CV). Based on previous work with electroactive ferrocene monolayers[12], we hypothesized that multilayers that show strong redox coupling will show a higher frequency of NDR than ones that do not show redox peaks. Cyclic voltammetry was first performed on 2 layers of BDMT/Cu^{2+} and BDMT/Zn^{2+} (Figures 3.2.7 and 3.2.8). These data do not show reversible redox activity. BDMT with Cu^{2+}or Zn^{2+} does not appear to be electrochemically active.

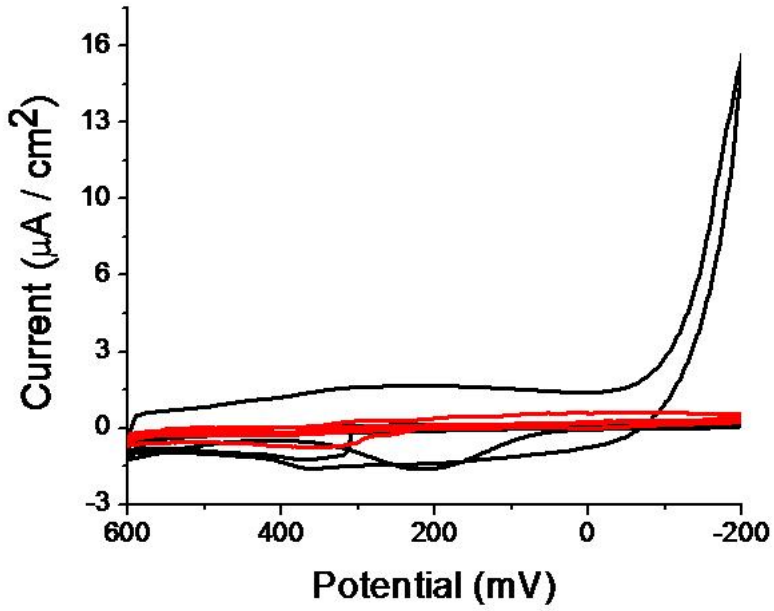

Figure 3.2.7 CV of 2 layers of BDMT/Cu^{2+} Black curve is a CV of bare gold the red curves are a CV of layers 1 and 2 of the BDMT/$Cu^{2+.}$ Scan rate = 100 mV/s vs Ag/AgCl

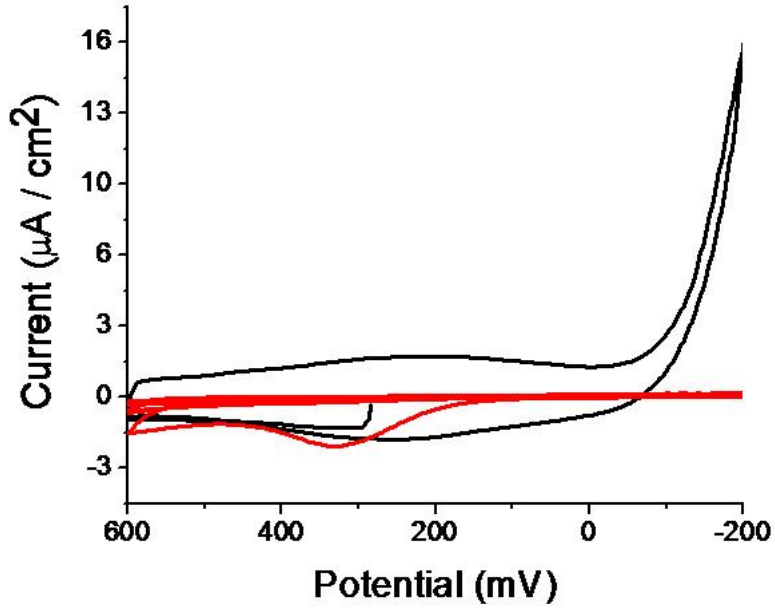

Figure 3.2.8 2 layers of BDMT/Zn^{2+} Black curve is a CV of bare gold the red curves are a CV of layers 1 and 2 of the BDMT/$Zn^{2+.}$ Scan rate = 100 mV/s vs Ag/AgCl

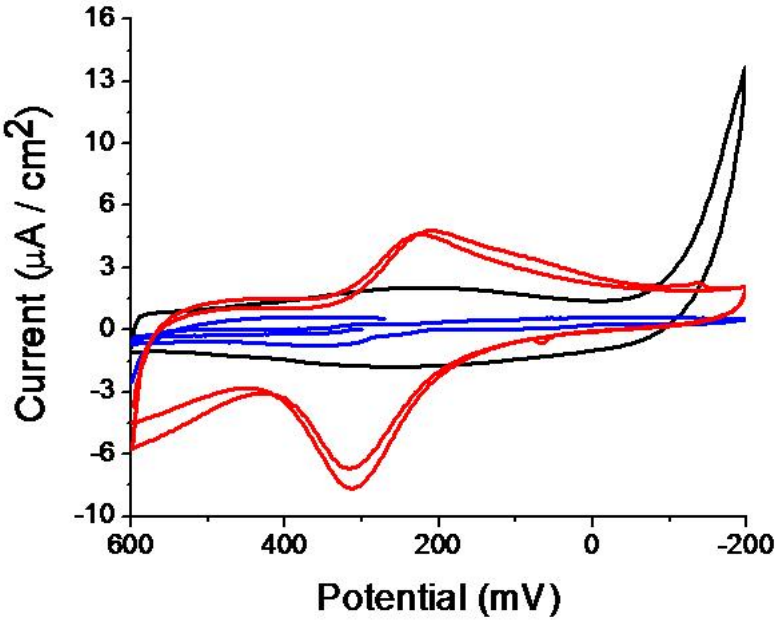

Figure 3.2.9 3 layers of MPA/Cu^{2+} Black curve is a CV of bare gold, blue curve is a CV of just the MPA and the red curves are CVs of layers 1 thru 3 of the MPA/Cu^{2+}. Scan rate = 100 mV/s vs Ag/AgCl

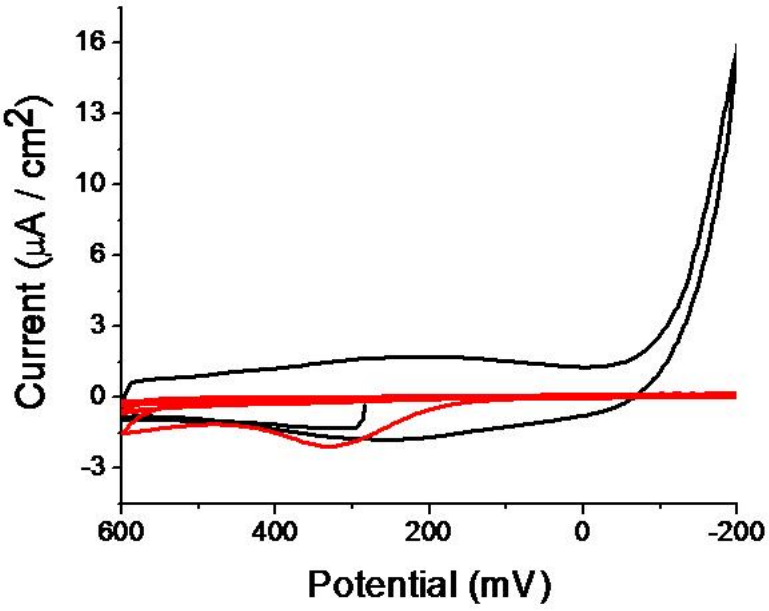

Figure 3.2.10 3 layers of MPA/Zn^{2+} Black curve is a CV of bare gold and the red curves are CVs of layers 1 thru 3 of the MPA/Zn^{2+}. Scan rate = 100 mV/s vs. Ag/AgCl

Multilayers of MPA/Cu^{2+} and MPA/Zn^{2+} were then formed. Figure 3.2.9 shows CVs of MPA/Cu^{2+} multilayers. A total of three samples with 1, 2, and 3 layers are shown. Additionally a CV of the bare gold is shown in black. The double layer capacitance decreases significantly when the initial acid terminated SAM is grown (blue curve). The acid terminated SAM is not electrochemically active until the first layer of Cu^{2+} ions (red curves) is put on. Cathodic and Anodic peaks were not seen in the same bias window for MPA/Zn^{2+} (Figure 3.2.10).

Using $CuFe(CN)_6$ as the metal source in between the organic chains, Bharathi et al. had shown that as the number of layers increased, the peak current increased.[13] Figure 3.2.11 shows CV's of two layers of BDMT/$CuFe(CN)_6$ again reversible electrochemistry is not seen. However, a chemically irreversible reduction occurs with the addition of the $Fe(CN)_6$ complex. This peak shifts to more negative potentials with increasing layers. When MPA is substituted for BDMT reversible redox peaks are seen (Figure 3.2.12). A total of 5 layers are shown and as can be seen the current in a MPA/$CuFe(CN)_6$ monolayer does increase with layer thickness. Figure 3.2.13 shows that the anodic peak current increases linearly. Based on the results of the CV's the first system to be probed using a STM was the MPA multilayers.

Later studies determined that two multilayers of MBA/$CuFe(CN)_6$ could be formed and the same current increase was seen (Figure 3.2.14). A comparison of the MPA/$CuFe(CN)_6$ to the MBA/$CuFe(CN)_6$ is shown in Figure 3.2.15. As expected, due to increased conjugation in the molecule, a higher peak current is observed with the MBA.

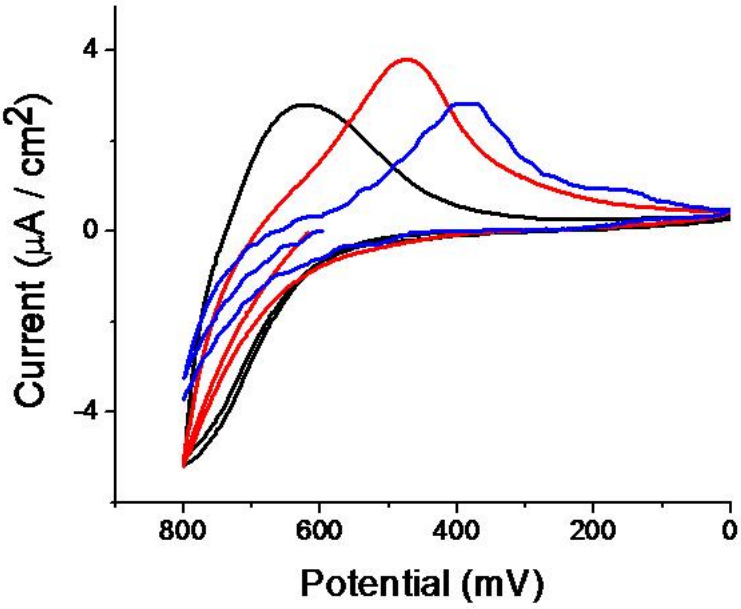

Figure 3.2.11 CV of 1 thru 3 layers of BDMT/$CuFe(CN)_6$ (Layer 1: black curve, Layer 2: red curve, Layer 3: blue curve) Scan rate = 100 mV/s vs Ag/AgCl

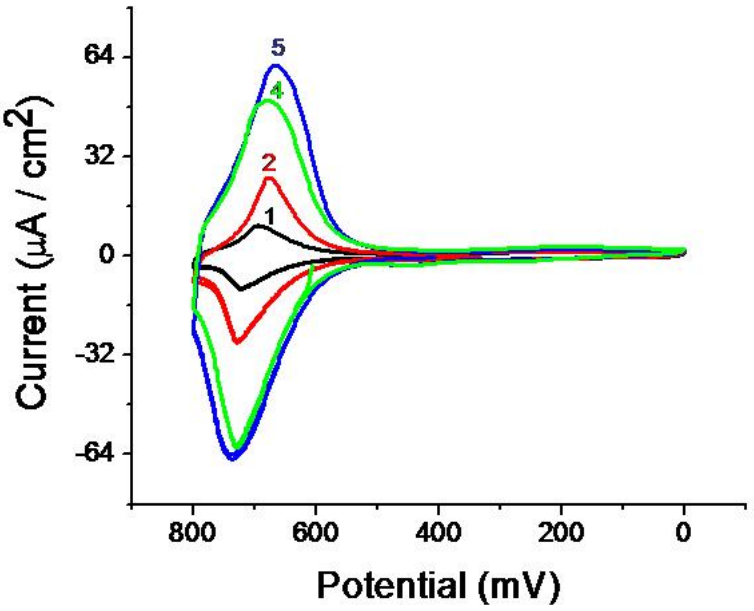

Figure 3.2.12 CV of 1 thru 5 layers of MPA/$CuFe(CN)_6^-$ Scan rate = 100 mV/s vs Ag/AgCl

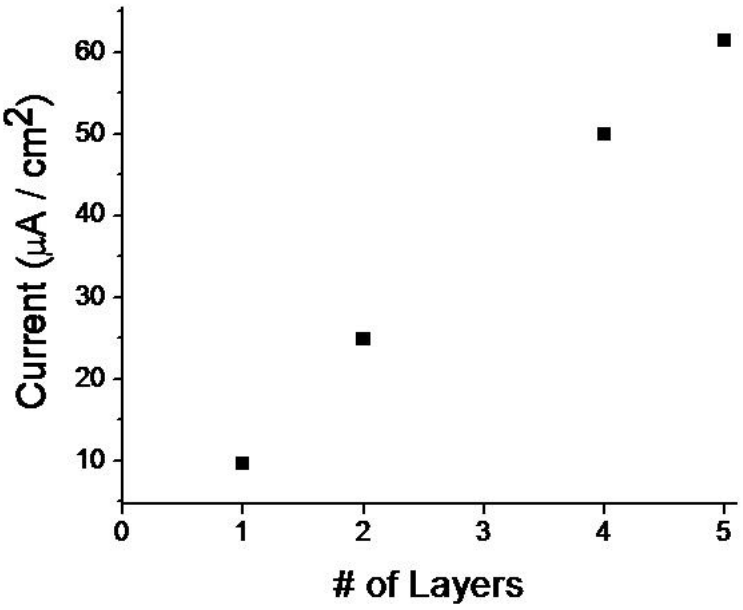

Figure 3.2.13 Anodic peak current of 1 thru 5 layers of MPA/$CuFe(CN)_6^-$ Scan rate = 100 mV/s vs Ag/AgCl

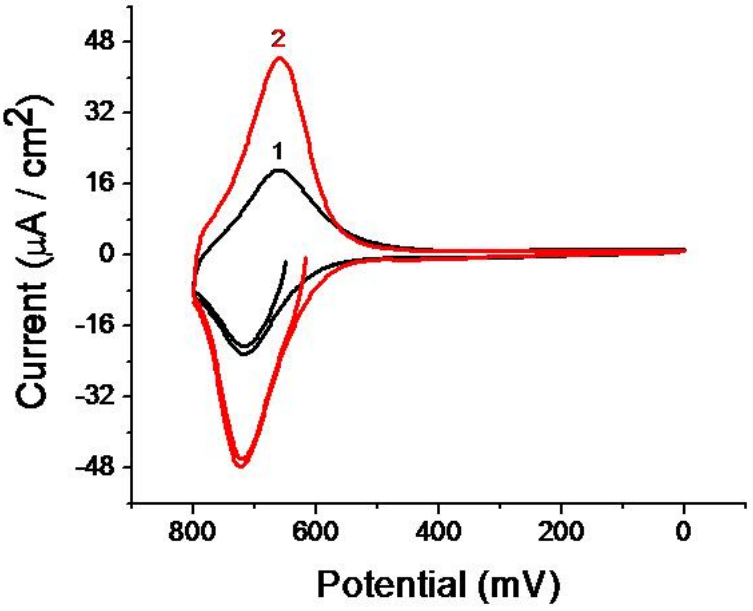

Figure 3.2.14 CV of 1 ad 2 layers of MBA/CuFe(CN)$_6$. Scan rate = 100 mV/s vs Ag/AgCl

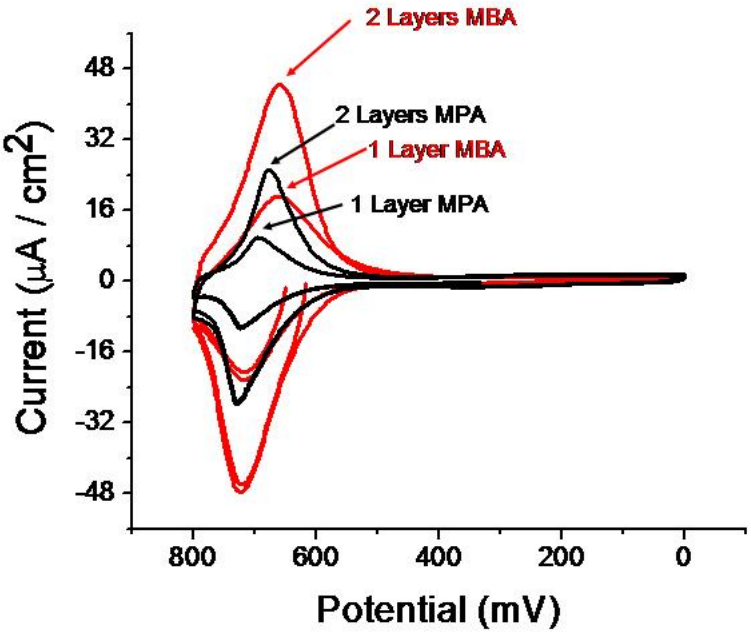

Figure 3.2.15 Comparison of CVs of 1 ad 2 layers of MBA/CuFe(CN)$_6$ (red curve) vs. MPA/CuFe(CN)$_6$ (black curves) . Scan rate = 100 mV/s vs Ag/AgCl

3.2.2b NDR and Continuous Imaging Tunneling Spectroscopy

NDR in Fc-SAM was investigated by using CITS. In discussing NDR and CITS data collection it is important to talk about how the data are analyzed. As discussed in Chapter 2 and Appendix 1, CITS mode, imaging feedback is temporarily interrupted allowing for the current to be measured in 32 individual voltage sweeps along a fast scan line (x) and this process is iterated 32 times along the slow scan axis, resulting in 1024 I-V curves. Between 5 and 10 samples are taken per Au substrate.

Table 3.2.1

	MPA	MPA / Cu	MPA / Zn
# of curves rejected out of 1024	74	531	541
# of curves that show NDR by visual inspection	8	10	6
# Of PVR with Peak height > .2nA and PVR > 1	7	36	16
Avg. peak current from PVR data	0.29 nA	0.36 nA	0.32 nA
Avg. peak current from visually selected curves	0.48 nA	0.67 nA	0.50 nA

Table (3.2.1) shows a typical breakdown of data extracted from a statistical analysis of 1024 curves. A discussion of the methods of data analysis follows: The number of curves rejected refers to the initial number of curves that show zero or saturated peak current response. It is interesting to note that only

74 curves were rejected from the monolayer, but once either Zn or Cu is added, the number of curves that gets rejected is greater that 500, this could be due to the increased saturation of the signal due to limitations of the instrument (i.e. the metal ions cause the current to increase beyond the measurable limits of the STM). The average peak current of the entire data set and the average peak current from visually selected curves did not show any statistical difference between the three types of SAMs. The numbers of curves that show NDR by visual inspection refers to the I-V curves that show the best response. In order for a curve to be considered as showing good NDR, the peak height must be greater than a threshold level of 0.2 nA (> 20% maximum signal level).

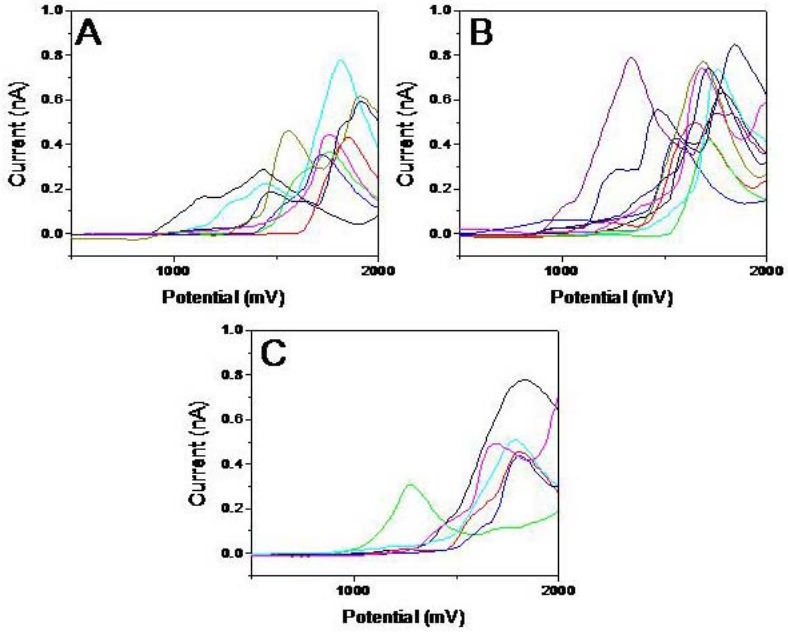

Figure 3.2.16 Visually selected IV curves of (A) MPA, (B) MPA/Cu^{2+}, (C) MPA/Zn^{2+}

This selection is subjective but provides a method for comparing different data sets. Comparison of NDR from visually selected I-V curves in a MPA monolayer

to Zn and Cu multilayers shows that there is no significant difference between the monolayer and the Zn and Cu multilayers (Figure 3.2.16 A, B and C respectively). The 10 best I-V curves for each system were also averaged together for comparison (Figure 3.2.17). To gain a statistical representation of the number of occurrences of NDR the peak position can be plotted as a histogram. Figure 3.2.18 shows histograms of the MPA monolayer and the Cu and Zn multilayers. All three histograms show the same amount of NDR within experimental error.

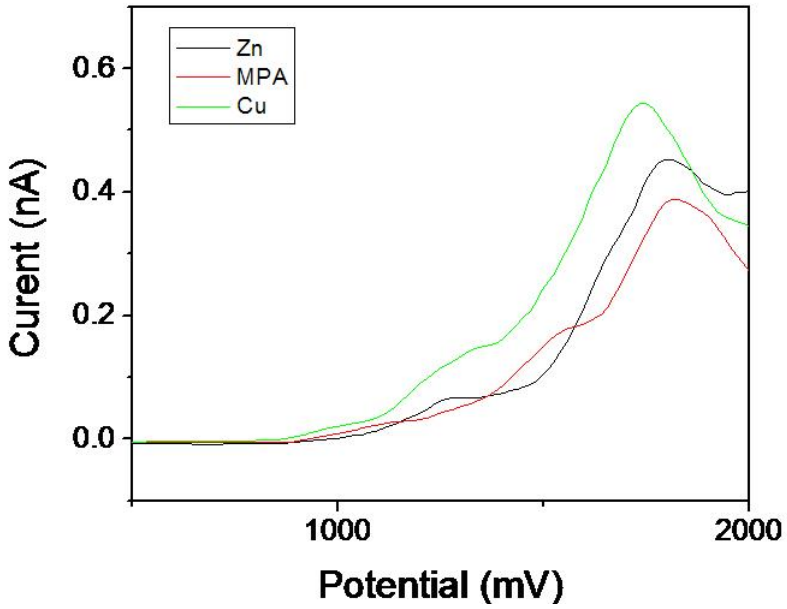

Figure 3.2.17 I-V curves of MPA, MPA/Cu^{2+}, MPA/Zn^{2+} each curve is the average of ten other representative curves.

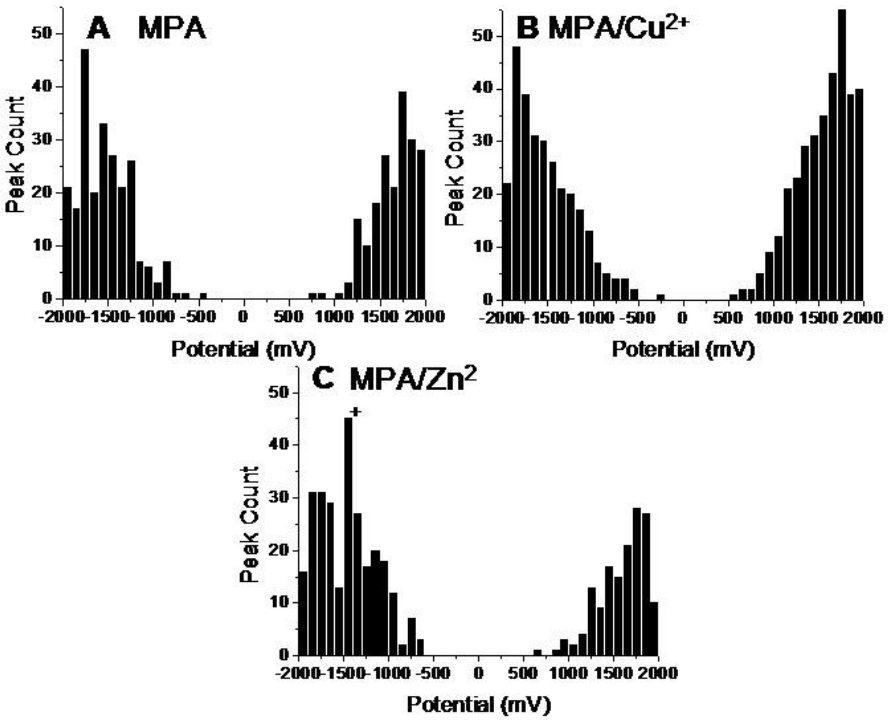

Figure 3.2.18 Histograms of NDR peak positions of MPA (A), MPA/Cu^{2+} (B), and MPA/Zu^{2+}(C)

3.3 Conclusion

Multilayers can be built, as shown by various analytical surface spectroscopic techniques. These multilayers have been shown to produce very interesting and complex redox behavior. I-V curves can be collected over them and NDR can be seen. Histograms of these systems show the same level of NDR however if more rigid criteria for what counts as NDR are used then some differences can be seen. For example, if only curves that have a peak current greater then 0.2 nA and a calculated peak to valley ratio (PVR) greater than 1 is used; then, differences could be seen between the MPA, MPA/Cu^{2+}, and MPA/Zn^{2+} data sets. The Zn layer shows twice as much NDR as the monolayer and the Cu layer shows 5 times as many NDR responses as the monolayer.

Neither the average peak current taken from the PVR data nor those taken from the visually selected curves, shows any significant difference.

As discussed in Chapter 2, variability in these systems makes it difficult to draw any real conclusions. These data suggest that NDR is much more complex than our resonant tunneling model suggests. The fact that NDR can be seen in both the Cu^{2+} and the Zn^{2+} multilayers as well as in the MPA monolayer and is seen in the same location as the Fc and MV terminated alkanethiolates suggests that there is some other electronic factor that is dominant over the position of the molecular orbitals. It is possible that the voltage drop between the tip and substrate is the dominating force and the electric field moves the MOs. NDR is not seen in methyl terminated alkanethiols but is seen in acid terminated alkanethiols. High surface free energy of the acid terminated thiolate may lead to increased surface contamination which could influence NDR. Surface contamination could also be a possibility with the charged ions (i.e., Cu^{2+} and Zn^{2+}) in the multilayers. While there are many more experiments that need to be done to further understand the nature of NDR a few general conclusions can be drawn from the existing data. NDR seems to be a phenomenon that can be seen in any molecule that has accessible molecular states. Redox activity is a good way to select molecules for I-V spectroscopy but no correlation can be made as to whether the redox potential can be correlated to NDR peak position. A better understanding of how the electronics collect the I-V curves and how NDR is influenced by them needs to be developed. As with almost all molecular

electronics experiments nailing down a mechanism for NDR may not be possible due to the complexity of the systems and the way the data are collected.

3.4 Experimental

Materials. Dodecane ($C_{12}H_{26}$), Zinc perchlorate hexahydrate ($Cl_2O_8Zn \cdot 6H_2O$) , 1,4 benzenedimethanethiol, mercaptopropionic acid and butanethiol were purchased from Aldrich and were used without further purification. Copper(II) perchlorate hexahydrate ($Cl_2O_8Cu \cdot 6H_2O$) was purchased from Acros. 4-mercaptobenzoic acid (HSC_6H_4COOH) was purchased TCI America. $K_{23}Fe(CN)_6$ was purchased from Fischer Thiols were dissolved in anhydrous ethanol (AAPER Alcohol and Chemical Co.) to form 1 mM stock solutions. Metal ions were dissolved in 18 MΩ - cm deionized water to from 50 mM stock solutions. All solutions were discarded after each use.

SAM Preparation. Evaporated gold on glass with a titanium adhesion layer were perchased from Evaparated Metals Inc. (Ithaca NY). These slides were used for all electrochemistry, XPS, surface IR and ellipsometry experiments. Prior to monolayer deposition the slides were cleaned in piranha solution (3:1 H_2SO_4:H_2O_2 (30%) by volume) for 30 seconds, rinsed with deionized water and dried under a N_2 stream. (*Caution: Piranha solution is corrosive.* In addition, care should be taken to not store piranha solution for extended lengths of time due to the formation of explosive oxides.) Au(111) substrates were incubated in 1 mM ethanol solution of various thiols for 1 hour at room temperature to form a self-assembled monolayer. After copious rinsing in ethanol and deionized water the sample was immersed into a 50 mM Cu^{2+} or Zn^{2+} solution for 1 hour. This

process was iterated until the desired number of layers was achieved. The slides were given a final rinse with ethanol and then dried in a dinitrogen stream.

For use in scanning tunneling microscopy (STM): Sample substrates were flame-annealed Au(111) facets on a gold bead formed at the end of a gold wire (Alfa Aesar, 99.999%). The wire stem was alloyed to a platinum foil (Alfa Aesar) base. Prior to monolayer deposition, the substrates were flame annealed. Au(111) substrates were incubated in 1 mM ethanol solution of various thiols for 1 hour at room temperature to form a self-assembled monolayer. After copious rinsing in ethanol and deionized water the sample was immersed into a 50 mM Cu^{2+} or Zn^{2+} solution for 1 hour. This process was iterated until the desiered number of layers was achieved. The sample substrate was mounted in a custom Kel-F fluid cell in preparation for scanning in solvent. Samples were subsequently studied by STM without further delay. The STM tips used in this work were mechanically cut Pt:Ir (90:10, Alfa Aesar, 0.254 mm diameter) wire.

VASE Spectroscopic Ellipsometer.

The VASE spectroscopic ellipsometer data uses a 75W Xe lamp as its source with a HS-190 monochromator. Thicknesses are calculated assuming a refractive index of 1.45. The angle of incidence in all studies was 68° and 70° and the wavelength was swept from 500 to 1000 nm at 1 nm/s.

X-ray Photoemission Spectroscopy (XPS).

The XPS spectra were obtained using a Riber XPS dual Mg/Al (12kV) anode source with a 14 mA emission and a spot size of 1 mm on the sample.

Electrochemistry. Cyclic voltammetry experiments were carried out in 0.1 M aqueous KCl or K_2SO_4 solution using a BAS Model 50 potentiostat and a three-electrode electrochemical cell with a Ag/AgCl reference electrode, a platinum wire counter electrode, and an evaporated gold on glass working electrode of 0.32 cm^2 surface area. All potentials are quoted with respect to Ag/AgCl.

Surface FT-IR The IR spectra were recorded on a Nicollet Ft-IR instrument with a liquid nitrogen cooled MCT-A. The spectra were recorded at room temperature at a resolution of 4 cm^{-1} and were the results of one scan with a spectral range of 900–4000 cm^{-1}. A freshly cleaned gold slide was used as a background.

Scanning Tunneling Microscopy (STM). All current–voltage data were collected on a Digital Instruments (Santa Barbara, CA) Nanoscope E, equipped with a multimode base, an E-scanner, and low-current converter with a picoamp boost stage. All experiments were performed at room temperature under ambient conditions. The sample substrate was placed in a custom-made Kel-F fluid cell and scanned in a low dielectric solvent (dodecane). Typical scanning conditions were a bias voltage of 1 V and a set-point current of 10 pA.

Scanning Tunneling Spectroscopy (I–V Data Collection). Current–voltage curves were collected for these experiments using the CITS (current imaging tunneling spectroscopy) mode in the Digital Instruments scanning

software. At least three data sets for each type of experiment were collected. Each set consisted of 1024 curves collected at regularly spaced intervals (32 x 32 array) when scanning a square region (typically 200 nm by 200 nm). During the collection of a current–voltage curve, the instrument stopped lateral tip scanning and turned off the feedback. The sweep time for each curve was 50 μs, and the bias limits were –2 V to +2 V.

Each data set was subjected to a screening process where saturated responses were removed as described previously.[12] The peak currents and valley currents were determined by analyzing the first derivative of each I–V curve. These values were used to calculate a peak-to-valley ratio (PVR) for each peak. The large number of samples per scanning area (1024 per 0.04 μm^2 area (200 nm x 200 nm)) permitted the collection of a large number of data for each sample.

3.5 References

(1) Lee, H.; Kepley, L. J.; Hong, H. G.; Mallouk, T. E. *J. Am. Chem. Soc.* **1988**, *110*, 618.

(2) Lee, H.; Kepley, L. J.; Hong, H. G.; Akhter, S.; Mallouk, T. E. *J. Phys. Chem.* **1988**, *92*, 2597.

(3) Evans, S. D.; Ulman, A.; Goppertberarducci, K. E.; Gerenser, L. J. *J. Am. Chem. Soc.* **1991**, *113*, 5866.

(4) Brust, M.; Blass, P. M.; Bard, A. J. *Langmuir* **1997**, *13*, 5602.

(5) Uosaki, K.; Sato, Y.; Kita, H. *Langmuir* **1991**, *7*, 1510.

(6) Bolink, H. J. *Photorefractive polymers*; University Library Groningen: Groningen, 1997.

(7) Koepp, H. M.; Wendt, H.; Strehlow, H. *Zeitschrift Fur Elektrochemie* **1960**, *64*, 483.

(8) Bard, A. J.; Faulkner, L. R. *Electrochemical Methods : Fundamentals and Applications*; 2 ed.; Wiley Text Books, 2000.

(9) Freeman, T. L.; Evans, S. D.; Ulman, A. *Thin Solid Films* **1994**, *244*, 784.

(10) Allara, D. L.; Parikh, A. N.; Rondelez, F. *Langmuir* **1995**, *11*, 2357.

(11) Bain, C. D.; Troughton, E. B.; Tao, Y. T.; Evall, J.; Whitesides, G. M.; Nuzzo, R. G. *J. Am. Chem. Soc.* **1989**, *111*, 321.

(12) Gorman, C. B.; Carroll, R. L.; Fuierer, R. R. *Langmuir* **2001**, *17*, 6923.

(13) Bharathi, S.; Nogami, M.; Ikeda, S. *Langmuir* **2001**, *17*, 7468.

Chapter 4

Attenuating Negative Differential Resistance in an Electroactive Self-Assembled Monolayer-Based Junction

This work was the subject of the publication, Ronald A. Wassel, Grace M. Credo, Ryan R. Fuierer, Daniel L. Feldheim, and Christopher B. Gorman, “Attenuating Negative Differential Resistance in an Electroactive Self-Assembled Monolayer-Based Junction”, Journal of the American Chemical Society, 2004, 126 (1), 295 - 300

4.1 Introduction

This chapter will discuss how the negative differential resistance (NDR) peak current observed in redox active self-assembled monolayer-based molecular junctions has been attenuated by controlling the composition of the molecular junction. The approach presented here involves capping the electroactive ferrocenyl groups with β – cyclodextrin.

Metal–molecule–metal junctions exhibiting nonlinear current voltage properties are currently the subject of several research efforts due to their proposed use as elements in molecule-scale electronic components. For example, junctions exhibiting nonlinear current–voltage properties such as negative differential resistance (NDR) are desirable because they could serve as nanoscale analogues of multistate electronic switches.[1-4] NDR behavior in conventional semiconductor-based resonant tunneling diodes (RTDs) has been tuned by modifying the materials, dopant concentration, and the physical configuration of the device.[5-9] However, control of the parameters governing NDR behavior in molecular systems is just beginning to be explored experimentally[3,10-12] and theoretically.[13-17] Recent scanning probe microscopy studies have described the use of electroactive moieties in molecular junctions to facilitate the appearance of nonlinear current–voltage behavior.[4,14,18-20] Several reports have examined the relationship between NDR and electroactivity in organic[4,18,21] and inorganic systems.[22,23] In semiconductor devices, one mechanism that results in observed NDR is resonant tunneling. A resonant tunneling diode consists of a quantum well separated from two electrical contacts by two tunnel barriers. In semiconductor devices, the quantum well is composed

of a narrow layer of material characterized by accessible quantized states (as in the well/barrier system GaAs/AlGaAs).[5] As discussed in Chapter 2, in resonant tunneling, the tunnel barriers control the probability of electrons moving from one electrode to the other through the quantum well. In an analogous molecular device (Figure 2.1.6), electroactive molecules appear to serve a similar role via accessible energy levels for electron tunneling. In RTDs, the magnitude of the NDR current peak, directly related to the resonant tunneling probability, is affected by the height and width of the barriers on each side of the well.[6-9] Tunability for conventional RTDs suggests that NDR behavior in molecular-scale systems should also exhibit predictable changes based on tunnel barrier modifications. Several relevant studies suggest that molecule-based tunnel barriers can be constructed in a rational manner.[24-30] In this paper, the results of modulating the tunnel barrier in a molecule-based system are reported. In the first example, the tunnel barrier between a ferrocene terminated self-assembled monolayer (FcC11S-SAM) and a probe STM tip was modulated by the formation of host–guest complexes consisting of cyclodextrin-ferrocene.

4.2 Results and discussion

It was hypothesized that the magnitude of the tunneling barrier between the ferrocenyl group and the STM tip could be changed by these structural modifications to the barrier. These modifications were expected and found to decrease the peak current observed through the junction as the result of increasing the effective barrier. The proposed mechanism for NDR based on resonant tunneling is illustrated qualitatively in Figure 4.2.1. A double tunnel junction was formed by the placement of an electroactive moiety between two

metal/molecule junction barriers. The tunnel junction was not likely to be symmetric due to the differences between the alkylthiolate Au–S bond on the substrate side and the gap between the ferrocene headgroup and STM tip.[31,32] The precise shape of the tunneling barriers is unknown, but the increase in tunnel barrier with increasing molecular length was precedented as discussed above. On the left side of Figure 4.2.1A, resonant tunneling through a ferrocenyl group is depicted using an unmodified tip. On the right side of Figure 4.2.1A, placing another chemical species between the tip and ferrocenyl group alters the tunnel barrier between tip and ferrocene (via an increase in the width and/or height of the barrier). Figure 4.2.1B depicts negligible resonant tunneling current with zero applied bias on the substrate. With an increase in substrate potential, a maximum in peak current was observed as tunneling occurs through a resonant molecular state (Figure 4.2.1C). Whether this is the highest occupied molecular orbital (HOMO)[33] or lowest occupied molecular orbital (LUMO)[34] is unclear but depends on the relative Fermi energies of the metal contacts with respect to the molecule in the junction. In Figure 4.2.1D, as the coupling between the tip and a resonant state in the molecule reaches a minimum value, current decreases. Finally, in Figure 4.2.1E, as the substrate potential becomes more positive, current continues to increase via other injection processes such as thermionic emission.

Negative Differential Resistance

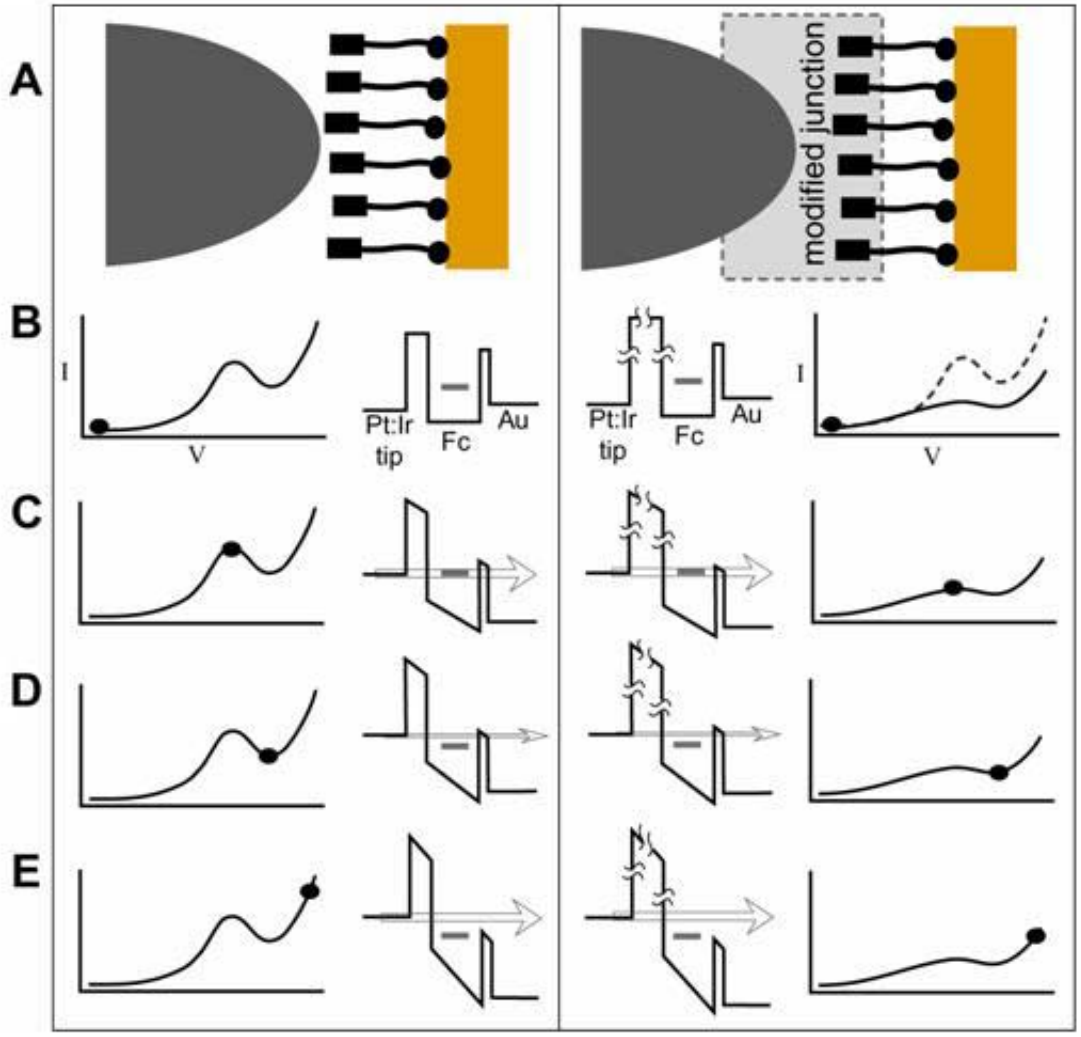

Figure 4.2.1Qualitative model for the attenuation of NDR peak current by modification of the STM tip/ferrocenyl tunnel junction. (A) Schematics of the two junctions and energy level diagrams indicating the two junctions (B) at zero applied bias, (C) in resonance with the molecular orbital (MO) associated with the ferrocenyl headgroups, (D) out of resonance with the MO associated with the ferrocenyl headgroups, and (E) exhibiting an increase in nonresonant current.

It was hypothesized that reduction in the electron-transfer rate due to the capping of the ferrocenyl (Fc) groups with β-cyclodextrin (β-CD) would result in a decrease in the magnitude of the observed NDR. Electrochemical studies of Fc-CD complexes in solution have exhibited slowed electron-transfer kinetics following exposure of the Fc to CD as a result of the formation of a 1:1 host–guest inclusion complex.[35-39] In an electrochemical experiment, the presence of the cyclodextrin slows the kinetics of electron transfer to the ferrocenyl moiety. Although the cyclodextrin has several effects on the electrochemistry that are not relevant here (e.g., its effect on the diffusion rate of the ferrocene and access of counter ions to the oxidized form), a similar complexation was expected to increase the magnitude of the tunnel barrier and result in a decrease in the steady-state current flowing through the ferrocenyl moiety in a tip–molecule–substrate junction. After scanning an unmodified $FcC_{11}S$-SAM, I–V curves exhibited the same NDR behavior as previously reported.[40] This sample was incubated in an aqueous solution containing β-CD, rinsed, and I–V curves were obtained by STM. Following exposure to the complexation agent, the I–V behavior of the $FcC_{11}S$-SAM exhibited a marked attenuation in peak current as can be observed in Figure 4.2.2. Figure 4.2.2A shows several representative I–V traces for an unmodified $FcC_{11}S$-SAM as probed by an STM tip. Figure 4.2.2B shows analogous I–V traces for a $FcC_{11}S$-SAM that had been incubated in β-cyclodextrin prior to collection of the data. Several traces are shown to indicate the variation observed across a large dataset.

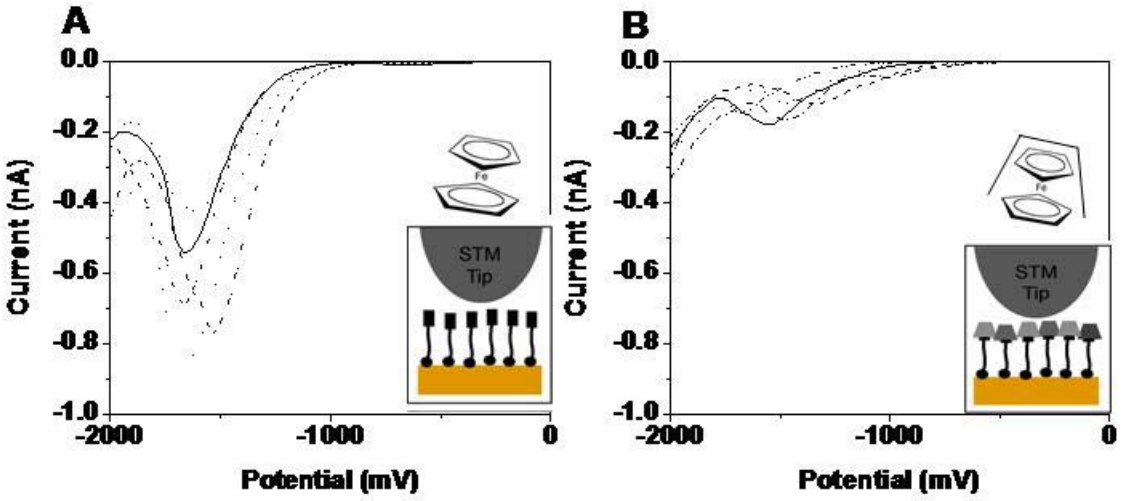

Figure 4.2.2 Current–voltage curves of $FcC_{11}S$-SAM and β-CD $FcC_{11}S$-SAM, as indicated. The insets are schematics of the STM tip-based molecular junctions and are not drawn to scale

However, the peak current was observed to decrease by approximately a factor of 4 as the result of complexation with the β -CD. To rule out nonspecific binding, similar samples were exposed to α-cyclodextrin (α-CD), a molecule that is too small to bind to ferrocene. Attenuation of the peak NDR current was not observed as the result of complexation with α -CD. Data were also obtained on a dodecanethiolate SAM ($C_{12}S$-SAM), which had no electroactive functionality, to verify that this system did not exhibit NDR response.[31,32,40] The curves shown in Figure 4.2.2 are representative of a larger data set. Sets of 1024 current–voltage traces captured across several regions of each sample were examined. The peak-to-valley ratio (PVR)[35,41] of each curve was tabulated. The PVR indicates the ratio of the peak current to the minimum current measured in the region of

negative differential resistance. An average peak to valley ratio (PVR) of 2.14 ± 1.56 was determined for FcC11S-SAMs, which was larger than the average PVR of 1.39 ± 0.48 determined for FcC11S-SAMs complexed with β-CD. Representative histograms comparing the FcC11S-SAM with the β-CDFcC11S-SAM are show in Figure 4.2.3A and B. The histograms do not show any difference between the two, supporting the conclusion that the mechanism of NDR was not changed by the complexation of β-CD, only the tunneling barrier was changed.

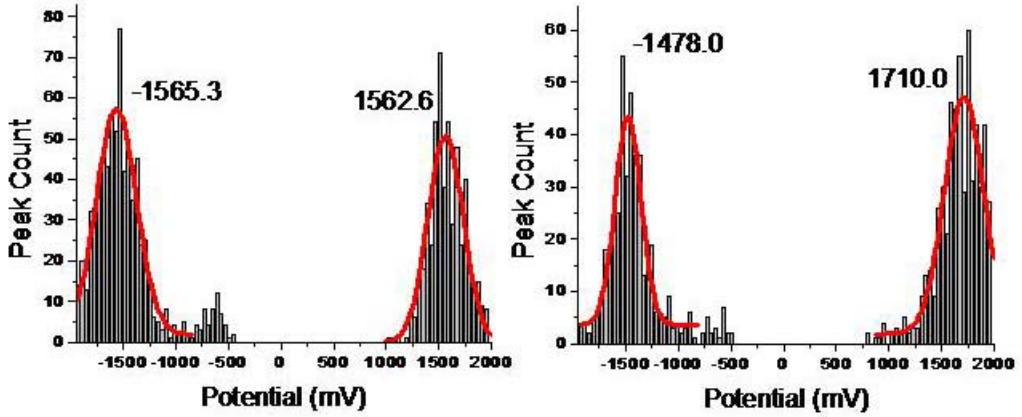

Figure 4.2.3 Representative histograms of NDR peak position of A) $FcC_{11}S$-SAM and B) β-CD $FcC_{11}S$-SAM Histograms are fit to a Gaussian model

Current - distance (I–z) spectroscopy was employed as a complementary method to quantify the change in tunnel barrier upon β-CD complexation. In this experiment, the exponential decrease in current was measured as the tip was retracted vertically from the substrate (Figure 4.2.4). This type of analysis was originally employed for the measurement of tunnel barriers in clean, metal/vacuum/metal[42] and semiconductor[35,43,44] junctions.

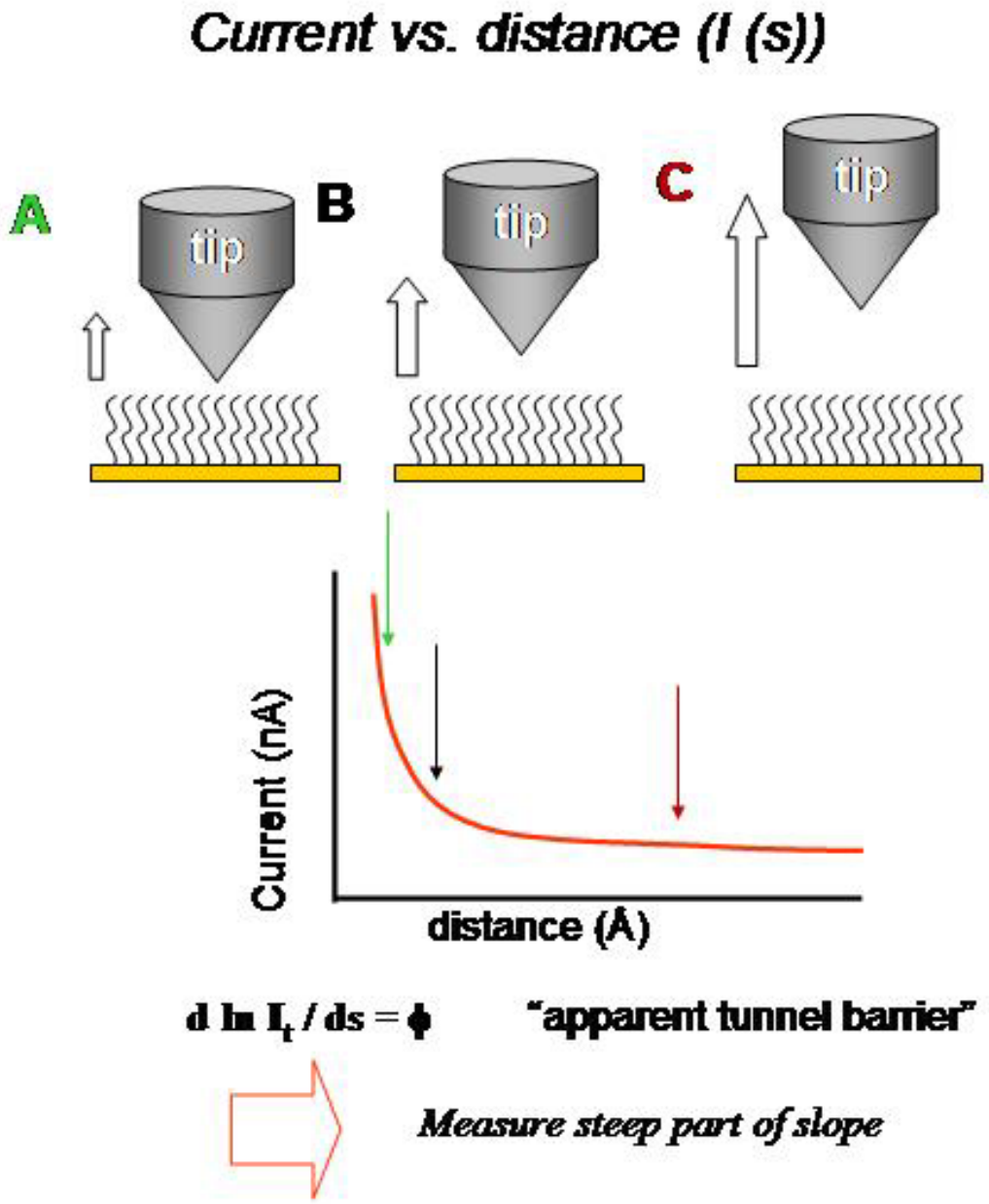

Figure 4.2.4 Schematic of current distance spectroscopy performed over a SAM. As the tip was retracted (A-C) the current decays exponentially.

This technique then evolved into the study of tunneling through thin water layers.[45,46] Most recently, I–s spectroscopy has been employed in the analysis of metal/molecule/metal junctions.[32,47] In this latter case, the physical significance

of the tunnel barrier calculated from these data is more ambiguous since the distance between the tip and the SAM is unknown.[32] Nevertheless, I–s spectroscopy appears to be a quantitative way to show that the modification of the tunnel junction affects the current–voltage behavior. Note that this type of measurement, in which the tip is moved relative to the SAM, is not the same as that in which the current through a molecule-based junction is measured for a set of iso-structural molecules of differing length. This latter type of experiment calculates a distance dependence of a steady-state current, β, where $i = i_o \exp(-\beta d)$ and d is the length of the molecule.

To measure the variation in the tunneling barrier, current versus distance measurements were obtained on four types of samples: dodecanethiolate self-assembled monolayers on gold (C_{12}S-SAMs), FcC_{11}S-SAMs, FcC_{11}S-SAMs that had been exposed to β-CD (abbreviated β-CD-FcC_{11}S-SAM), and FcC_{11}S-SAMs that had been exposed to α-CD (abbreviated α -CD-FcC_{11}S-SAM, although this latter molecule was not expected to bind to the FcC_{11}S-SAM). The α-CD-FcC_{11}S-SAM was employed as a control experiment to rule out modulation of tunneling due to adventitious adsorption onto the SAM. From these data, an apparent tunneling barrier (ϕ) was calculated. This quantity is defined as:

$$\phi = \left(\frac{1}{1.025}\right)\frac{\partial \ln I}{\partial \ln S}$$

where S is the relative distance of the tip as it was retracted from the sample.[42] The use of this equation in establishing tunneling barriers has been discussed in detail previously.[42] Because the initial distance of the tip from the SAM was unknown, the relative interaction of the tip with the SAM was unknown, leading to

ambiguity in the physical significance of this quantity. For our purposes, we are only concerned with the comparison of ϕ between the various monolayers studied. Figure 4.2.5 illustrates the range of ϕ values measured across several data sets with different tips and samples. Variation in each type of assembly was observed (similar to that observed in the current–voltage data shown in Figure 4.2.3. Reasons for this variation that have been previously proposed include fluctuation in tip–sample geometry, the orientation of the molecules on the surface, and the shape of the tip during the experiment. Nevertheless, trends in the variation of this ϕ value can be obtained. As compared to a C_{12}S-SAM (with an average ϕ, ϕ_{avg} = 1.1 ± 0.3, Figure 4.2.5A), the average tunneling barrier for FcC_{11}S-SAMs (ϕ_{avg} = 0.31 ± 0.22, Figure 4.2.5B) was reduced by a factor of approximately 4. Upon complexation, the β-CD-FcC_{11}S-SAM substrate shows an increased average tunnel barrier (ϕ_{avg} = 0.92 ± 0.67, Figure 4.2.5C). This result was anticipated, given the expected increase in tunnel barrier through the β-CD. Notably, these data show a wider distribution. This plausibly was due to incomplete encapsulation of every ferrocenyl group by a β -CD. In contrast, little change in the α-CD-FcC_{11}S-SAM data was observed (ϕ_{avg} = 0.39 ± 0.32 Figure 4.2.5D) as compared to those in Figure 4.2.5B, consistent with a non-complexed FcC_{11}S-SAM. This result ruled out alteration of the tunnel barrier due to nonspecific adsorption or other contamination during the incubation step.

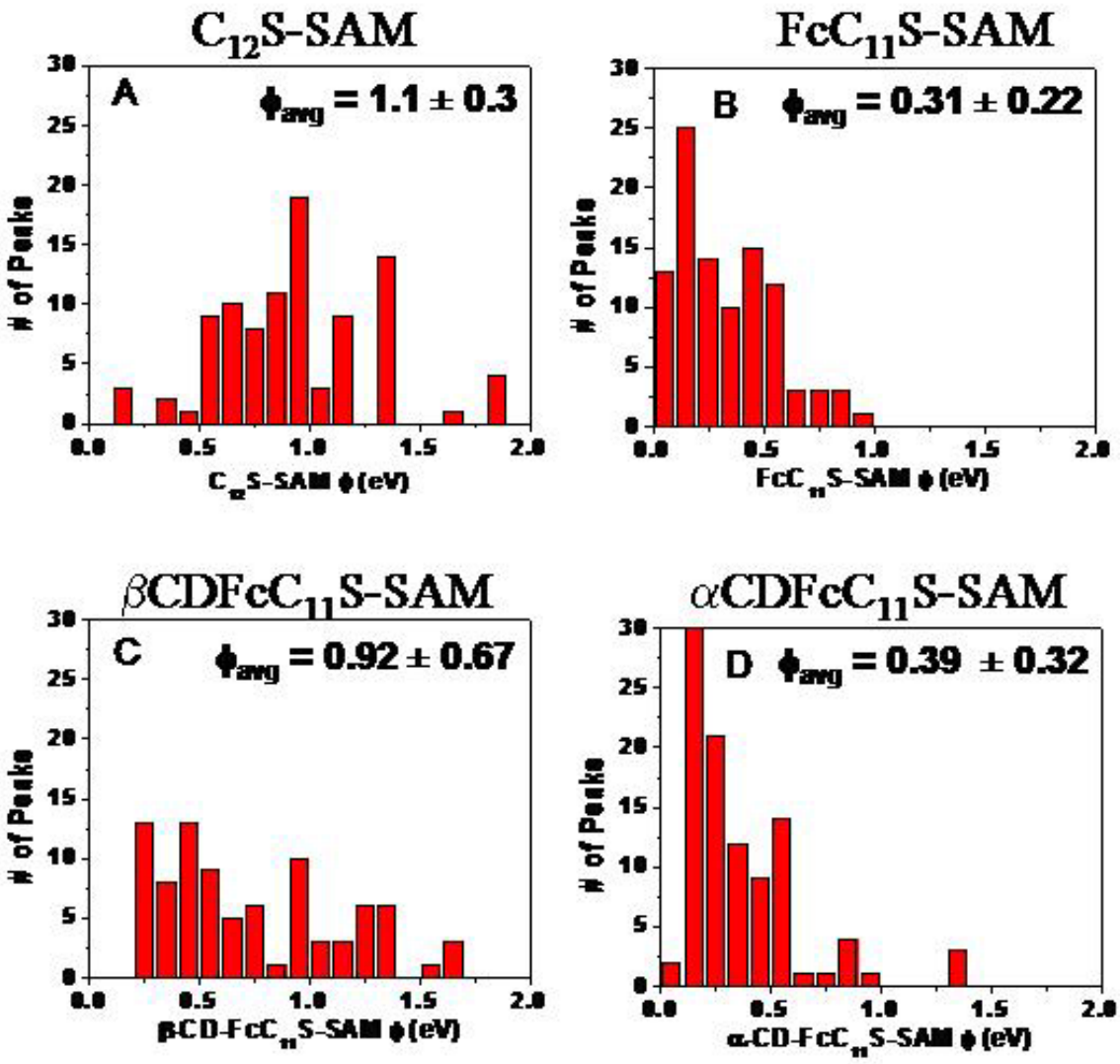

Figure 4.2.5 Histograms tabulating the apparent tunnel barriers measured for (A)C_{12}S-SAM, (B) FcC_{11}S-SAM, (C) β-CD-FcC_{11}S-SAM, and (D) α-CD-FcC_{11}S-SAM. Average values (one standard deviation; Φ_{avg} are indicated.

.

To further support the contention that β-CD complexes with FcC_{11}S-SAM but α-CD does not, Polarization Modulation Infrared Reflection Absorption Spectroscopy (PM-IRRAS) spectra were obtained on FcC_{11}S-SAM (Figure 4.2.6A), β -CD-FcC_{11}S-SAM (Figure 4.2.6C), and FcC_{11}S-SAM that had been incubated with α -CD (Figure 4.2.6B indicated as α -CD-FcC_{11}S-SAM). The most

diagnostic peak in the $FcC_{11}S$-SAM was a strong peak at 1107 cm^{-1} which was assigned as a γ(CH) mode on the ferrocenyl moiety based on assignments previously reported by Porter et al.[48] In the α-CD-$FcC_{11}S$-SAM samples, no differences were observed as compared to the $FcC_{11}S$-SAM samples. When β-CD-$FcC_{11}S$-SAM samples were prepared in an identical fashion (e.g., incubation with the cyclodextrin for 24 h followed by rinsing with water and ethanol), the γ (CH) mode on the ferrocenyl moiety shifted to 1085 cm^{-1} and a new mode at 1157 cm^{-1} was observed. This latter band was assigned to C–O stretching in the cyclodextrin. These data are all consistent with surface-bound complexation of β-CD and $FcC_{11}S$-SAM but a lack of complexation between α-CD and $FcC_{11}S$-SAM.

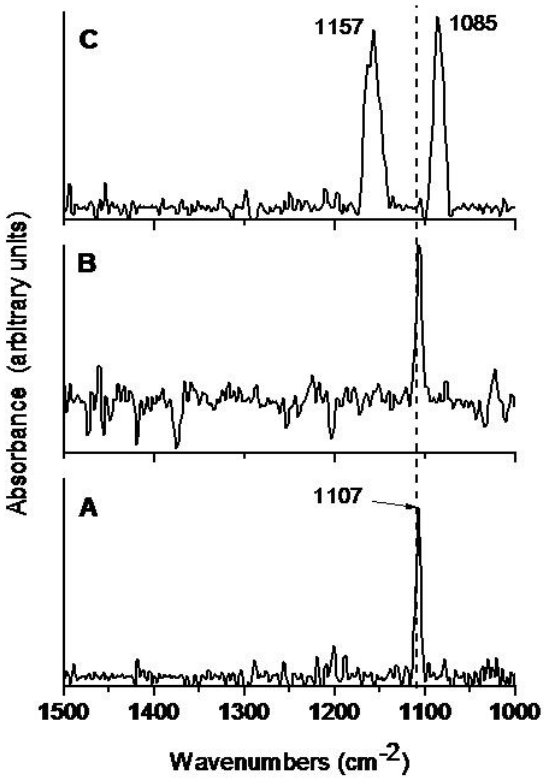

Figure 4.2.6 PM-IRRAS spectra of A) $FcC_{11}S$-SAM, B) α-CD-$FcC_{11}S$-SAM and C) β-CD-$FcC_{11}S$-SAM

4.3 Conclusions

The rational attenuation of molecule-based NDR behavior in electroactive, ferrocene-terminated thiolate SAMs at room temperature has been demonstrated. This result has been obtained via noncovalent encapsulation of the ferrocenyl groups using β-cyclodextrin. The magnitude of the peak tunneling current was shown to decrease with increasing tunnel barrier, as been proposed in conventional resonant tunneling diodes. This tunnel barrier has also been quantitatively probed using current–distance spectroscopy. From the standpoint of device engineering, functionalization of one contact in an RTD to reduce the peak current was desired in some cases. These include lower power consumption due to lower turn-on voltage and faster switching time, since it would take less time to reach the peak current.[5] Ideally, this was done without decreasing the signal-to-noise ratio. In the case of semiconductor-based RTDs, the quantitative relationship between the tunnel barrier and observed peak current was complex.[9,31,42] In general, however, an increase in tunnel barrier height or width reduces the steady-state current through the device. These data provide a measure of how tunnel barriers attenuate peak current at the molecular level in a SAM-based system.

4.4 Experimental

Materials. Dodecane and n-alkanethiols ($HS(CH_2)_{n-1}CH_3$ (n = 3, 6, 7, 12, 16) were purchased from Aldrich and were used without further purification. 11 Ferrocenylundecanethiol ($Fc(CH_2)_{11}SH$, abbreviated here as $FcC_{11}SH$) was prepared according to previously published procedures.[49,50] n-Alkanethiols were

dissolved in anhydrous ethanol (Aaper Alcohol and Chemical Co.) to form 1 mM stock solutions. β-Cyclodextrin (β-CD) was purchased from Fluka ,and α-cyclodextrin (α -CD) was purchased from Sigma. Both cyclodextrin molecules were used without further purification. Cyclodextrins were dissolved in deionized water to form 5 mM stock solutions. All solutions were discarded after each use.

SAM Preparation. Prior to monolayer deposition, the substrates were cleaned in piranha solution (3:1 H_2SO_4:H_2O_2 (30%) by volume). *Caution: Piranha solution is corrosive.* In addition, care should be taken to not store piranha solution for extended lengths of time due to the formation of explosive oxides. Sample substrates were flame-annealed Au(111) facets on a gold bead formed at the end of a gold wire (Alfa Aesar, 99.999%). The wire stem was alloyed to a platinum foil (Alfa Aesar) base. Au(111) substrates were incubated in 1 mM ethanol solution of ferrocenyl undecylthiol for at least 24 h at room temperature to form a ferrocenyl-terminated self-assembled monolayer ($FcC_{11}S$-SAM). After copious rinsing in ethanol and drying in a dinitrogen stream, the sample holder was mounted in a custom Kel-F fluid cell in preparation for scanning in solvent.

Ferrocene-Cyclodextrin Complexation. Au(111) substrates coated with a FcC11S-SAM were incubated in 5 mM aqueous solution of β-CD or α-CD for at least 12 h at room temperature. Samples were rinsed in water and then ethanol and dried in an N_2 stream. Samples were subsequently studied by STM without further delay.

Scanning Tunneling Microscopy (STM). All current–voltage data were collected on a Digital Instruments (Santa Barbara, CA) Nanoscope E, equipped

with a multimode base, an E-scanner, and low-current converter with a picoamp boost stage. All experiments were performed at room temperature under ambient conditions. Current–distance (I–d) measurements were performed using a RHK (Troy, MI) SPM 1000 controller with the same Digital Instruments multimode base, E-scanner, and low-current converter. The sample substrate was placed in a custom-made Kel-F fluid cell and scanned in a low dielectric solvent, such as dodecane or mesitylene. Typical scanning conditions for both types of measurements were a bias voltage of 1 V and a set-point current of 10 pA.

Scanning Tunneling Spectroscopy (I–V Data Collection). Current–voltage curves were collected for these experiments using the CITS (current imaging tunneling spectroscopy) mode in the Digital Instruments scanning software. At least three data sets for each type of experiment were collected. Each set consisted of 1024 curves collected at regularly spaced intervals (32 x 32 array) when scanning a square region (typically 200 nm by 200 nm). These results were comparable to those obtained when the tip was not scanning (zero scan size). During the collection of a current–voltage curve, the instrument stopped lateral tip scanning and turned off the feedback. The sweep time for each curve was 150 μs, and the bias limits were –2 V to +2 V. Each data set was subjected to a screening process where saturated responses were removed as described previously. The peak currents and valley currents were determined by analyzing the first derivative of each I–V curve. These values were used to calculate a peak-to-valley ratio (PVR) for each peak. The large number of samples per

scanning area (1024 per 0.04 μm2 area (200 nm x 200 nm)) permitted the collection of a large number of data for each sample.

Current–Distance Spectroscopy. Current–distance (I–d) spectroscopy data were also collected on at least three samples with three different tips for each type of sample (C_{12}S-SAM, FcC_{11}S-SAM, β-CD-FcC_{11}S-SAM, and α-CD-FcC_{11}S-SAM). The tip was placed at various positions on the substrate, and the current was recorded as the tip was retracted 2 Å. At least 50 curves were collected for each individual sample. Each curve was acquired at a set point of 10 Pa and 1 V, and 32 points per curve were taken with an acquisition time of 100μs.

Polarization Modulation Infrared Reflection Absorption Spectroscopy (PM-IRRAS). The PM-IRRAS spectra were recorded on a Digilab FTS 6000 spectrometer equipped with a step scan interferometer, liquid nitrogen cooled narrow band MCT detector, globar source, and a UDR-4 filter. The IR radiation was typically phase modulated at frequencies of 400 or 800 Hz at an amplitude of 1.0 or 2.0 λ HeNe while stepping at 0.5–2.5 Hz. A gold grid polarizer was used to obtain either s- or p-polarized radiation, which was then modulated by a Hinds ZnSe PEM operating at 37 kHz and amplitude of 0.5 λ (strain axis 45° degrees to the polarizer) before reflecting off the sample at an incident angle of 80□degrees from the surface normal. The spectra were recorded at room temperature at a resolution of 4 cm^{-1} and were the results of one scan with a spectral range of 900–4000 cm^{-1}. The digital signal processing (DSP) algorithm incorporated into the Digilab spectrometer software was used to obtain the spectra, which eliminates the need for a separate reference gold slide.

4.5 References

(1) Sze, S. M. *Physics of Semiconductor Devices, 2nd ed.* New York, 1981; Vol. John Wiley & Sons.

(2) Chen, J.; Reed, M. A.; Rawlett, A. M.; Tour, J. M. *Science* **1999**, *286*, 1550.

(3) Selzer, Y.; Salomon, A.; Ghabboun, J.; Cahen, D. *Angew. Chem.-Int. Edit.* **2002**, *41*, 827.

(4) Gorman, C. B.; Carroll, R. L.; Fuierer, R. R. *Langmuir* **2001**, *17*, 6923.

(5) Sun, J. P.; Haddad, G. I.; Mazumder, P.; Schulman, J. N. *Proc. IEEE* **1998**, *86*, 641.

(6) Zhao, P. J.; Cui, H. L.; Woolard, D.; Jensen, K. L.; Buot, F. A. *J. Appl. Phys.* **2000**, *87*, 1337.

(7) Huang, C. Y.; Morris, J. E.; Su, Y. K.; Kuo, T. H. *Electron. Lett.* **1994**, *30*, 1012.

(8) Zhao, P. J.; Cui, H. L.; Woolard, D. L.; Jensen, K. L.; Buot, F. A. *IEEE Trans. Electron Devices* **2001**, *48*, 614.

(9) Schulman, J. N.; Santos, H. J. D.; Chow, D. H. *IEEE Electron Device Lett.* **1996**, *17*, 220.

(10) Xue, Y. Q.; Datta, S.; Ratner, M. A. *J. Chem. Phys.* **2001**, *115*, 4292.

(11) Lu, X.; Hipps, K. W. *J. Phys. Chem. B* **1997**, *101*, 5391.

(12) Song, I. K.; Kaba, M. S.; Barteau, M. A. *Langmuir* **2002**, *18*, 2358.

(13) Leonard, F.; Tersoff, J. *Phys. Rev. Lett.* **2000**, *85*, 4767.

(14) Karzazi, Y.; Cornil, J.; Bredas, J. L. *J. Am. Chem. Soc.* **2001**, *123*, 10076.

(15) Paulsson, M.; Stafstrom, S. *Phys. Rev. B* **2001**, *6403*.

(16) Han, J. E.; Crespi, V. H. *Appl. Phys. Lett.* **2001**, *79*, 2829.

(17) Seminario, J. M.; Zacarias, A. G.; Tour, J. M. *J. Phys. Chem. A* **1999**, *103*, 7883.

(18) Tao, N. J. *Phys. Rev. Lett.* **1996**, *76*, 4066.

(19) Hipps, K. W.; Barlow, D. E.; Mazur, U. *J. Phys. Chem. B* **2000**, *104*, 2444.

(20) Scudiero, L.; Barlow, D. E.; Hipps, K. W. *J. Phys. Chem. B* **2000**, *104*, 11899.

(21) Chen, J.; Wang, W.; Reed, M. A.; Rawlett, A. M.; Price, D. W.; Tour, J. M. *Appl. Phys. Lett.* **2000**, *77*, 1224.

(22) Kinne, M.; Barteau, M. A. *Surf. Sci.* **2000**, *447*, 105.

(23) Kaba, M. S.; Song, I. K.; Barteau, M. A. *J. Vac. Sci. Technol. A-Vac. Surf. Films* **1997**, *15*, 1299.

(24) Boulas, C.; Davidovits, J. V.; Rondelez, F.; Vuillaume, D. *Phys. Rev. Lett.* **1996**, *76*, 4797.

(25) Holmlin, R. E.; Haag, R.; Chabinyc, M. L.; Ismagilov, R. F.; Cohen, A. E.; Terfort, A.; Rampi, M. A.; Whitesides, G. M. *J. Am. Chem. Soc.* **2001**, *123*, 5075.

(26) Holmlin, R. E.; Ismagilov, R. F.; Haag, R.; Mujica, V.; Ratner, M. A.; Rampi, M. A.; Whitesides, G. M. *Angew. Chem.-Int. Edit.* **2001**, *40*, 2316.

(27) Wold, D. J.; Frisbie, C. D. *J. Am. Chem. Soc.* **2000**, *122*, 2970.

(28) Wold, D. J.; Frisbie, C. D. *J. Am. Chem. Soc.* **2001**, *123*, 5549.

(29) Cui, X. D.; Primak, A.; Zarate, X.; Tomfohr, J.; Sankey, O. F.; Moore, A. L.; Moore, T. A.; Gust, D.; Harris, G.; Lindsay, S. M. *Science* **2001**, *294*, 571.

(30) Cui, X. D.; Zarate, X.; Tomfohr, J.; Sankey, O. F.; Primak, A.; Moore, A. L.; Moore, T. A.; Gust, D.; Harris, G.; Lindsay, S. M. *Nanotechnology* **2002**, *13*, 5.

(31) Appenzeller, J.; Knoch, J.; Martel, R.; Derycke, V.; Wind, S. J.; Avouris, P. *IEEE Trans. Nanotechnol.* **2002**, *1*, 184.

(32) Beebe, J. M.; Engelkes, V. B.; Miller, L. L.; Frisbie, C. D. *J. Am. Chem. Soc.* **2002**, *124*, 11268.

(33) Damle, P.; Rakshit, T.; Paulsson, M.; Datta, S. *IEEE Trans. Nanotechnol.* **2002**, *1*, 145.

(34) Bhatt, J.; Fung, B. M.; Nicholas, K. M. *J. Organomet. Chem.* **1991**, *413*, 263.

(35) Altfeder, I. B.; Golovchenko, J. A.; Narayanamurti, V. *Phys. Rev. Lett.* **2001**, *87*, 0568011.

(36) Isnin, R.; Salam, C.; Kaifer, A. E. *J. Org. Chem.* **1991**, *56*, 35.

(37) Ju, H. X.; Leech, D. *Langmuir* **1998**, *14*, 300.

(38) Schonherr, H.; Beulen, M. W. J.; Bugler, J.; Huskens, J.; van Veggel, F.; Reinhoudt, D. N.; Vancso, G. J. *J. Am. Chem. Soc.* **2000**, *122*, 4963.

(39) Fuierer, R. R.; Carroll, R. L.; Feldheim, D. L.; Gorman, C. B. *Adv. Mater.* **2002**, *14*, 154.

(40) Carroll, R. L.; Fuierer, R.; Gorman, C. B. In *Molecules as Components of Electronic Devices*; Amer. Chem. Soc.: Washington, 2003; Vol. 844, pp 10.

(41) Borgstrom, M.; Bryllert, T.; Sass, T.; Gustafson, B.; Wernersson, L. E.; Seifert, W.; Samuelson, L. *Appl. Phys. Lett.* **2001**, *78*, 3232.

(42) Besenbacher, F. *Rep. Prog. Phys.* **1996**, *59*, 1737.

(43) Hahn, J. R.; Hong, Y. A.; Kang, H. *Appl. Phys. A-Mater. Sci. Process.* **1998**, *66*, S467.

(44) Grandidier, B.; Nys, J. P.; Stievenard, D.; de la Broise, X.; Delerue, C.; Lannoo, M. *Appl. Phys. A-Mater. Sci. Process.* **1998**, *66*, S977.

(45) Barteau, M. A.; Song, I. K.; Lyons, J. E. *Abstr. Pap. Am. Chem. Soc.* **2002**, *223*, U22.

(46) Fleming, M. S.; Walt, D. R. *Langmuir* **2001**, *17*, 4836.

(47) Bogozi, A.; Lam, O.; He, H. X.; Li, C. Z.; Tao, N. J.; Nagahara, L. A.; Amlani, I.; Tsui, R. *J. Am. Chem. Soc.* **2001**, *123*, 4585.

(48) Popenoe, D. D.; Deinhammer, R. S.; Porter, M. D. *Langmuir* **1992**, *8*, 2521.

(49) Gorman, C. B.; Touzov, I.; Carroll, R. L. *Abstr. Pap. Am. Chem. Soc.* **1998**, *216*, U44.

(50) Uosaki, K.; Sato, Y.; Kita, H. *Langmuir* **1991**, *7*, 1510.

Chapter 5

Stochastic Variation in the Relative Conductance of Electroactive Molecules

This was the subject of a publication, Ronald A. Wassel, Ryan R. Fuierer, Namjin Kim, and Christopher B. Gorman “Stochastic Variation in Conductance on the Nanometer Scale: A General Phenomenon” Nano Letters,2003, 3 (11),1617-1620 *

5.1 Introduction

Understanding how conductance changes with time in molecular junctions is extremely important to the rational design of future molecular based devices. The conductance of a nanometer-scale, metal-molecule-metal junction is dependent on several factors. Notable among these is the conformation and orientation of the molecules in the junction and any conformational changes that these molecules can undergo with respect to the metallic contacts. Stochastic switching (random changes) between various conductances should occur in any junction composed of a small enough collection of molecules. This phenomenon has been observed using a scanning tunneling microscope (STM) tip in contact with a self assembled monolayer (SAM) as one of the metallic contacts.

The Gorman group has previously observed that when replacement lithography (Figure 2.2.5) was performed with electroactive molecules, they spontaneously inserted themselves into the background SAM.[1,2] This type of replacement was labeled as “adventitious replacement” and occurred in areas where the monolayer was disordered such as step edges, pits and domain boundaries. Weiss et al. have observed the same behavior in their phenylene ethynylene-based oligomers (OPEs). He used this phenomenon to study the current – voltage properties of individual OPE molecules inserted into a *n*-alkanethiolate background SAM. The Weiss group also observed conductance changes over time (“blinking”) in the phenylene ethynylene-based oligomers inserted into a host SAM.[3-7] This change in conductance was attributed to conformational changes within the molecule. Lindsay et al. also observed conductance changes over time in

alkanedithiol SAMs on gold that had been capped with gold nanoparticles.[8] In this case the change in conductance was attributed to changes in the bonding between the molecule and the gold nanoparticle.

As the current used in STM feedback decreases exponentially with distance, an increase in the dimensions of the tip substrate gap is expected to result in an exponential decrease in the current. This phenomenon translates into order of magnitude changes in tunneling current for angstrom changes in the gap dimensions. Given that any metal-molecule-metal junction is likely to have enough variability on this length scale, conductance changes in these junctions (and thus stochastic switching) likely is completely general in this type of system.

This chapter shows that stochastic switching can be observed in two types of electroactive thiol molecules inserted into an n-alkanethiolate SAM on gold. Previously, it had been observed that negative differential resistance (NDR, decreasing current with increasing bias) occurs in these types of molecules when composed into a SAM.[9] At the applied bias in which these molecules show NDR, they show an enhanced transconductance compared to an *n*-alkanethiolate SAM background. This chapter will show that this enhanced transconductance behavior blinks on and off, presumably due to conformation and/or orientation changes of the inserted molecules with the SAM over time.

5.2 Results and Discussion

5.2.1 Adventitious Replacement

While observing adventitious replacement of $FcC_{11}SH$, attempts were made to measure the rate of replacement into an insulating $C_{12}S$- self assembled monolayer. The approach was to modify an annealed gold (111) surface with an organic self-assembled monolayer and then image the surface with an STM tip. Once a flat area of the substrate was found, electroactive molecules could be inserted into the background monolayer. Images following this replacement were collected over a period of time.

To measure the rate of adventitious replacement and the subsequent stochastic switching of the replaced molecules a series of STM images were collected over time. These images monitored the transconductance of two types of electroactive thiols that were adventitiously inserted into a $C_{12}S$-SAM. Samples were prepared using a modified protocol originally described by Weiss et al. [10-13] A $C_{12}S$-SAM was exposed to ca. 1 mM solution of the desired electroactive molecule for a predetermined amount of time. The amount of time is dependent on the desired concentration of replaced thiol. A longer deposition time leads to more replacement. In the first system, ferrocenyl-undecanethiol ($FcC_{11}SH$)[14] was inserted into a dodecanethiolate SAM ($C_{12}S$-SAM) host matrix; in the other a viologen-terminated thiol ($MVC_{11}SH$)[15] was inserted into a decanethiolate SAM ($C_{10}S$-SAM) host matrix. Table 5.2.1 shows the molecules used for this study as well as their calculated heights on the surface. In the bias region in which NDR is observed for these electroactive molecules (ca. 1.6 V), they appear as bright spots in the darker

n-alkanethiolate SAM background matrix. At lower bias, the relative transconductance of these two species is similar and little or no contrast between these molecules is observed. This phenomenon had previously been illustrated for $FcC_{11}S$-SAM regions that had been nanopatterned into a $C_{12}S$-SAM (Figure 2.2.6).[2,9] In Figure 5.2.1, the same behavior is shown for $MVC_{11}SH$ inserted into $C_{10}S$-SAM. Specifically, at 0.2 V applied bias between tip and substrate, little contrast is observed in an STM image of this sample. Increasing the applied bias to 1.0 V reveals a number of bright features of approximately molecular dimensions. These are assigned to adventitiously inserted $MVC_{11}SH$ molecules.

The rate at which inserted molecules replaced into the background SAM was also of interest. Understanding the rate of replacement will provide more control over the insertion individual molecules and is also relevant to replacement lithography. Figure 5.2.2 shows a schematic of Fc-C_{11}-SH inserted into an insulating background C_{12}-SH SAM. This is a very general cartoon and should not be taken literally as to how the $FcC_{11}S$- inserts into the baackgournd SAM. It has been observed that the rate of adventitious replacement is slower for ferrocenyl-undecanethioacetate (Fc-C_{11}-SAc - the acetate is a protecting group that prevents the formation of disulfide) than the deprotected thiol.

Table 5.2.1

Molecule	Height
A) 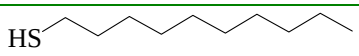	11.7Å
B) 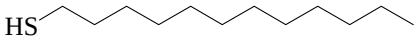	13.9Å
C) 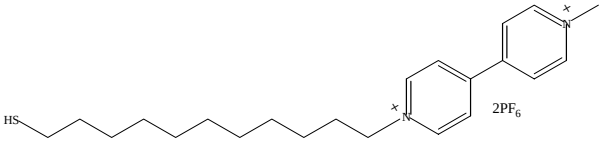	19.9Å
D) 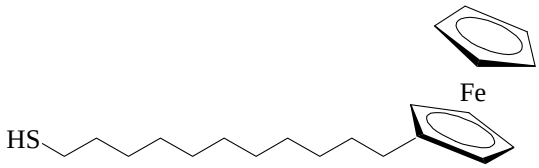	16.8Å

A) Decanethiol ($C_{10}SH$), B) Dodecanethiol ($C_{12}SH$), C) Viologen terminated thiol ($MVC_{11}SH$), D) ferrocenyl-undecanethiol ($FcC_{11}SH$). All heights were calculated using standard bond lengths and angles and assumed a fully extended conformation and a 30 degree tilt of the molecules on the Au substrate

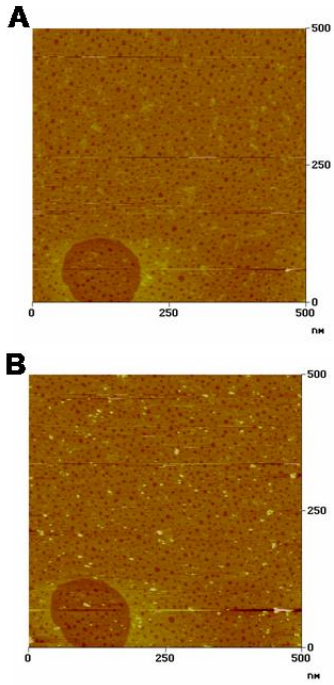

Figure 5.2.1 Bias dependent height contrast of MVC11S-SAM (z scale = 3 nm) inserted into a C10S-SAM. A) The MVC11S-SAM does not appear to be any higher than the C10S-SAM at 0.2V with a 10 pA setpoint B) At 1.0V with a 10 pA setpoint the MVC11S-SAM exhibits increased apparent height vs the C10S-SAM.

No one has ever attempted to quantify the rate of replacement. In an attempt to quantitatively describe the rate of replacement of Fc-terminated thiols into a background SAM, STM images were captured for several hours. A C_{12}-S-SAM was imaged on Au under dodecane with standard imaging conditions. Then a small amount of Fc-C_{11}-SH was added to the cell. The concentration of Fc-C_{11}-SH replaced

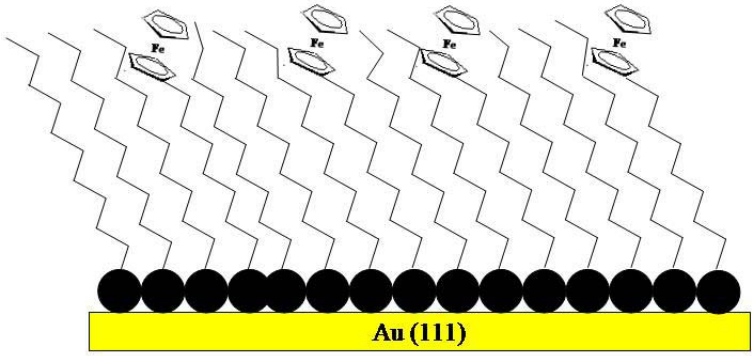

Figure 5.2.2 Schematic of $FcC_{11}SH$ inserted into $C_{12}S$-SAM (not drawn to scale)

into the background SAM was shown to increase with time. Figure 5.2.3 shows selected images over the course of 16 hours of $FcC_{11}SH$ replacing into the background SAM. The bright spots are the Fc-C_{11}-SH which show a higher apparent height contrast then the $C_{12}S$-SAM as discussed previously. To make a qualitative analysis of the kinetics these images were then thresholded so that the background SAM was represented as black and the $FcC_{11}S$- appeared as white spots in the black background (Figure 5.2.4 A and B). The thresholded images allowed the calculation of the number of black and white pixels which then were converted into an area of coverage (Table 5.2.2).

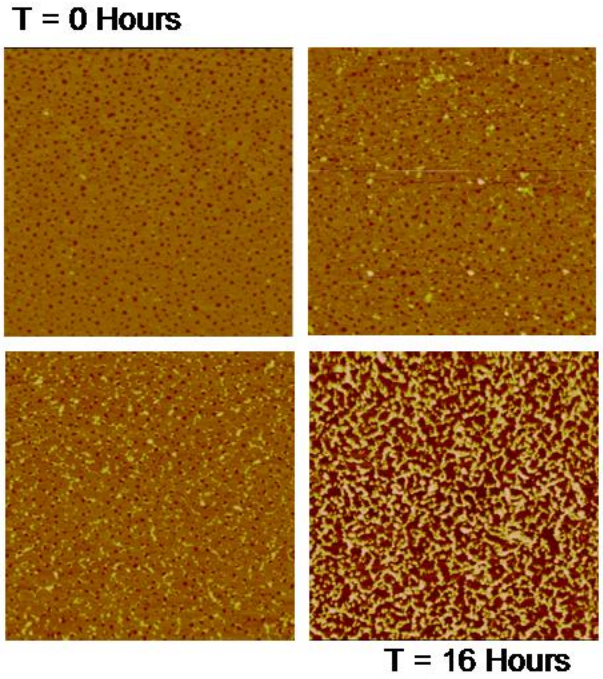

Figure 5.2.3 Representative images of $FcC_{11}SH$ inserted into a background $C_{12}S$-SAM taken over a 16 hour period.

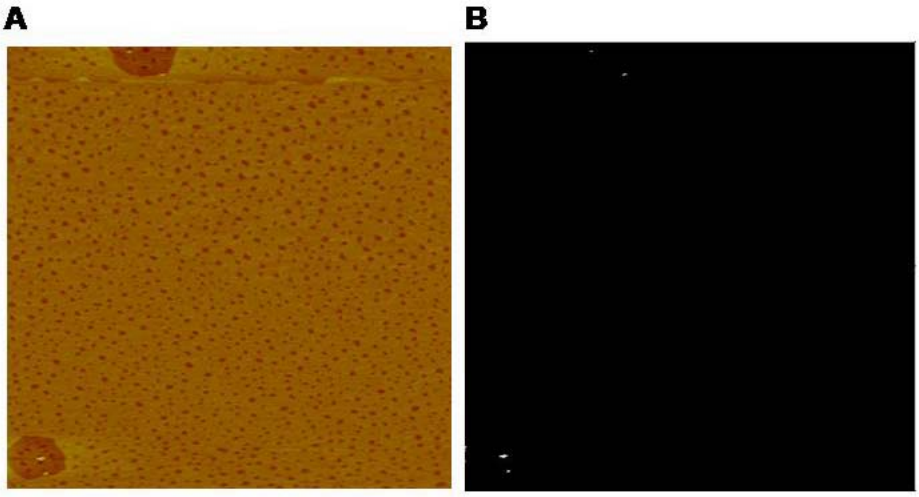

Figure 5.2.4 A) $C_{12}S$-SAM B) $C_{12}S$-SAM thresholded so that only the $FcC_{11}SH$ will show up as bright spots.

Table 5.2.2

Scan Size (nm)	500
Total Area (nm^2)	250,000
Total Area *(cm^2)	2.5×10^{-9}
Total # of pixels	250,000
Total # of pixels / Total Area	1
# of pixels in black region	241,211
# of pixels in the white region	8,789
Total area in black region (cm^2)	2.41211×10^{-9}
Total area in white region (cm^2)	$8{,}789 \times 10^{-11}$
# of molecules inserted	5,295
#of moles	8.79206×10^{-21}
Surface Coverage Γ (moles / cm^2)	3.51682×10^{-12}

Example of a typical spreadsheet showing data for calculating the surface coverage from the # of pixels (representing inserted $FcC_{11}SH$) The area of one $FcC_{11}SH$ molecule is estimated to be ~1.66×10^{-14} cm^2

These data can be plotted as a percent surface coverage of $FcC_{11}S$- vs. time. Figure 5.2.5 shows a plot of percent surface coverage vs. time for continuously imaged $FcC_{11}S$- (A), intermittently imaged $FcC_{11}S$-(B) and intermittently imaged $FcC_{11}SAc$-.(C) Figure 5.2.5 A shows that there are two sigmoidal regions to this plot. First a relatively slow increase in surface coverage is followed by a plateau after 400 minutes and then a very rapid increase in surface coverage followed, which plateaus again. It was hypothesized that the initially rapid replacement was due to the fact that the thiol replaces into defect sites in the background SAM first.

The thiol then begins to displace the background SAM which should be a much slower process because the thiol has to insert itself into a well packed monolayer. As the SAM becomes more disordered and more sites are available to the Fc-C_{11}-SH the surface coverage increases at a much faster rate.

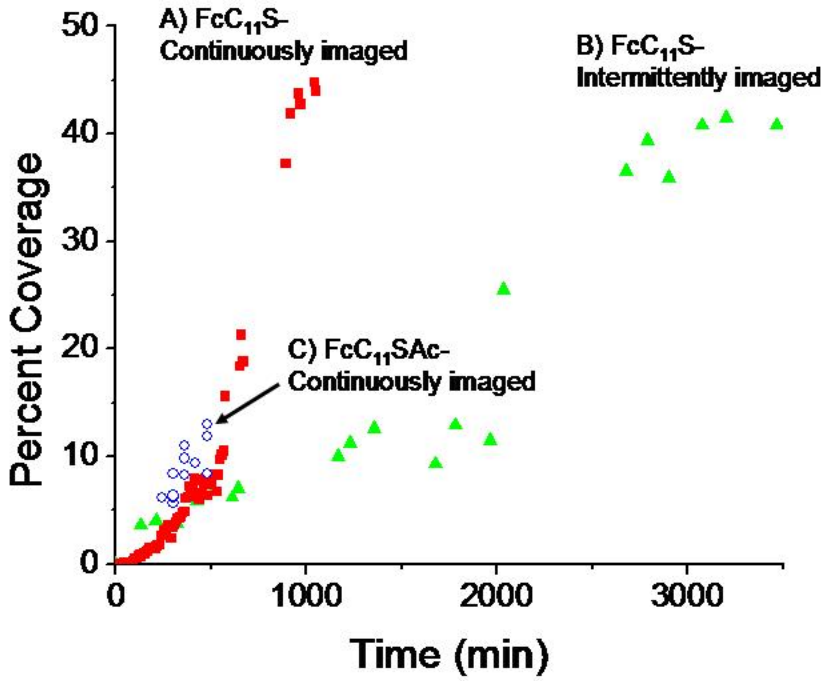

Figure 5.2.5 A) Plot of % surface coverage vs. time for $FcC_{11}SH$ inserted into a $C_{12}S$-SAM under constant imaging (red squares). B) Plot of % replacement vs. time for $FcC_{11}SH$ inserted into a $C_{12}S$-SAM under intermittent imaging (green triangles). C) Plot of % replacement vs. for $FcC_{11}SH$ inserted into a $C_{12}S$-SAM (blue circles).

However, it was possible that the rate of replacement was being artificially induced by the electric field (~1V/nm) produced by the tip. In order to rule this out another experiment was performed where a background SAM was imaged and FcC11SH was added to the cell. Scanning was then stopped and images were captured at intermittent periods for the next 58 hours. The surface coverage was calculated the same way as previously discussed. Figure 5.2.5B shows a plot of the percent

replacement vs time. Again a sigmoidal curve is observed but over a much longer time frame than the $FcC_{11}SH$ that adventitiously replaced into the background SAM under constant imaging., The percent replacement of the $FcC_{11}S$- that was scanned continuously increased at a much faster rate than the sample that was only scanned periodically.

FcC11SAc- was also replaced into a background $C_{12}S$- SAM in this case it was decided to make up multiple samples and incubate them for various times. This way there would always be a fresh sample where replacement could not be perturbed by the electric field from the tip. Figure 5.2.5C shows the percent replacement of $FcC_{11}SAc$-. A comparison of the percent replacement of $FcC_{11}SAc$ vs $FcC_{11}SH$ (not constantly scanned) showed the slope of the initial replacement was the same. These data clearly show that the constant scanning of the tip over the substrate induces a faster rate of replacement than if the scanning is done periodically or if the insertion is performed in solution out side of an STM set up.

5.2.2 Stochastic Switching

$FcC_{11}S$- SAMs and $MVC_{11}S$-SAMs were shown to change their transconductance over time relative to the *n*-alkanethiolate SAM background. Figure 5.2.6A shows a series of STM images of the same region of a sample in which the relative height (e.g., relative transconductance) of several inserted $MVC_{11}SH$ molecules varies over time. Each bright spot is likely a small bundle of molecules rather than just one. Two of these groups are labeled A and B. In the first panel (at time = 0) the molecules labled A are “on” while the molecules labeled B are “off”.

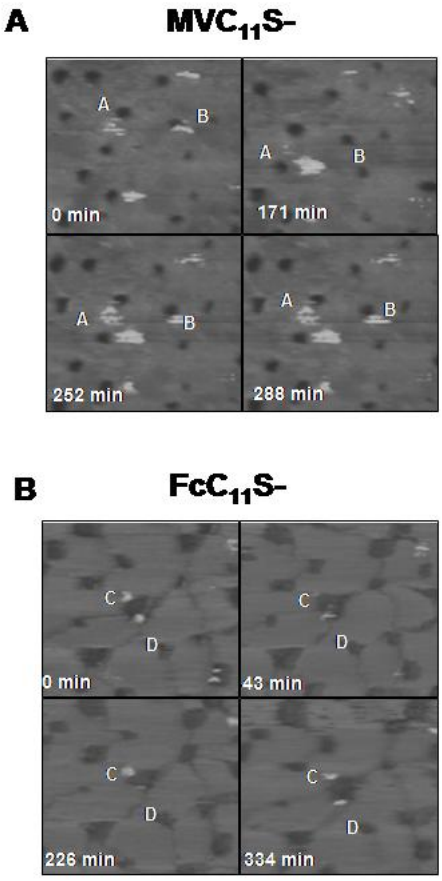

Figure 5.2.6 Four images from a series of time lapse images. A) These images of MVC11S-SAM were acquired at times of 0 min, 117 min, 252 min and 288 min. Each image is 70 nm x 70 nm and was acquired at +1.2V at 10 pA with a z range of 2 nm. B) These images of FcC11S-SAM were acquired at times of 0 min, 117 min, 252 min and 288 min. Each image is 47 nm x 47 nm and was acquired at +1.0V at 10 pA with a z range of 2 nm. These molecules labeled A,B,C,D were found to switch conductance states several times.

The second panel shows an image at time = 171 min, where the conductance of A has decreased such that only a small spot is observed and is considered to be “off”. B is still “off”. At time = 252 min, in the third panel, A is back “on” and B is also “on”. In the fourth panel B is still “on” and while A is still considered to be “on” it is exhibiting a slight decrease in transconductance. In this lat panel a bundle of molecules nest to A which has been “on” in the previous 3 panels in “off”. Figure

5.2.6B shows a similar behavior for inserted $FcC_{11}SH$ molecules. Two of these groups are labeled C and D. In the first panel (at time = 0) both C and D are “on”. The second panel shows an image at time = 43 min, where the conductance of C has decreased such is considered to be “off”. D is still “on” however, the conductance is greatly decreased. At time = 226 min, in the third panel, C is back “on” and B is “off”. In the fourth panel both C and D are “on” again. The molecules “blink” independently of one another, consistent with the contention that the “blinking” was not due to the direction the STM was scanning in (up and down scans could presumably represent two different orientations of the tip and therefore two different pathways for the current to tunnel through), or a tip perturbation applied consistently to each inserted molecule.

Figure 5.2.7A shows a time-lapse series of images of one or a small collection of inserted MVC11SH molecules. The relative change in transconductance could be quantified by taking a cross section of the height of the inserted molecules for each image in Figure 5.2.7A and plotting the height versus time (Figure 5.2.7B). The molecules were considered to be “off” when no height contrast could be observed between them and the background SAM. The molecules were decided to be “on” at a height contrast of 0.8 nm. A similar series of images (Figure 5.28A) and apparent height versus time plot (Figure 5.2.8B) was obtained in a similar

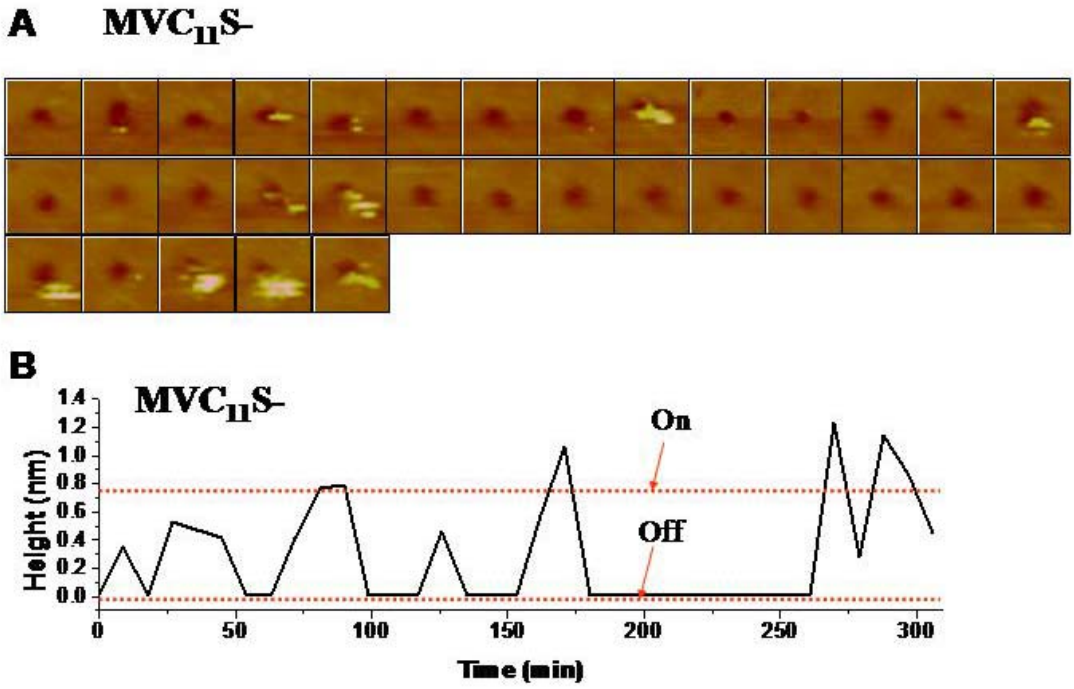

Figure 5.2.7 A)Full time-lapse series of images for MVC11S-SAM these images are 24.6Å x 24.6Å and were used to calculate the heights shown in B

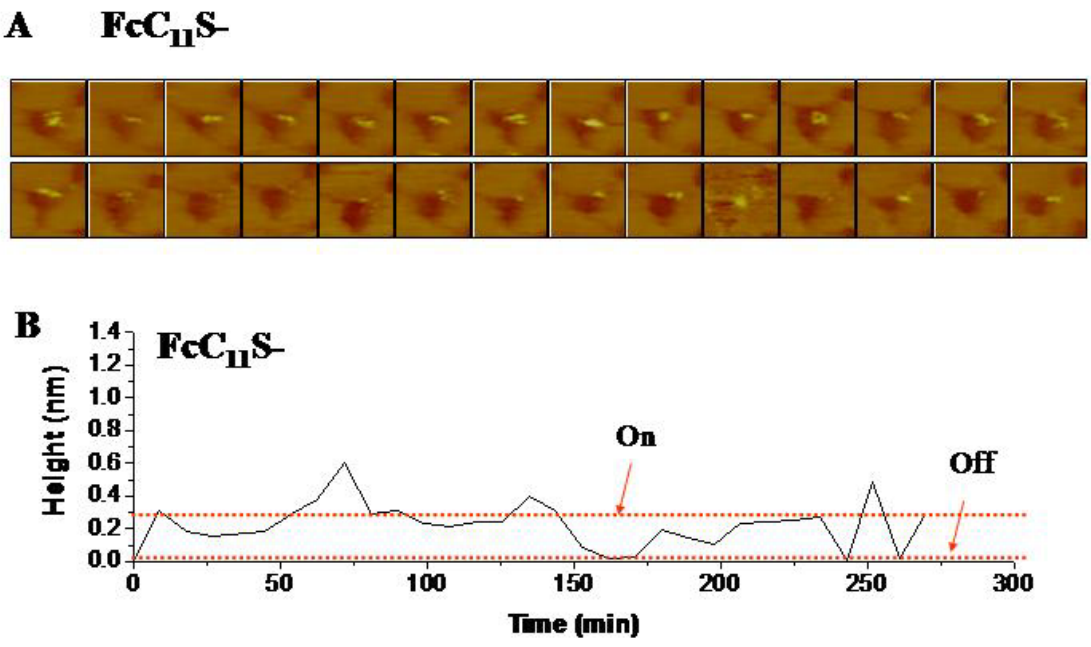

Figure 5.2.8 A)Full time-lapse series of images for FcC11S-SAM these images are 15.6Å x 15.6Å and were used to calculate the heights shown in B

fashion for inserted FcC11SH. The molecule was “off” then the height contrast was 0 and “on” when the height contrast was greater than 0.5 nm. The apparent height contrast between the higher and lower conductance states of the MVC11S- and FcC11S- fluctuates through the series of images in a manner similar to the stochastic switching behaviors reported previously in the introduction. This behavior is consistent with both types of molecules assuming different conformations and/or orientations in the SAM.

5.3 Conclusion

It was not anticipated that the process of scanning in an STM configuration would influence the rate of adventitious replacement. The data presented in this chapter show quite clearly that this assumption was incorrect. It is proposed that the electric field generated by the STM tip induces replacement of electroactive molecules into a background alkanethiolate SAM at a much faster rate then was expected. The influence of the electric field is important to remember when future studies of molecular conductance are performed on larger assemblies of patterned electroactive thiols using replacement lithography.

While this chapter has shown stochastic variation in the relative transconductance of electroactive molecules, it is likely a completely general phenomenon. It is illustrated here for two electroactive thiol molecules that are structurally quite different from one another and from molecules in which this phenomenon has been studied previously. This behavior is most simply rationalized as conformational and/or orientational changes of one or a small collection of

molecules over time. In cases relevant to molecular-scale electronics, the observation of these changes will not be averaged out over a large collection of molecules. While the work presented here does not indicate how many molecules will be required to create a junction with a consistent transconductance, it does illustrate the importance of addressing this issue in molecular-scale electronics studies.

5.4 Experimental

SAM Preparation

Prior to monolayer deposition the substrates were cleaned in piranha solution (3:1 H2SO4:H2O2 (30%) by volume). (Caution: Piranha solution is corrosive. In addition, care should be taken to not store piranha solution for extended lengths of time due to the formation of explosive oxides.) Sample substrates were flame-annealed Au(111) facets on a gold bead formed at the end of a gold wire (Alfa Aesar, 99.999%). The wire was alloyed to a platinum foil (Alfa Aesar) base.[9] n-Alkanethiolate SAMs were prepared on gold by refluxing gold [111] facets in 1 mM n-alkanethiol ethanolic solutions and for the Blinking experiments, briefly exposed them to 1mM ethanolic solutions of an electroactive guest species (FcC11S- or MVC11S-). This allowed small groups of the guest species to insert into the defects sites in the host matrix.[4,5,8] After copious rinsing in ethanol, the sample holder was mounted in a custom Kel-F fluid cell in preparation for scanning. For measuring the rate of adventitious replacement ~10 -20µl of $FcC_{11}SH$ or $FcC_{11}SAc$ dissolved in dodecane was added to the Kel-F fluid cell.

STM Imaging

All STM experiments employed a Digital Instruments (Santa Barbara, CA) Nanoscope IIIa equipped with an E-scanner in low-current mode to obtain STM images at room temperature in dry nitrogen. The samples were imaged at a setpoint of 10 pA and a bias of 1.0V for the FcC11S- and 1.2V for the MVC11S-. SAM images were continuously captured to monitor the variation in the apparent height of that species. Due to thermal drift and creep in the STM piezoelectric imaging system, the ability to keep the tip imaging in the same region required large scan areas (100 nm to 500 nm) to compensate for the drift. For measuring the rate of adventitious replacement, images were either captured continuously or the tip was retracted and then periodically engaged to capture one image.

5.5 References

(1) Fuierer, R. R.; Carroll, R. L.; Feldheim, D. L.; Gorman, C. B. *Adv. Mater.* **2002**, *14*, 154.

(2) Gorman, C. B.; Carroll, R. L.; He, Y. F.; Tian, F.; Fuierer, R. *Langmuir* **2000**, *16*, 6312.

(3) Chen, J.; Reed, M. A.; Asplund, C. L.; Cassell, A. M.; Myrick, M. L.; Rawlett, A. M.; Tour, J. M.; Patten, P. G. V. *Appl. Phys. Lett.* **1999**, *75*, 624.

(4) Donhauser, Z. J.; Mantooth, B. A.; Pearl, T. P.; Kelly, K. F.; Nanayakkara, S. U.; Weiss, P. S. *Jpn. J. Appl. Phys. Part 1* **2002**, *41*, 4871.

(5) Donhauser, Z. J.; Mantooth, B. A.; Kelly, K. F.; Bumm, L. A.; Monnell, J. D.; Stapleton, J. J.; Price, D. W.; Rawlett, A. M.; Allara, D. L.; Tour, J. M.; Weiss, P. S. *Science* **2001**, *292*, 2303.

(6) Chen, J.; Reed, M. A.; Rawlett, A. M.; Tour, J. M. *Science* **1999**, *286*, 1550.

(7) Chen, J.; Wang, W.; Reed, M. A.; Rawlett, A. M.; Price, D. W.; Tour, J. M. *Applied Physics Letters* **2000**, *77*, 1224.

(8) Ramachandran, G. K.; Hopson, T. J.; Rawlett, A. M.; Nagahara, L. A.; Primak, A.; Lindsay, S. M. *Science* **2003**, *300*, 1413.

(9) Gorman, C. B.; Carroll, R. L.; Fuierer, R. R. *Langmuir* **2001**, *17*, 6923.

(10) Allara, D. L.; Dunbar, T. D.; Weiss, P. S.; Bumm, L. A.; Cygan, M. T.; Tour, J. M.; Reinerth, W. A.; Yao, Y.; Kozaki, M.; Jones, L. *Molecular Electronics: Science and Technology*; Ann. NY Acad.Sci.: New York, 1998; Vol. 852.

(11) Cygan, M. T.; Dunbar, T. D.; Arnold, J. J.; Bumm, L. A.; Shedlock, N. F.; Burgin, T. P.; Jones, L.; Allara, D. L.; Tour, J. M.; Weiss, P. S. *J. Am. Chem. Soc.* **1998**, *120*, 2721.

(12) Bumm, L. A.; Arnold, J. J.; Cygan, M. T.; Dunbar, T. D.; Burgin, T. P.; Jones, L.; Allara, D. L.; Tour, J. M.; Weiss, P. S. *Science* **1996**, *271*, 1705.

(13) Weiss, P. S.; Bumm, L. A.; Dunbar, T. D.; Burgin, T. P.; Tour, J. M.; Allara, D. L. *Probing electronic properties of conjugated and saturated molecules in self-assembled monolayers*; Ann. NY Acad.Sci.: New York, 1998; Vol. 852.

(14) Uosaki, K.; Sato, Y.; Kita, H. *Langmuir* **1991**, *7*, 1510.

(15) Tang, X. Y.; Schneider, T. W.; Walker, J. W.; Buttry, D. A. *Langmuir* **1996**, *12*, 5921.

Appendix 1

Scanning Tunneling Microscopy

Electronics

A.1 Introduction

This appendix discusses the general operation of a Digital Instruments (DI) STM. The STM relies on the ability of electrons to tunnel through a very narrow vacuum gap between two conductive materials. When a voltage bias is applied between a conducting surface and an atomically sharp metal tip a tunneling current flows across the gap. The current's magnitude changes exponentially as the distance between the tip and the surface changes. The tunneling current depends on the electronic structure and the bias voltage; this dependence may be used to examine molecular structure -electronic property relationships. STM routinely reaches true atomic resolution. However, the sample must be at least moderately conducting; which rules out the use of STM on many interesting surfaces. Also, STM cannot be used in a conducting solution, which makes it unsuitable for many biological applications.

The quality of an STM image is determined by how precisely a tip-sample interaction can be monitored. Part of this interaction is determined by the quality of the scanner, which moves, either the sample or the tip. In the DI scanner configuration, the tip is held in a stationary position while the sample is scanned beneath it. The DI scanner uses piezo materials combined in a single tube. Each tube consists of five or more independently operated piezo elements. Piezo materials contract or expand as a voltage is applied to them. The polarity of the bias determines whether the piezo expands or contracts. The size of the piezo determines the maximum size that can be imaged. Shorter scan tubes contain shorter piezo elements that can be controlled more precisely than larger piezo tubes.

However, shorter piezo tubes can not scan as large an area as larger tubes. There is, therefore, a trade off of precision for scan size. If molecular resolution is desired smaller piezo tubes are preferred.

The tip- sample distance is controlled by a feedback mechanism that is designed to keep the tip- sample distance constant. This is achieved by maintaining a constant tunneling current. The feedback is monitored as the sample is scanned. The feedback changes the tip sample distance due to physical surface features or changes in the conductance of the substrate. The scanner motion is correlated point by point with the feedback status to produce an image which is a three dimensional topographic relief.

A.2 Vacuum Electron Tunneling

Tunneling is a quantum –mechanical phenomenon that arises because the wave function (Ψ) that describes a particle can extend into areas where it is classically forbidden. The Fermi energy (E_F) of a typical metal is around 4 eV below the vacuum potential. If two metals are separated by a vacuum gap they have about a 4 eV energy barrier (ϕ) between them. Tunneling theories are based on the perturbative-transfer Hamiltonian. In this theory the interaction between the two electrodes is weak enough to be neglected and the tunneling current can be evaluated from the eigenfunctions Ψ_u and Ψ_v in the region of the tunnel barrier.[1] These eigenfunctions have eigenenergies E_u and E_v which represent the energies of the tip and sample electrode potentials respectively. The following equation is obtained

$$I_t = \frac{2\pi e}{\hbar}\sum_{v,u} f(E_v)\left[1 - f(E_v + eV_t)\right]\left|M_{uv}\right|^2 \delta(E_u - E_v) \qquad (1)$$

Where the tunnel matrix element is:

$$M_{uv} = \frac{\hbar}{2m}\int_{S_0} dS \cdot (\psi_u^* \nabla \psi_v - \psi_v \nabla \psi_u^*) \qquad (2)$$

The integral is over any surface (S_0) which lies completely in the barrier region.[1] The delta function in equation 1 suggests that the electron does not lose energy during tunneling (elastic tunneling) and the energy shift eV_t is the result of the tunnel bias voltage (V_t).

This transfer Hamiltonian can be applied to STM by considering the limit of small V_t and assume that the geometry of the tip is spherical with a radius of curvature R. The following expression for the tunneling conductance can be obtained:

$$G_t \equiv \frac{I_t}{V_t} \approx 0.1R^2\, e^{2kR}\rho s(r_t, E_F)$$

$$\rho s(r_t, E_F) \equiv \sum_v \left|\psi_v(r_t)\right|^2 \delta(E_v - E_f) \qquad (3)$$

where $\rho s(r_t, E_F)$ is the local density of states (LDOS) of the sample surface at the Fermi level calculated at the center position r_t of the tip. $\kappa = \hbar^{-1}(2m\phi)^{1/2}$ is the decay length for the wave function in vacumm and ϕ is the tunneling barier height relative to the Fermi Level (E_F).[1] given that $\left|\psi_v(r_t)\right|^2 \propto e^{-2k(R+z)}$, from equation 3 the tunneling conductance can be rewritten as:

$$G_t = \frac{I_t}{V_t} \propto e^{-2kz} = \exp(-1.025\sqrt{\phi}z) \qquad (\phi \text{ is in eV and z is in Å}) \qquad (4)$$

The tunneling conductance (i.e. current) decays exponentially with increasing distance (z). For a typical ϕ of 4 eV a change in the tip –substrate distance by 1 Å willl result in a ten fold change in I_t. This sensitivity to distance is what allows the STM to achieve molecular resolution.

A.3 Continuous Imaging Tunneling Spectroscopy

I-V curves were collected at room temperature under dodecane. current imaging tunneling spectroscopy (CITS) was used to collect the I-V curves (a more detailed description of CITS can be found in appendix 1). In CITS mode the tip scans one line in feedback and records the tips distance from the surface at 32 evenly distributed points along the line. The tip then goes out of feedback and uses the recorded height information to collect an I-V curve at each designated point. This procedure is iterated over the scan area creating a 32 by 32 array of collection points. For a total of 1024 I-V curves. Figure A.1 shows graph of Bias vs time for a typical I-V curve. The voltage is ramped to a user defined start potential (in this case +2000 mV) and then is swept to an end potential (-2000 mV). The time the potential sweep takes can be set by the user. This is done by selecting how many points the computer should sample in an I-V curve, and the time between each sample point (sample period) The sample period is the time it takes in between each feedback cycle in the bias sweep. The feedback turns on between ramps of the bias voltage. The time required for each bias sweep then is the sample period multiplied by the number of points collected for each curve and the scan rate is determined by dividing the sample period by the bias window. Typically we set the bias window to

sweep from -2000 mV volts to 2000 mV with 256 samples collected and a sample period of 50 µs.

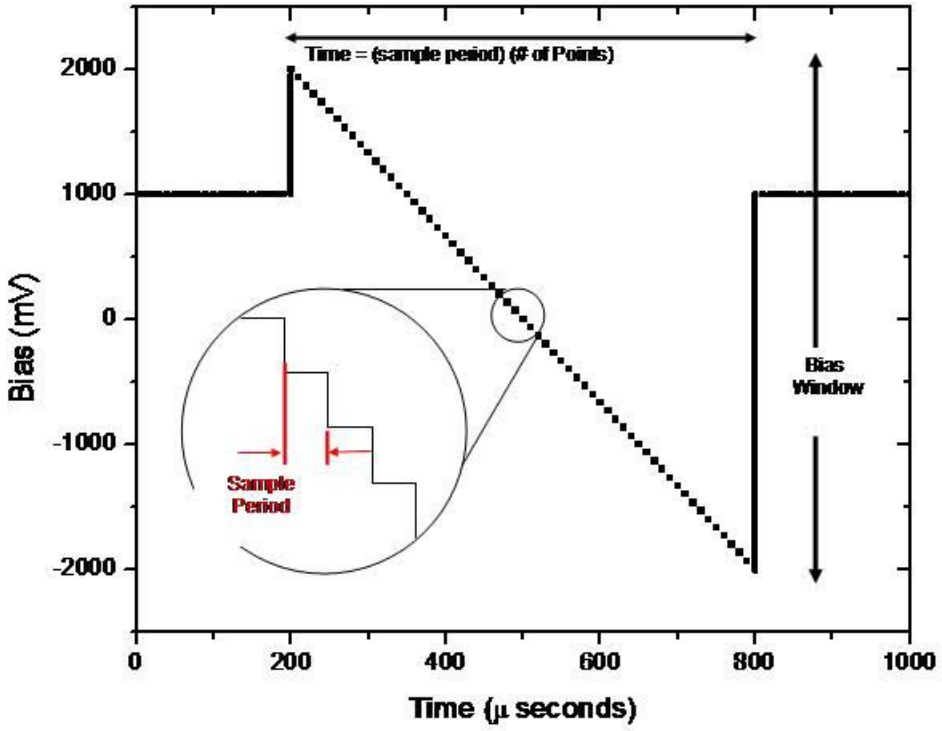

A.1 Schematic of the bias sweep during the collection of an I-V curve

A sample period of 50 µs is selected because of bandwidth limitations in the electronics of the instrument. The STM is able to operate in a low current configuration (typically 5 12 pA) with the help of l booster box that has three low pass filter options (400Hz, 1.5 kHz, and 4 kHz). It is therefore necessary for the frequency of the NDR peak be less then the low pass filter setting that is used. The booster box does not allow the filters to be bypassed. Typically I-V curves are collected with the 1.5 kHz filter selected. The average peak width of NDR is approximately 850 mV. The time it takes for an I-V curve to be collected can be calculated (assuming 256 points per curve):

$$(256\ \text{points})\left(\frac{50\times10^{-6}\,\text{seconds}}{\text{point}}\right)=0.0128\ \text{seconds}$$

once the time it takes for I-V curev to be taken the rate can be determined by dividing the bias window the I-V collection time:

$$\frac{4.0\ V}{.0128\,\text{seconds}}=312.5\,V/\text{second}$$

The frequency can then be calculated by assuming a peak width of .850 V:

$$\left(\frac{312.5\,V}{\text{seconds}}\right)\left(\frac{1}{.850\,V}\right)=368\ s^{-1}\ or.\ 368\ kHz$$

This is well below the cutoff frequency of the low pass filter.

A.4 Imaging and I-V spectroscopy with RHK Controller

The RHK controller was a new piece of equipment that was acquired by the Gorman group. There were many technical challenges in trying to get the RHK to work properly. The RHK works in the same way as the DI but has a different set of filters and control of the tip is better as well as it has the ability to compensate for drift. The same DI base and scan tube was used, but connected to the RHK controller. There is a first stage preamp in the DI STM head. In the case of the DI a different head is used that has an external first stage preamp that is connected to the head via a BNC cable. The current is then boosted with a second stage preamp that is much more versatile than the DI low current boost box. The RHK second stage preamp allows for more low pass filter choices (500 Hz, 1.5 kHz, 5 kHz, 15 kHz, 50 kHz and 150 kHz) as well as an option to bypass the filters; which the DI

does not allow. To asses the capabilities of the RHK it was desirable to compare images and I-V curves to those observed with the DI. To make sure the tip was of sufficient quality for molecular resolution. Imaging was first performed on the DI, then the tip was retracted and the same tip was inserted into the scanning head for the RHK. The DI base was disconnected from the DI controller and connected directly to the RHK controller. Individual I-V curves were taken with the RHK instead of CITS. The RHK allows for precise placement of the tip over surface features. Figure A.2 shows representative I-V curves of a $C_{12}S$- SAM for each filter setting available to the RHK.

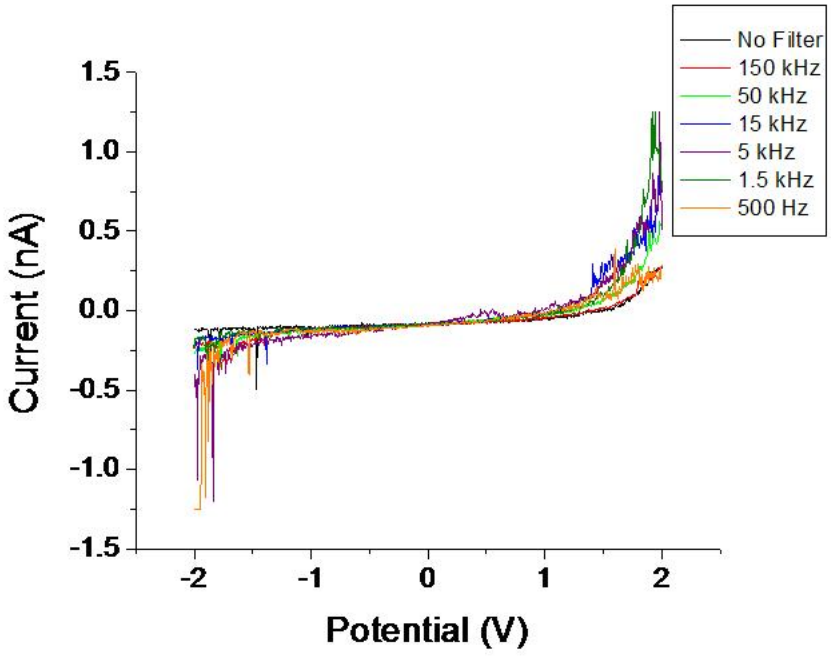

A.2 I-V curves at various filter settings on the RHK.

From these curves it can be seen that there is not much difference in the noise between the filter settings.

A direct comparison of the two controllers could be achieved by using replacement lithography.[2-5] Figure A.3 shows a $FcC_{11}S$- SAM was replaced into a decanethiolate monolayer ($C_{10}S$- SAM). With the RHK an image is collected and then the tip can be moved by the user to anywhere in the image and single or multiple I-V curves can be acquired at the designated location. Replacement can be performed again and I-V measurements taken and a direct comparison to the DI can be made.

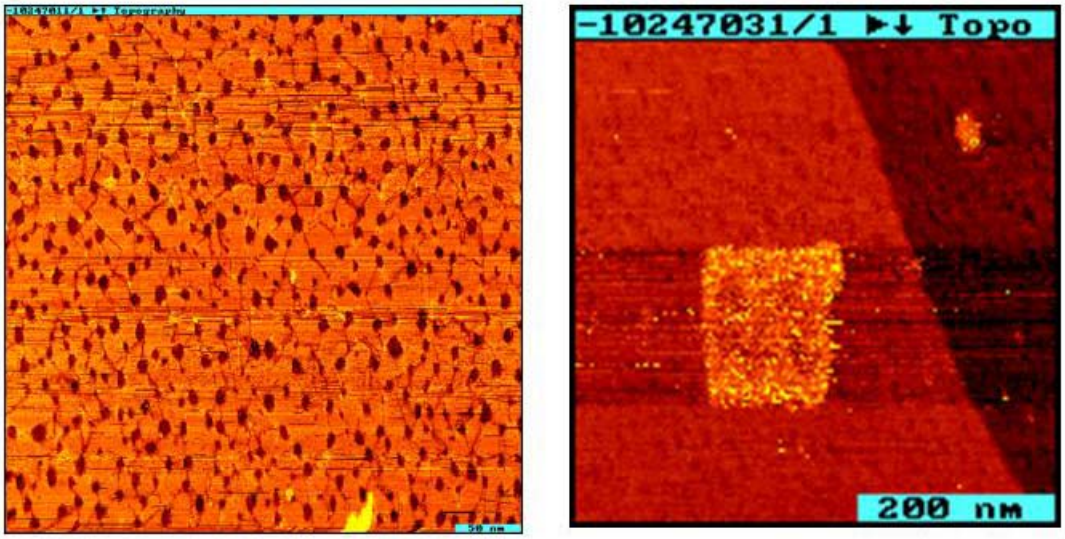

A.3 Replacement of Fc in to $C_{10}S$-SAM usenig a RHK controller

This is very useful because one can alternate between taking an I-V curve inside the replaced $FcC_{11}S$- region and the $C_{10}S$-. With the Di set up all the data is filtered through a low pass filter. There is never a chance for the I-V collection to be performed without the filters. The curves we see with the DI are not the curves in their raw form. They have been filtered.

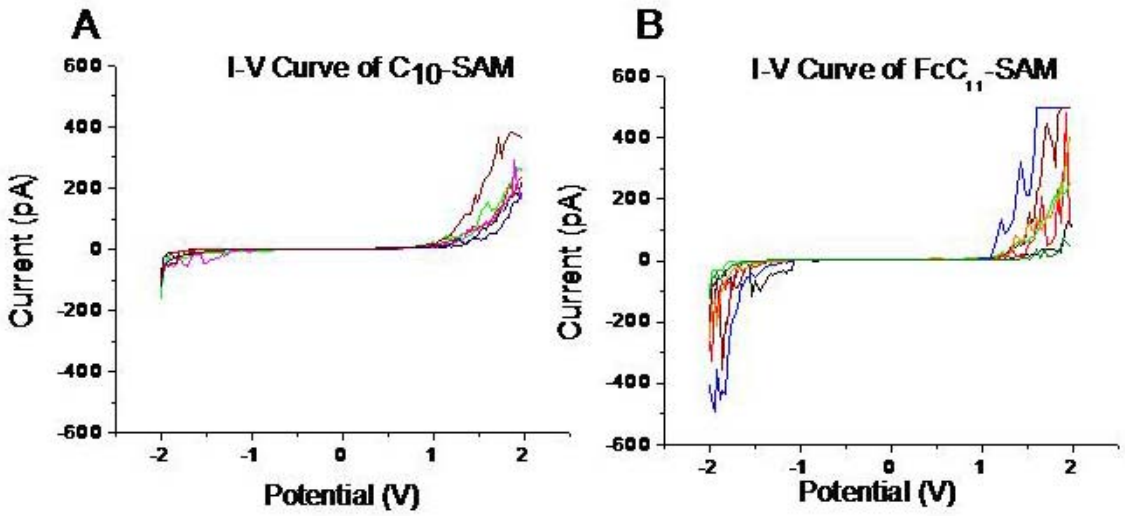

A.4 (A) I-V curves over C_{10}S- (B) I-V curves over replaced Fc region

All of the curves are collected with a booster box that has been set to a maximum filter cut off frequency of 1.5 kHz. Figure A.4A shows several I-V curves taken over a C_{10}S- SAM, as can be seen the curves show non linear I-V behavior associated with tunneling. There is however much more noise in these samples that in the DI curves. Figure A.4B shows several I-V curves taken in the replaced FcC_{11}S- as expected with a molecule with higher conductance the maximum current is increased, However, NDR could not be seen due to the increase in noise. More work need to be done to better optimize the RHK.

A.5 References

(1) Besenbacher, F. *Rep. Prog. Phys.* **1996**, *59*, 1737.

(2) Fuierer, R. R.; Carroll, R. L.; Feldheim, D. L.; Gorman, C. B. *Adv. Mater.* **2002**, *14*, 154.

(3) Gorman, C. B.; Carroll, R. L.; He, Y. F.; Tian, F.; Fuierer, R. *Langmuir* **2000**, *16*, 6312.

(4) Fuierer, R. *Probing the Electronic Properties of Materials that Self-Assemble*; North Carolina State University: Raleigh, 2004.

(5) Gorman, C. B.; Carroll, R. L.; Fuierer, R. R. *Langmuir* **2001**, *17*, 6923.